# Advanced Turbine Technology

# ATTAP

## Applications Project

DOE/NASA 0336-5
NASA CR-195446
EDR 17038



## 1992 Annual Report

**Allison**
**Gas Turbine Division**
General Motors Corporation
P.O. Box 420
Indianapolis, Indiana 46206-0420

**December 1993**

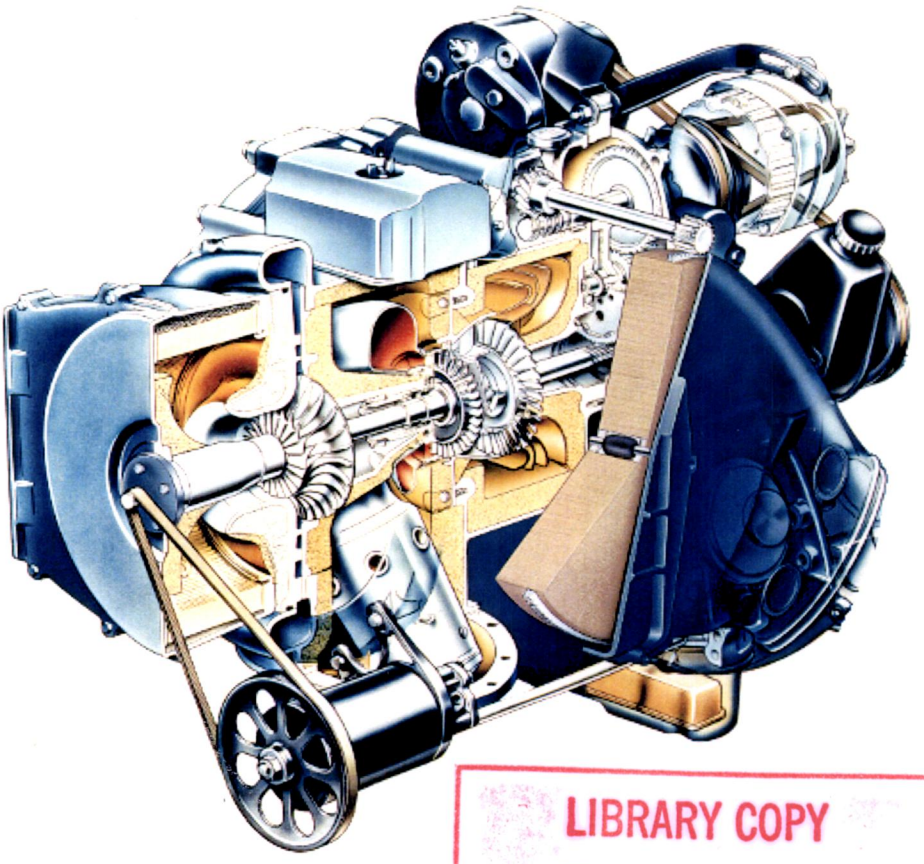

Prepared for
National Aeronautics
and Space Administration
Lewis Research Center
Cleveland, Ohio 44135
Under Contract DEN 3-336

For U.S. Department of Energy
Conservation and Renewable Energy
Office of Vehicle and Engine R&D
Washington, D.C. 20545
Under Interagency Agreement DE-AI01-90CE50300

# NOTICE

# FOREWORD

This report presents a technical summary of work accomplished on the Advanced Turbine Technology Applications Project (ATTAP) under NASA contract DEN3-336 for calendar year 1992. The report is set up and arranged per the original Work Breakdown Structure (WBS). Only WBSs with activity in 1992 are reported herein.

This technology project is funded by the U.S. Department of Energy, Conservation and Renewable Energy, Office of Transportation Technologies, Propulsion Systems, Advanced Propulsion Division. Project management and technical direction are provided by the NASA Lewis Research Center (LeRC), Aeronautics Directorate, Propulsion Systems Division, Terrestrial Propulsion Office.

The overall intent of the ATTAP is to bring the automotive gas turbine engine to a technology state at which industry can make commercialization decisions. Key to this goal is the development and demonstration of structural ceramic component technology as the critical high risk/high payoff element in this type of engine. Such ceramic technology is the prime ATTAP focus. Automotive gas turbine attractions include the following potential advantages:

- Significantly increased fuel economy
- Ability to meet Federal emission standards with untreated exhaust
- Ability to operate on a wide range of alternate fuels
- Inherently smooth, low-vibration operation

General Motors (GM) is addressing the ATTAP with a team that draws on:

- The extensive ceramic design, analysis, and materials data base and expertise in place at the Allison Gas Turbine Division (Allison)
- The substantial experience, design and test capabilities, automotive gas turbine technology and hardware, and test vehicle resources developed under GM funding as background to this project and in place at GM's Advanced Engineering Staff (AES)
- The infrastructure of expertise and resources in place in the American ceramics industry and the working relationships between the industry and Allison
- The unique capabilities and resources existing at universities and at national laboratories, such as the High Temperature Materials Laboratory (HTML) at the Oak Ridge National Laboratory (ORNL)

In this arrangement, Allison serves as prime contractor. Major ceramics industry development subcontractors to date are The Carborundum Company (CBO); Corning Inc.; Schuller International, Inc.; Ceramics Process Systems (CPS); and Norton/TRW Ceramics (N/TRW). A major ceramic component supplier is the Kyocera Industrial Ceramics Corporation.

TABLE OF CONTENTS

## LIST OF ILLUSTRATIONS

LIST OF ILLUSTRATIONS (cont)

## LIST OF ILLUSTRATIONS (cont)

## LIST OF TABLES

# SUMMARY

ATTAP activities during the past year included reference powertrain design (RPD) updates, test-bed engine design and development, ceramic component design, materials and component characterization, ceramic component development and fabrication, ceramic component rig testing, and test-bed engine fabrication and testing.

RPD revisions included updating the baseline vehicle as well as the turbine RPD. Comparison of major performance parameters shows that the turbine engine installation exceeds critical fuel economy, emissions, and performance goals, and meets overall ATTAP objectives.

Test-bed engine design and development included engine mechanical design, with gasifier housing and regenerator seal systems, combustion system design, alternate aerodynamic designs of ceramic scrolls and rotors, and engine system integration, all aimed at upgrading the AGT-5 from a 1038°C (1900°F) metal engine to a durable 1372°C (2500°F) structural ceramic component test-bed engine. A 3-D CAD surface model of the revised gasifier housing insulation mandrel was generated, which in turn was used to build a full size polycarbonate rapid prototype for analysis of machining and fabrication processes. Two versions of the regenerator L-seal system were analyzed, designed, fabricated, and tested. Combustion system development included analysis of two designs and fabrication of components, including fuel nozzles, for one design. In the aerodynamics area, flow testing of alternative scrolls and RPD size gasifier rotors was completed. Engine control development efforts included consolidation of EDM-800 controller program versions to accommodate magnetoresistive N1 sensors, the burner variable geometry actuator, automatic setting of minimum fuel, and starting logic.

ATTAP-defined ceramic and associated ceramic/metal component design activities completed include the ceramic gasifier turbine static structure, the gasifier turbine rotor, and the ceramic power turbine rotor. Efforts on the ceramic gasifier turbine static structure included analysis of gasifier turbine vanes with cold assembly structural analysis, steady-state maximum power thermal and structural/probability of survival (POS) analyses, and cold start transient thermal and structural/POS analyses. Results of analyses reveal component stresses below design limits and ceramic component POS above design criteria for the cold assembly conditions, minimal ceramic component maximum power steady-state stresses with the corresponding ceramic assembly POS exceeding design goals, and metal component stresses below design limits at the maximum power steady-state condition. Work on gasifier turbine rotors included analysis of rework for 26-blade gasifier rotor to reduce high blade fillet stresses, but the rework was not predicted to increase the POS enough to warrant reworking the parts. Power turbine development efforts analyzed and corrected designs and hardware for further testing.

Materials and component characterization efforts have focused on the testing and evaluation of five candidate ceramic materials from three separate suppliers to establish a data base of appropriate material characteristics supporting the design, analysis, development, and testing of hot section ceramic components. The material characterization activities dealt with microstructural, density, flexural strength, and fracture toughness evaluations. Fractographic analyses of ceramic component hardware failures allowed the separation of design features from material deficiencies, defects, or nonoptimum fabrication procedures.

Ceramic component process development and fabrication proceeded for the thermal insulation, extruded ceramic regenerator disk, gasifier turbine rotor, and gasifier turbine scroll. Major ceramic industry development subcontractors are Schuller, Corning, Ceramics Process Systems, and Norton/TRW. Efforts at Schuller were directed at developing injection moldable insulation and manufacturing processes for low cost, high volume production of both simple and complex engine components. Process demonstrations performed in the last year appear to be viable candidates for high volume injection molding production parts. Corning worked to develop materials and processes to yield reli-

able, low cost, high performance, one-piece extruded ceramic regenerator discs. Materials work developed an LAS additive that greatly improved salt resistance. Die development tested alternative cell geometries and demonstrated the feasibility of large 1100 cpsi tools. CPS development programs addressed tooling, processing, and fabrication of gasifier turbine rotors using CM200 and SRS201 sialon materials and the Quickset injection molding fabrication process. Work was completed for a 26-blade rotor application. Norton/TRW Ceramics efforts were focused on the gasifier turbine rotor and turbine scroll fabrication using pressure slip casting techniques. Rotor configurations with 20 and 26 blades, respectively, as well as four turbine scrolls were fabricated and delivered to Allison for rig/engine test activities, demonstrating the feasibility of the process.

Component rig activities included the development of rigs and test procedures, as well as actual testing of ceramic components and assemblies. Rigs were developed and testing was performed on a rotor/shafting system rig, a hot gasifier rig, and a regenerator rig. The rotor/shafting system rig was capable of evaluating seals, bearings, rotor shaft dynamics, and lubrication systems, and acquired some steady-state and slow acceleration shaft dynamics data. The hot gasifier rigs were used to screen/proof test and evaluate structural ceramic components prior to introduction into the engine. The rigs were used to assess insulation degradation, and one was run during the past year with an exhaust bypass system. The rigs also accumulated test hours using ceramic components, including ceramic scrolls and ceramic rotors.

Test-bed engine fabrication, testing, and development activities supported improvements in ceramic component technology that permit the achievement of both program performance and durability goals. More than 40 gasifier and engine builds were supported in the past year, including a 100-hour engine durability test on a new regenerator seal system, engine insulation exhaust emissions test work, and test-bed vehicle installation preparation. Total test time in 1992 is shown in Table I.

*Table I.*
*Total test hours.*

| | Pre-1992 | 1992 | Cumulative |
|---|---|---|---|
| Engine test hours | 1720 | 147 | 1867 |
| Hot rig test hours | 1571 | 452 | 2023 |
| Total hours | 3291 | 599 | 3890 |

# INTRODUCTION

This is the fifth of a series of annual reports documenting work performed on the ATTAP. This work is being conducted by a team directed by GM, with significant activities underway at GM's Allison Gas Turbine Division (which serves as prime contractor), at GM's AES located at the General Motors Technical Center, and at the several domestic ceramic suppliers who are under development subcontracts. The U.S. Department of Energy (DOE) sponsors this work, which is managed and technically directed by NASA-Lewis Research Center under contract DEN3-336.

## GOAL AND OBJECTIVES

ATTAP is intended to advance the technological readiness of an automotive ceramic gas turbine engine. Specifically, ATTAP aims to develop and demonstrate the technology of structural ceramics that have the potential for competitive automotive engine life cycle cost and for operating for 3500 hr (automotive engine life) in a turbine engine environment at temperatures up to 1371°C (2500°F). Project objectives are the following:

- Enhance the development of analytical tools for ceramic component design using the evolving ceramic properties data base
- Establish improved processes for fabricating advanced ceramic components
- Develop improved procedures for testing ceramic components
- Evaluate ceramic component reliability and durability in an engine environment

## PROGRAM SCHEDULE AND CONTENT

Figure 1 shows the scheduled activities in the 61-month program. Materials assessment occurred at the initiation of ATTAP and resulted in the targeting of ceramic component technology goals and the identification of materials, processes, and manufacturers to address those goals. The materials assessment was updated in Year 3 and in Year 5, at which time the state of the art was reassessed for each component and required technology improvements were

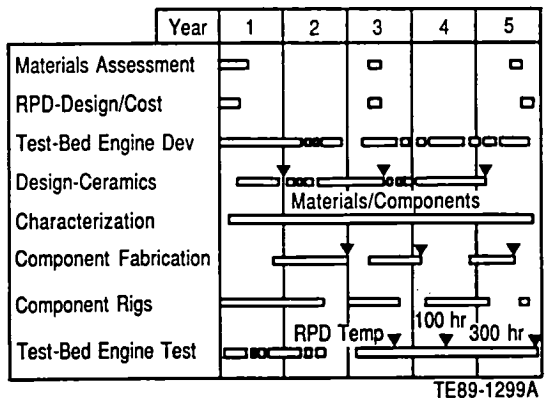


*Figure 1. ATTAP schedule.*

of materials, processes, and manufacturers are ongoing, continuous activities in ATTAP, and promising candidates are integrated into the program as merited. Similarly, those technologies and/or ceramic component suppliers that do not productively evolve to address program goals are truncated from ATTAP.

RPD activities include the preliminary design of a powertrain system that could meet performance, cost, and reliability design goals. Such a design was executed at the beginning of ATTAP using a high temperature derivative of the AGT-5 automotive gas turbine engine. The RPD was updated in Year 3 to reflect current ceramic component technology and goals, and again in Year 5.

Test-bed engine development, shown in Figure 1 as an intermittent activity, includes those efforts aimed at ensuring the availability and functionality of the AGT-5 gas turbine engine as the test-bed for the high temperature ceramic components. Although engine development is not a primary focus of ATTAP, these activities recognize the need for continuing evolution of the engine to handle the power and thermal loads, as well as design changes resulting from the integration of a high temperature flow path.

Central to the logic of Allison's ATTAP approach is an iterative component development cycle. Three such cycles are shown in Figure 1 and include the design/fabrication/characterization/rigs/engine test sequences of activities.

These three development cycles reflect anticipated improvements in ceramic materials and the associated component processing technologies, and the incorporation of laboratory characterization data and rig/engine test results into succeeding designs. The initial design activity, shown with a milestone at the end of Year 1, features then-current monolithic ceramic technology in the design of the gasifier turbine stage of the AGT-5 engine for 1371°C (2500°F) turbine inlet temperature (TIT) plus other required hot flow-path pieces. The second design phase incorporated toughened monolithic materials, used in the same gasifier stage components. The third phase will incorporate advanced (e.g., from Oak Ridge's Ceramic Technology for Advanced Heat Engines [CTAHE] project) materials and processes as they become available. Additionally, the succeeding design phases include other necessary ceramic components in the high-temperature test-bed engine, notably power turbine flow-path pieces. Component fabrication includes those process development activities executed by ceramic suppliers that result in the fabrication of engine-usable components. Characterization involves those laboratory activities, both at suppliers and at Allison, that measure and define the various properties and qualities of ceramic materials in both test bar form and in components. Examples are microstructural evaluation and measurements of density, strength, oxidation resistance, toughness, etc. Included are the development and application of nondestructive evaluation (NDE) techniques.

Component rig activity includes the development of rigs for component verification and testing (e.g., hot gasifier turbine rigs) as well as the actual testing activities. Test-bed engine test includes those testing activities associated with test-bed engine development plus the verification and development testing of the ceramic components. Note that each of the three component development cycles begins with design, followed by component fabrication, characterization, then rig testing, and finally engine testing. This rigorous development process, shown in Figure 2, is iterative between the users and the ceramic supplier community and ensures developing an understanding of the behavior of components in service and the continuous identification of areas for improvement.

## TEST-BED ENGINE

Figure 3 shows the automotive gas turbine engine being used as the ceramic component development test-bed for the ATTAP. This GM-developed engine, the AGT-5, is a two-shaft, regenerative configuration with axial-flow gasifier and power turbines. The engine produces approximately 110 hp at its original full-power TIT of 1038°C (1900°F).

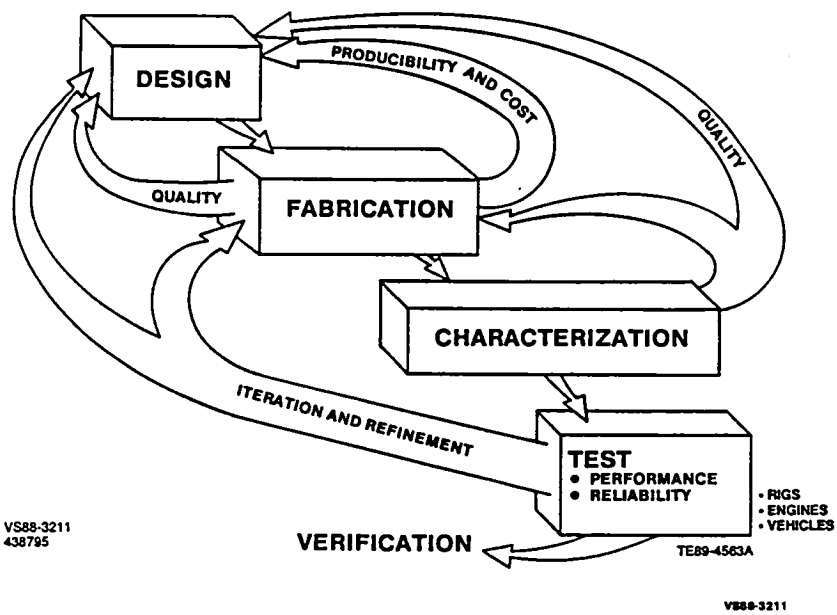


*Figure 2. Ceramic component development cycle.*

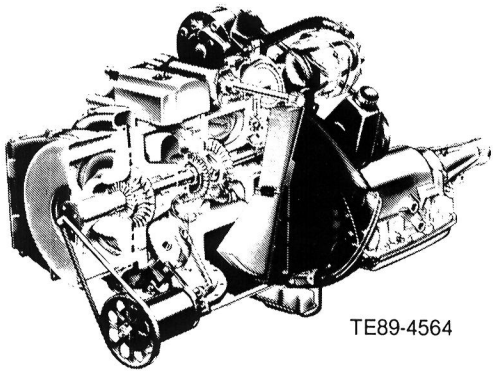


*Figure 3. ATTAP test-bed engine – AGT-5.*

The emissions and alternate fuels goals are considered achievable based on demonstrated GM experience. For example, the AGT100 (from the AGT project) engine's combustion system has displayed laboratory steady-state emissions of oxides of nitrogen ($NO_X$), CO, and unburned hydrocarbons (UHC) well within current Federal Emissions Standards using diesel fuel, jet fuel, and methanol. The AGT-5 engine has successfully run on dry powdered coal. Although such systems have demonstrated the potential for low emission/alternate fuel gas turbine combustion, much work remains to achieve a fully-functional system suitable for automotive application. Such efforts are outside the scope of ATTAP. The definition of power plant cost and reliability goals, in addition to performance, is included in ATTAP.

## CRITICAL COMPONENTS

Consistent with the strong ATTAP emphasis on ceramic component technology is the focus on specific gas turbine components as development/demonstration targets. Four ceramic components and the engine insulation have been identified as critical development components because (1) their functional success is critical to the viability of the ceramic automotive gas turbine engine; and (2) each requires some further technological development to be proven reliable and durable in the automotive engine environment, as well as cost effective. These critical elements, shown in Figure 4, are the following:

- gasifier turbine rotor
- gasifier turbine vanes

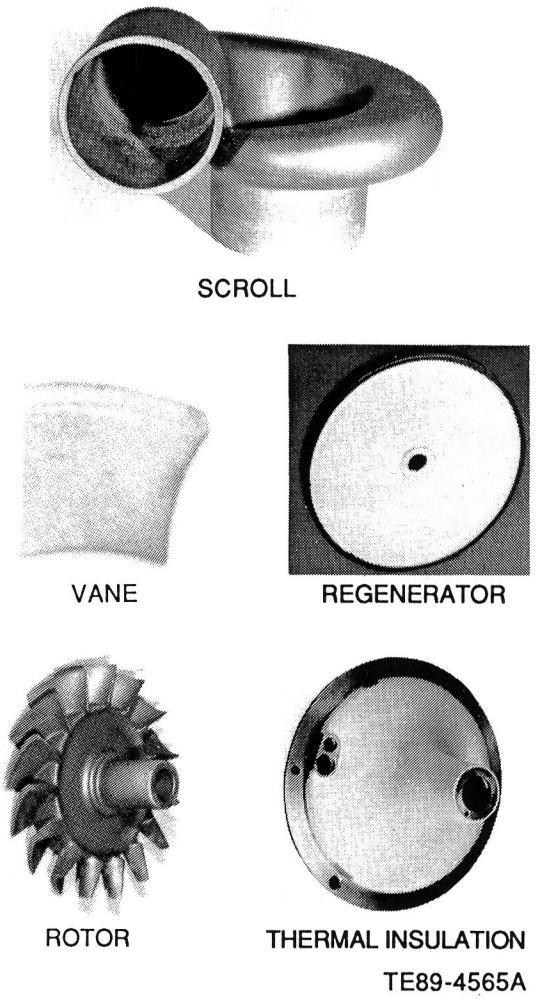


*Figure 4. Ceramic components selected for development.*

- gasifier turbine scroll
- regenerator disks
- thermal insulation

For each component, specific areas and parameters requiring improvement have been identified and quantified where possible.

# I. ENGINE/POWERTRAIN DESIGN AND DEVELOPMENT, ANALYSIS, AND MATERIALS ASSESSMENT

## 1.2 REFERENCE POWERTRAIN DESIGN (RPD)

A Reference Powertrain Design (RPD) was completed at the outset of ATTAP in order to ensure that the AGT-5 type power plant has the potential to fulfill the overall goals that underlie the DOE's sponsorship of automotive gas turbine technologies. This original RPD was a preliminary engineering design of a powertrain system that integrates with vehicle characteristics to provide a system with the potential for meeting not only performance, but also cost and reliability goals. Specific performance goals were originally set for the program as follows:

- 30% improvements in fuel economy over the reference 1988 Pontiac Grand Am equipped with a 2.5 liter, 4-cylinder, spark ignition engine over the combined Federal Driving Cycle
- competitive vehicle drivability and performance with the reference 1988 Grand Am
- gaseous emissions and particulate levels less than the following (based on diesel fuel No. 2):
  - NOx = 0.249 gm/km (0.4 gm/mile)
  - HC = 0.255 gm/km (0.41 gm/mile)
  - CO = 2.11 gm/km (3.4 gm/mile)
  - particulates = 0.129 gm/km (0.2 gm/mile)
- ability to use a variety of fuels

As the program progressed, the RPD was periodically updated to reflect the current state of the art in automotive turbine development. In addition, with the introduction of California ULEV automotive emissions standards to the industry, these standards were incorporated into the project as a further objective (see Section 1.4.2).

Since the inception of the ATTAP in late 1987, production spark-ignition automotive engines have continued to improve. In order to make the RPD comparable to current technology, this 1992 RPD study considers a current Grand Am as a new baseline reference.

Table 1-I shows the results of the most recent RPD performance simulation, based on the AGT-5 type engine, versus the new baseline reference vehicle.

The data show that the RPD gas turbine equivalent vehicle exceeds critical fuel economy and performance goals.

*Table 1-I.*
*1988-1992 baseline vehicle versus RPD.*

| Original RPD | 1988 spark-ignition piston powered Grand AM | RPD (turbine) |
|---|---|---|
| Urban mpg | 25.5 | 42.51 |
| Highway mpg | 40.7 | 57.87 |
| Composite mpg | 30.7 | 48.30 |
| 0-60 mph time (sec) | 13.5 | 13.10 |
| **1992 RPD revision** | **Baseline quad - OHC 1992 Grand AM** | **RPD (turbine)** |
| Urban mpg | 25.55 | 32.12 |
| Highway mpg | 39.70 | 45.56 |
| Composite mpg | 30.44 | 40.80 |
| 0-60 mph time (sec) | 12.20 | 12.20 |

## 1.4 TEST-BED ENGINE DESIGN AND DEVELOPMENT

### 1.4.1 Mechanical

Development efforts are required to ensure that the test-bed engine(s) can accept the improved ceramic components and operate at the 1371°C (2500°F) TIT conditions of the reference powertrain design (RPD). Specific design/development activities include the metal power turbine static structure for the 1371°C (2500°F) ceramic flow path, as well as the regenerator seal system.

#### Gasifier Housing - Objective/ Approach

One objective of engine mechanical design is to generate a polycarbonate model of the revised metal gasifier housing and associated insulation mandrel using a rapid prototype process. This approach validates the design of the static structure.

#### Accomplishments/Results

- A CAD (ANVIL 5000) 3-D surface model of the revised gasifier housing geometry and insulation mandrel was generated.
- The DeskTop Manufacturing (DTM) selective laser sintering (SLS) process was used to generate a full-size polycarbonate prototype of the revised gasifier housing and mandrel.
- The gasifier housing prototype was instrumental in identifying a required design modification. Identification of the design deficiency prevented the fabrication of defective hardware.
- The insulation mandrel prototype was subsequently utilized in insulation injection molding development while metal components were being fabricated.

#### Discussion

The AGT-5 metal gasifier housing (Figure 1-1) is a multifunction static structural component. The housing supports and supplies lubrication to the gasifier rotor bearings, provides a mount for the ceramic gasifier scroll and vane platform, and provides a mount for the gasifier shaft seal carriers. The geometry was redesigned in order to provide space for additional insulation thickness on the housing exterior (T3 cavity).

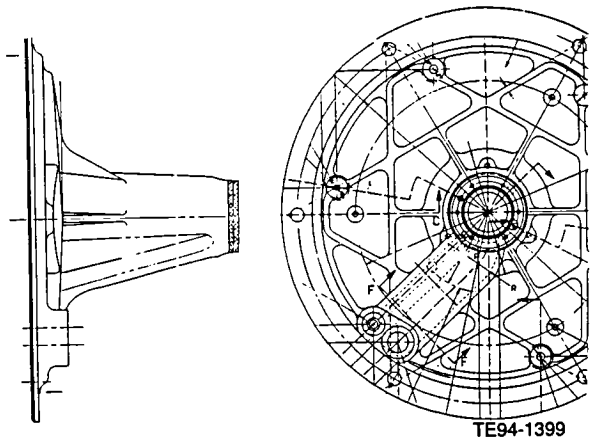


*Figure 1-1 AGT-5 metal gasifier housing.*

Due to the complex 3-D geometry, it was determined that DTM's SLS prototype process would be a cost effective method for design verification of the housing modifications and the associated insulation mandrel. The required 3-D surface models were generated on Allison's ANVIL 5000 CAD system. The CAD data bases were converted into .STL format files and submitted to DTM for prototype fabrication. Upon inspection of the gasifier housing polycarbonate model, it was discovered that a grinding wheel tool path had broken through the housing wall near the forward bearing oil drain (Figure 1-2). Generation of the prototype was therefore responsible for identifying the tool path error, which would have otherwise resulted in scrap metal hardware. A second polycarbonate housing was fabricated using an intermediate design modification that eliminated the tool path breakout by adding material to the casting exterior. Subsequent design reviews have led to a final housing geometry that incorporates a combination of material addition and re-definition of the compressor bearing support tool path.

A gasifier housing insulation mandrel is also required for the insulation injection molding effort. The cavity formed between the inner surface of this mandrel and the housing exterior defines the insulation envelope. Figure 1-3

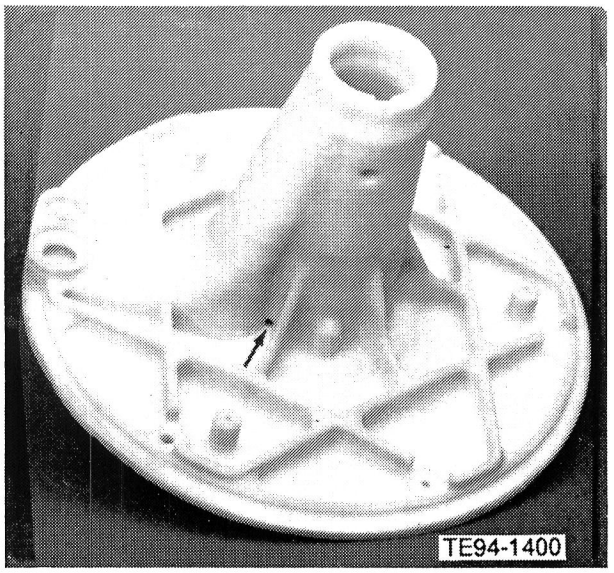


*Figure 1-2. Gasifier housing polycarbonate prototype (arrow shows tool path breakout area).*

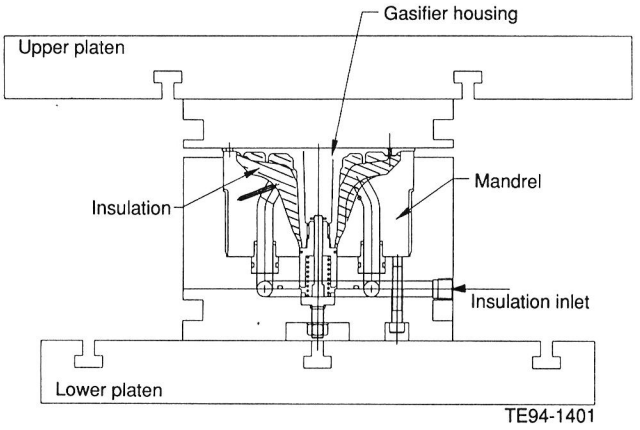


*Figure 1-3. Gasifier housing injection molding setup.*

illustrates one of the configurations for the gasifier housing injection molding setup. The polycarbonate insulation mandrel is shown in Figures 1-4 and 1-5. Schuller utilized the mold and housing polycarbonate prototypes for insulation injection molding development while metal housing and mold hardware were being fabricated.

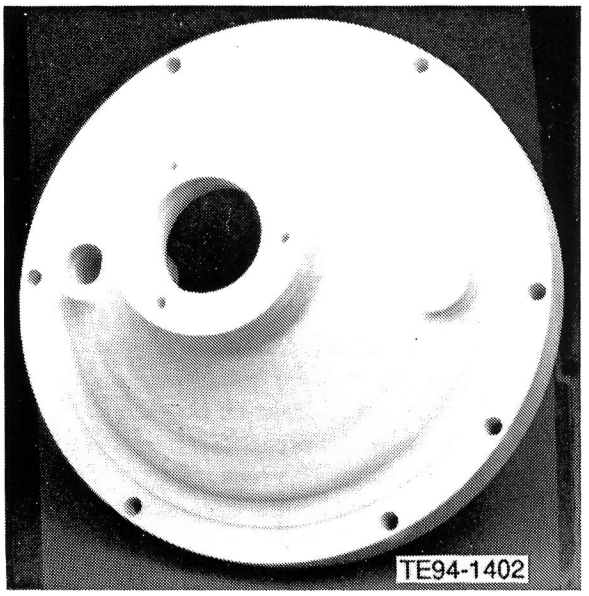


*Figure 1-4. Gasifier housing insulation mandrel polycarbonate prototype (aft surface).*

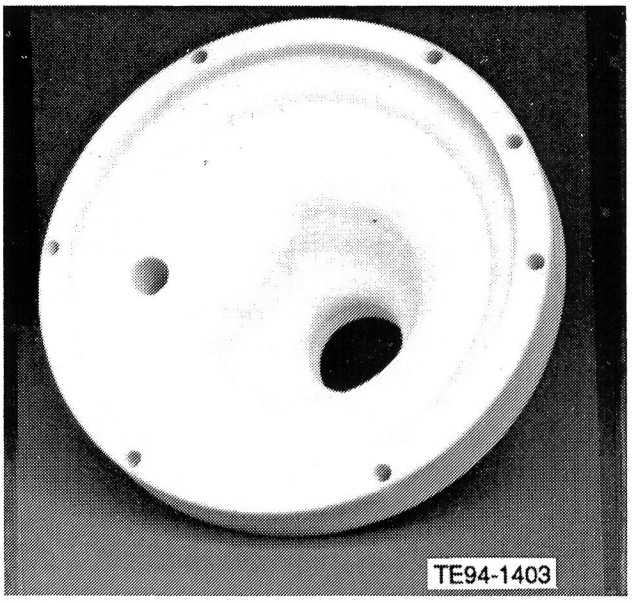


*Figure 1-5. Gasifier housing insulation mandrel polycarbonate prototype (forward surface).*

## Regenerator Seal System - Objective/Approach

Development of the materials and mechanism for the regenerator seal system is required to

ensure that the test-bed engine(s) can accept improved ceramic components and operate at the 1371°C (2500°F) TIT conditions of the RPD.

## Accomplishments/Results

- Analysis, detail design, and fabrication of L-seal regenerator seal system components was completed, including L-seals, wearface assemblies, engine housing and covers, and all accessory components.
- Two versions of a hot crossarm insulating insert were analyzed and tested. Initial cold flow testing of aluminum titanate (AT) inserts was successful, but a low-cost stainless steel design was selected for engine testing. Thermocouple data taken during full-engine testing showed the insert was successful in reducing the critical hot crossarm seal leaf thermal gradients.
- Accurate, low-cost L-seal fabrication techniques were developed.
- One-thousand hour L-seal cyclic durability flow fixture testing goals were exceeded.
- Full-engine assembly of S/N 15 (L-seal engine) and cold static regenerator leakage testing was completed, showing a 75% reduction in regenerator leakage.
- L-seal system durability was proof tested in engine S/N 15 with over 100 hr of cyclic durability, accelerations, and baseline running.
- Initial monolithic (HAYNES 230) hot crossarm regenerator seal wearface testing was conducted.
- Engine performance with L-seal system components showed improvements over prior configurations.

## Discussion

**Completion of L-Seal System Components.** Analysis, detail design, and fabrication of L-seal regenerator system components were completed, including all components required for full-engine testing of the L-seal system. These components included L-seal and wearface assemblies, engine housing and covers, as well as accessory parts. The design utilizes a thin metal L-shaped static seal first tried in the Chrysler-updated gas turbine shown in Figure 1-6. A straight seal crossarm was adopted for

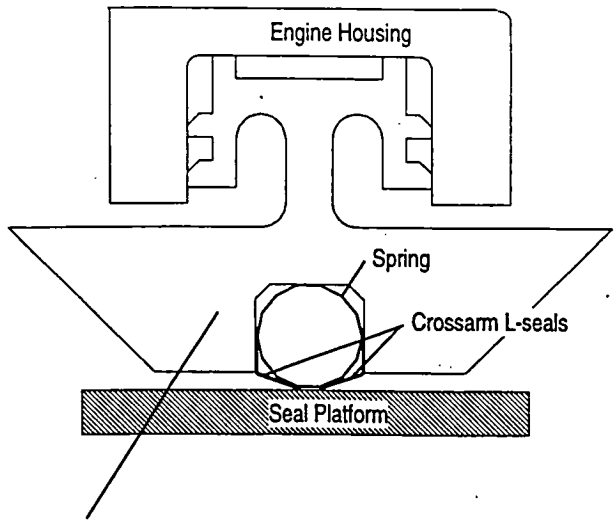


*Figure 1-6. Regenerator L-seal and insulator.*

simplicity. The L-seal system had 228 fewer parts than the previously used platform-leaf seal system (an 87% reduction), eliminating many difficult and expensive manufacturing and assembly steps. Modeling and analysis of the L-seal system has predicted full survivability and long-term durability of the seal system under full 1371°C (2500°F) TIT ceramic gas turbine engine conditions.

**Development of the Hot Crossarm Insulating Insert.** The previous seal had experienced thermal distortion and cracking of its thin metal sealing leaf. Analysis had attributed this to excessive thermal gradient across its width. One edge contacts the hot seal crossarm wearface, while the other contacts the cooler engine bulkhead. An insert or cap for the engine bulkhead was conceived to insulate the L-seal, and provide a lower thermal gradient. After the initial development of an AT ceramic insulating insert, an alternative low-cost stainless steel insulating insert was analyzed and designed. It was successfully installed and cyclic pressure tested, but despite the initial testing success, it was abandoned for the simpler, lower cost stainless steel. Long-term manufacturing costs for the ceramic insert appeared prohibitive compared to the costs associated with stainless steel.

Iterative two-dimensional (2-D) finite element heat transfer analysis was used on several low-cost insert designs to configure the shape of a

stainless steel insert to minimize heat transfer, utilizing a lengthened heat transfer path and minimized contact resistance. The finite element model of the selected stainless steel insert design demonstrated a maximum leaf temperature gradient of 245°C (473°F). This was within the original goal of 260°C (500°F) leaf maximum thermal gradient, meriting further testing and consideration.

Following the successful analytical design effort, the low-cost stainless steel insulating insert for the hot crossarm section of the engine was fabricated and installed in turbine engine housing S/N 15. Inserts were welded into an existing engine housing and regenerator covers to provide matching sealing surfaces for initial tests. While designed for extrusion in production quantities, the two engine test inserts were machined using conventional tooling. Discussions with several extrusion houses have indicated that the design is acceptable for low-cost/high-volume extrusion. After machining, the inserts were press fit into the hot crossarm region of S/N 15, readying the housing for full-engine assembly.

The insulating performance of the hot crossarm insulating insert is critical to the high-temperature survivability of the regenerator seal leafs at 1371°C (2500°F) TIT operation. Instrumentation was installed on the right-hand-side hot-crossarm insulating insert of S/N 15, which allowed for empirical evaluation of the insert system during actual engine operation. Thermocouple data taken while running engine S/N 15 indicated that the insert was holding a 200°C (392°F) thermal gradient between the leaf contact area and the engine housing. This insulating characteristic was sufficient to prevent any thermal distortion of the hot crossarm L-seal leafs. Post durability inspection of the hot crossarm L-seal leafs showed little thermal discoloration of the leafs, indicating a low maximum leaf temperature. This also indicates that the leakage of the P2/T2 air down the center channel of the hot crossarm insert is sufficient to provide substantial cooling of the seal leafs.

**L-Seal Fabrication Technique.** Through collaboration with General Motors' Advanced Manufacturing Engineering (AME) and General Motors' Parts Fabrication (GMPF) groups, a low-cost, highly accurate fabrication technique for L-seals was developed. The technique replaces the costly, inaccurate stamping method previously used to fabricate the seals.

The new L-seal fabrication process is a highly repeatable technique that produces L-seal leafs free of surface defects and with almost zero scrap. Inspection of these seals revealed that the standard deviation of critical seal dimensions part-to-part was less than 1.0% of the nominal dimension, which is well within acceptable repeatability for dimensional variance.

**L-Seal Cold Cyclic Durability Testing.** The goal of 1000 hr of cold cyclic durability testing of the L-seal system was met and exceeded during 1992. The durability L-seals were run to over 1600 hr without distress. At that point, the test was stopped due to other needs for the flow fixture hardware. Flow fixture leakage measurements showed continuous improvement of L-seal sealing performance with operating time. Estimated total engine seal leaf leakage was found to have decreased an additional 30% from leakage values measured at 100 hr of durability running. After over 1600 hr of durability running, no degradation of the seals or groove interfaces had occurred.

**Full-Engine Assembly and Baseline Testing of Engine S/N 15.** Assembly of automotive gas turbine engine S/N 15 was completed utilizing a full set of L-seal type regenerator seals and standard metal turbomachinery. Prior to hot running, a cold static leakage test was performed on the complete engine, which showed up to a 75% reduction in leakage over the old seal system. This test also verified a new leaf retaining method, which has been designed for low cost and ease of manufacturing and assembly.

Following engine assembly and leak check, S/N 15 was installed in dynamometer test cell 19. On October 29, 1992, engine S/N 15 was started for the first time. A baseline power run of L-seal engine S/N 15 was performed to test the engine and seal system performance. Low cold static leakage numbers measured on S/N 15 prior to running predicted good power and cooler TIT running for the engine. This was found to be the case, as S/N 15 produced equal power as

S/N 4 with the same power turbine turbomachinery, while running an average of 75°C (167°F) TIT cooler. This improvement can be attributed to the significantly reduced regenerator seal leakage due to the L-seal system.

**Proof-Tested L-Seal System Durability.** In order to determine the long-term durability potential of the L-seal system, engine S/N 15 was run for over 100 hr. The L-seal system was found to be in excellent condition following the 100.7 hr of running, with 5.6 hr of steady-state running, 21.3 hr on a 16 sec/48 sec (100% N1/idle) step acceleration schedule, and 73.3 hr on a modified ATTAP durability schedule.

During the 100-hr test, the various new component designs of the L-seal system were evaluated. Both hot and cold wear surfaces showed excellent regenerator wear patterns, indicating proper wear face pressure balance and good wear face positioning and retaining. The seals looked excellent, showing no signs of thermal or mechanical distress after 100 hr. No degradation of L-seal sealing capability occurred during testing. Cold static leakage tests before, during, and after the 100-hr test showed consistently low leakage values. The L-seal system performance showed the same beneficial "break-in" characteristics as seen in cold rig testing – TIT decreased 30°C (86°F) as the seals were run over the 100 hr of testing. The press-fit hot crossarm insulating insert showed no signs of thermal distress, mechanical deformation, or dislocation. The plugged hub regenerator cores showed no thermal or mechanical distress, and the graphite regenerator core bushings appeared to be sufficiently protected from the T6 temperatures. The supporting components such as clips, pins, and locators all worked as designed. During testing, no problems were observed with the seal system assembly, seal and wear face location during running, or component durability.

Using P5 total pressure and engine run data for S/N 15 BU 01, it was determined that the increased turbine mass flow due to low regenerator leakage was causing the gasifier rotor to choke at too low a gasifier speed, leading to losses in engine efficiency as well as gasifier/power turbine turbomachinery mismatch. It was determined that a larger gasifier rotor and shroud would be beneficial to both power and economy of the engine. The recommended shroud and rotor combination is slated to be built as gasifier assembly 'N' for use as BU 02 for S/N 15.

**Initial Monolithic Hot Crossarm Wear Face Test.** Collaborative efforts between GM Advanced Engineering and Argonne National Laboratories/Wear Sciences, Inc. have led to investigation of monolithic hot crossarm wear face materials to replace the expensive plasma-sprayed system currently used. In preliminary discussions with Wear Sciences, Inc., two standard off-the-shelf materials were identified for testing as monolithic wear face materials – Haynes alloy 230 and Inconel X750. The intent was that a hot crossarm wear face made of those materials, subjected to the 1800°F (982°C) exhaust of a ceramic engine would provide a self-replenishing layer of lubricious surface oxides, sufficient to support long-term operation in an automotive gas turbine.

A preliminary testing program was pursued for testing of the two identified materials. Two existing high-temperature friction and wear test rigs were brought back on line. Current vibration problems with the rigs are being addressed. When fully operational, the rigs will give quantitative friction and wear data for ceramic disk/monolithic wear face sliding contacts, at temperatures up to 982°C (1800°F). Monolithic hot crossarm components in AGT-5 sizes were also fabricated from Haynes 230. Parts were made for both platform-leaf and L-seal AGT-5 engines. Engine testing of these components allows qualitative evaluation of viability of the monolithic wear face system under actual engine conditions.

The L-seal engine monolithic hot crossarm wear face (Haynes 230) was run in engine S/N 15 for one hour on ATTAP durability. Prior to running, the wear face was preoxidized in a standard-atmosphere oven at 982°C (1800°F) for two hours, producing a deep green lubricious nickel oxide coating. The system ran acceptably in the engine. An intermittent audible squeak coming from the monolithic wear face was noted, which progressively increased during the one hour test to an almost constant squeak. The one hour inspection at the conclusion of the test revealed that the preoxidized nickel oxide coat-

ing had been worn away without replenishing, leaving a bare, polished metal wear surface. However, no damage or excessive wear to the ceramic (alumino silicate) regenerator disk was seen.

In post test discussions with Wear Sciences Inc. personnel, it was determined that the cool metal flow-path engine temperatures of S/N 15 were insufficient to promote lubricious oxide formation on the Haynes 230 material. For this metal engine, operating in the 649-760°C (1200-1400°F) range was inadequate to replenish the oxide. It is believed, however, that ceramic flow-path engine temperatures will be sufficient to produce lubricious oxides. It is valuable to note that no damage to the seal system or regenerator occurred even when the lubricious oxide layer was completely worn away, which is the "worst case" operational condition. This means that time may be allowed for an initial lubricious layer to form during engine operation without damage to the regenerator system. Further data are needed to determine the minimum temperatures for oxidation layer formation as well as the rate of oxide formation needed to attain a self-replenishing layer.

## 1.4.2 Combustion Systems

### Objective/Approach

The objective of the combustion system development effort is to meet 1997 California ULEV automotive emissions standards (0.2 gm/mi NOx, 1.7 gm/mi CO, 0.04 gm/mi HC) on diesel fuel. A prevaporizing/premixing combustor will be required to achieve this goal. The objective must be met without exhaust gas aftertreatment, i.e. no catalytic converter, and while maintaining carbon-free operation for the protection of ceramic turbine components. Other requirements for the low emissions combustor include fuel flexibility, combustion stability, cold start capability, driveability, and reliability.

### Accomplishments/Results

- A four-year low emissions combustor development program was initiated.
- The first low emissions combustor design concept was completed and parts were ordered.
- Screening tests of fuel nozzles for the initial design concept were completed.
- Preliminary sizing for the second design concept was completed.

### Discussion

The low emissions combustor development program for the automotive gas turbine is a planned four-year effort beginning in 1992. Three low emissions combustor concepts will be evaluated during the first three years with the best concept selected for design optimization and emissions validation in 1995. The first concept, called the poppet valve combustor, uses a translating valve to control primary zone airflow. The second concept, the sliding pad combustor, is a derivative of the AGT100 combustor developed under an earlier DOE/NASA contract, DEN 3-168. Airflow distribution is controlled by pads that slide on the outside surface of the combustor to cover and uncover openings in both the primary and dilution zones. The third concept is a two-stage combustor in which fuel staging is substituted for variable geometry.

There is no combustor rig for this program; all testing will be performed in AGT-5 engines. As part of the continuing development program, combustor development will take place on an engine dynamometer and emissions validation in a vehicle on a chassis dynamometer. Initial testing will be conducted in engines with metal hot sections with subsequent proof of high temperature operation in ceramic engines. Metal engines are sufficient for operating over the EPA emissions driving cycle.

The final design of the poppet valve combustor is shown in Figure 1-7. Air enters the combustor through two paths. One path is an annular passage between the combustor inner and outer liners that provides for convective cooling of the inner liner. This path leads to the fuel preparation zone where fuel is sprayed into the air by the main nozzle; evaporation of fuel and mixing of fuel and air take place in this region. The mixture then passes around the poppet valve and enters the reaction zone, where

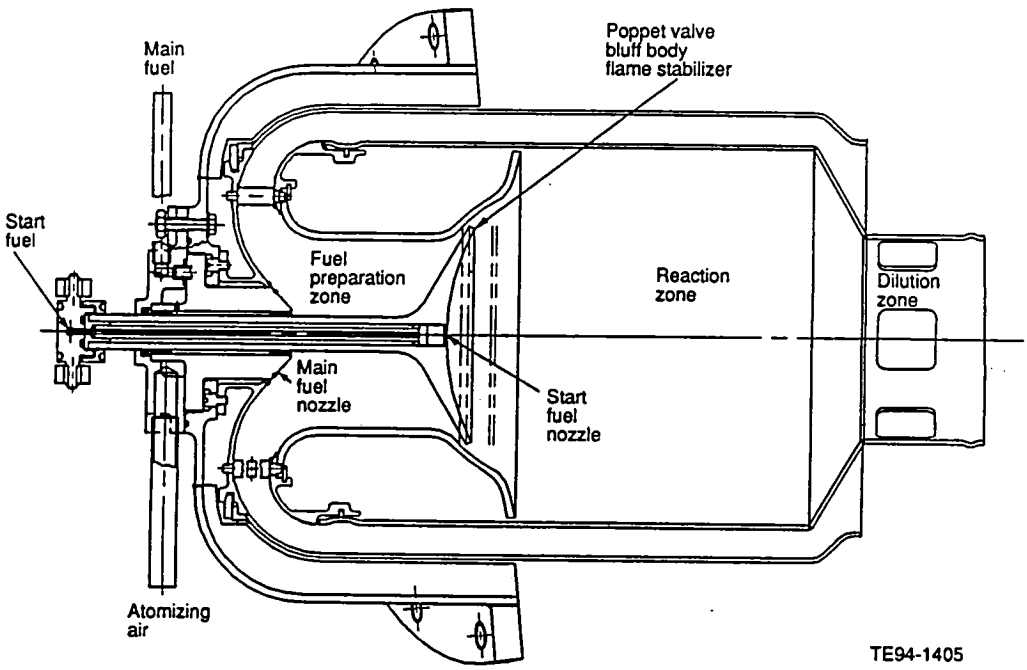


*Figure 1-7. Poppet valve premixing low emissions combustor final design.*

combustion takes place. Recirculation of combustion products downstream of the valve stabilizes the flame. Hot combustion products then pass through the dilution zone before exiting the combustor. Air can alternatively take the second path, entering the dilution zone directly through holes in the combustor inner liner and bypassing the fuel preparation and reaction zones.

Axial movement of the poppet valve regulates the open area between the valve and valve seat controlling the flow of air to the reaction zone. Fuel/air ratio and flame temperature in the reaction zone are controlled in this manner. Light-off is accomplished by a start nozzle positioned on the axis of the valve. The combustor operates in the diffusion flame mode until the engine reaches idle speed, at which time fuel is transferred from the start to the main nozzle. After transfer, the start nozzle is purged with air that continues to flow during operation at temperature for cooling. The start nozzle is a pressure atomizer, whereas the main nozzle is a continuous air assist atomizer.

The poppet valve combustor went through various design changes in 1992 before reaching the configuration shown in Figure 1-7. Initially, the parts exposed to hot combustion gases, the inner liner, valve, and valve seat, were to be fabricated from an oxide dispersion strengthed (ODS) high temperature alloy. A steady-state finite element heat transfer and stress analysis of the metal valve was performed at the maximum power operating condition to determine the benefits of cooling the valve head by flowing air between the head and a heat shield. Both cooled and uncooled cases were investigated. Predicted temperatures and stresses for the cooled case are shown in Figure 1-8. The results indicated a very steep thermal gradient in the heat shield leading to unacceptably high stresses. In the uncooled case, Figure 1-9, absolute temperatures were higher but gradients and thermally induced stresses were extremely low. With ODS material, the uncooled design met the life criterion of 100 hours at maximum power steady-state conditions, and therefore, the uncooled design was adopted.

Further analysis led to a decision to modify the combustor design so the valve and valve seat could be made of ceramic materials and the inner liner made of Haynes 230. These changes were significant enough to warrant additional heat transfer and stress analysis.

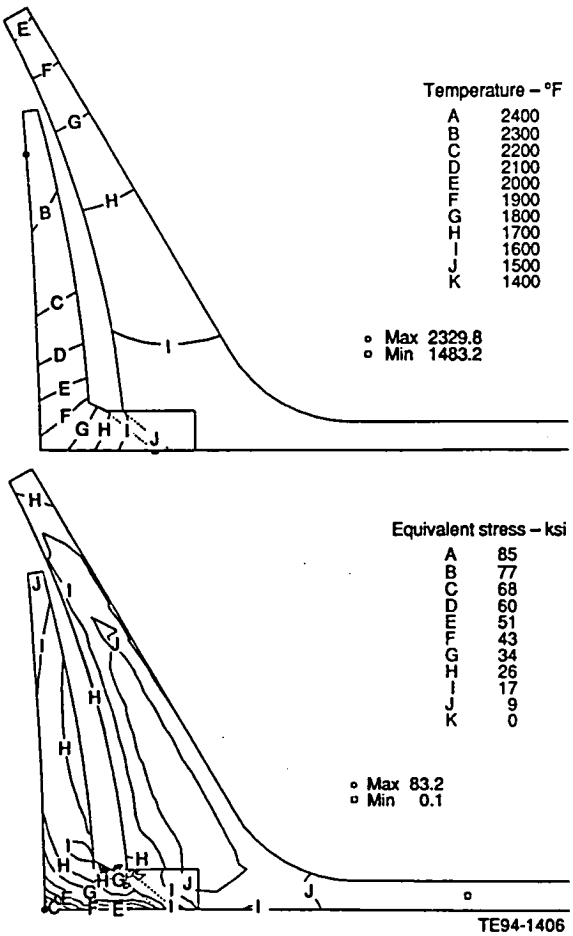


*Figure 1-8. Predicted temperatures and stresses for air-cooled poppet valve head, maximum power design point.*

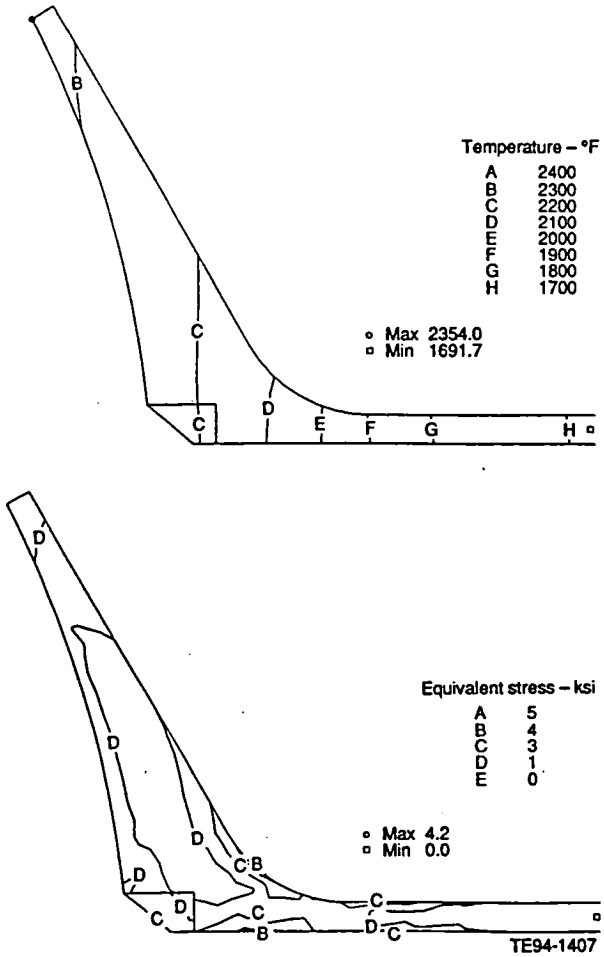


*Figure 1-9. Predicted temperatures and stresses for uncooled poppet valve head, maximum power design point.*

A 2-D axisymmetric finite element model of the entire combustor and supporting structure was generated to calculate temperatures and stresses. Figure 1-10 shows the finite element mesh and the computer aided design (CAD) drawing from which the mesh was made. Fuel spray on the ceramic valve seat was modeled in the analysis. The heat transfer boundary conditions were calculated for steady-state maximum power for a metal engine operating over the emissions driving cycle. These boundary conditions were used in generating a cold start transient.

The predicted temperatures and stresses for the ceramic valve and valve seat indicated no need for further modification of these parts. Calculated steady-state and worst case transient temperatures and stresses for the Norton NT230 siliconized silicon carbide valve seat are shown in Figures 1-11 and 1-12. The maximum temperature of the seat is high (143°C [2600°F]) under steady-state conditions, but the stress in this region remains low so the probability of survival (POS) remains high. For the Norton NT154 silicon nitride valve, the worst case temperature and stress occur under steady-state conditions. Plots shown in Figure 1-13 indicate that the temperatures and stresses are relatively low in the valve resulting in a high POS.

Predicted temperatures for the exit region of the HA230 combustor inner liner are shown in Figure 1-14. Temperatures were excessive in the initial configuration, which was run without back side convective cooling. The addition of back side cooling reduces the peak temperature by 201°C (362°F). Based on this analysis, the combustor outer liner was extended to cover the

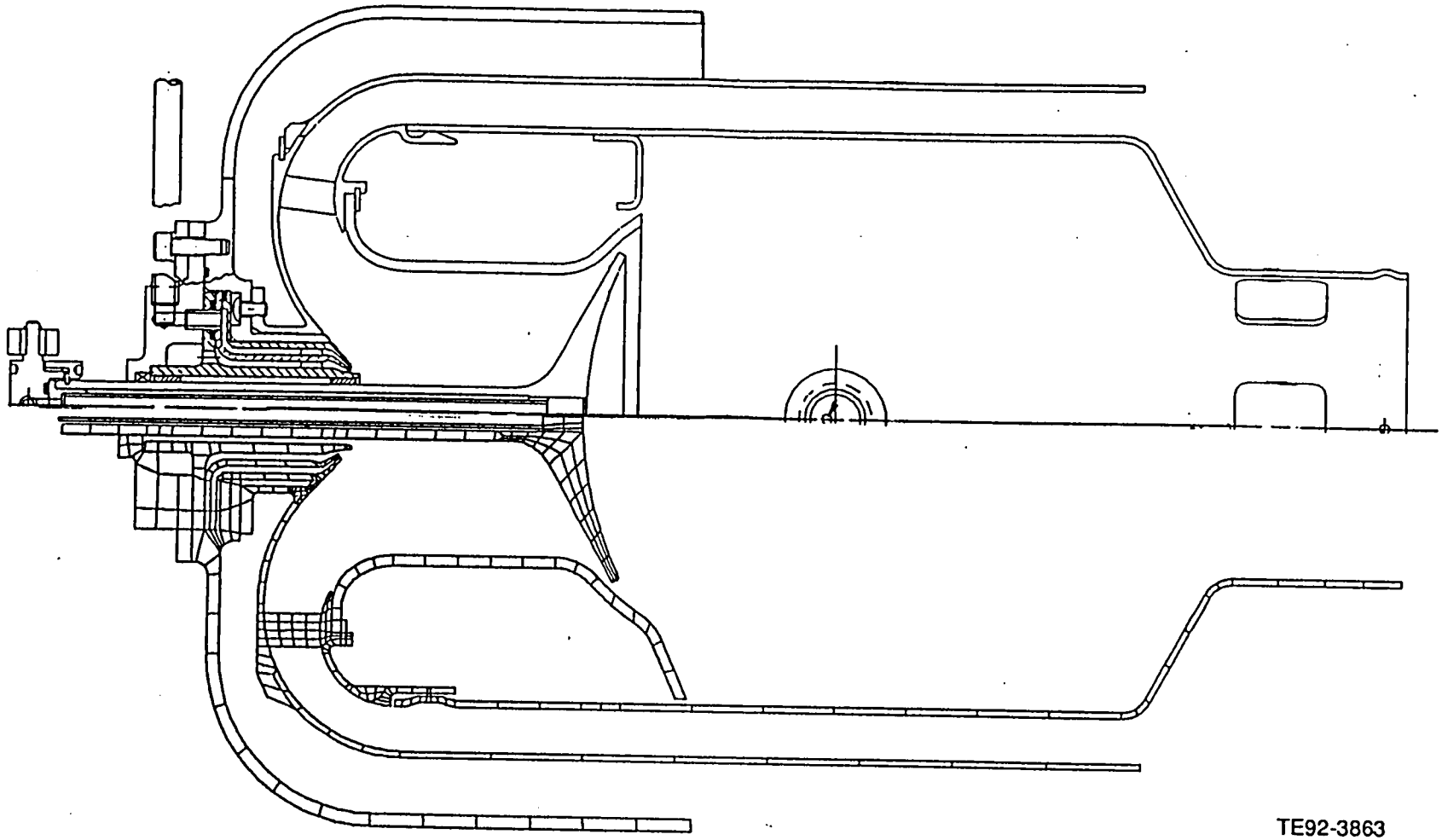


Figure 1-10. Finite element mesh and layout drawing of poppet valve combustor.

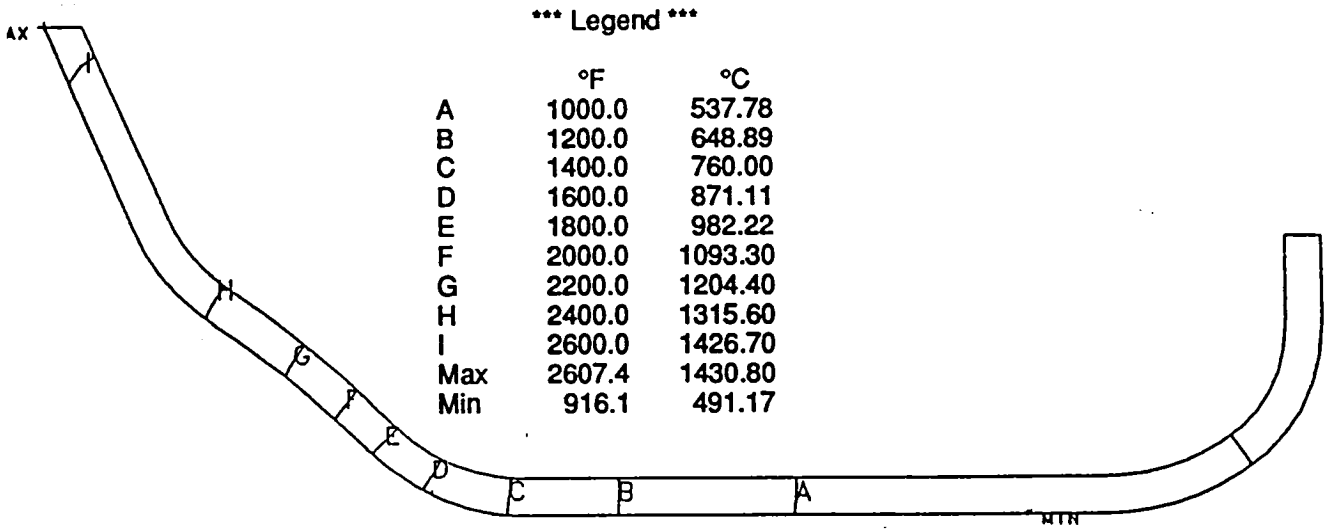


Temperature

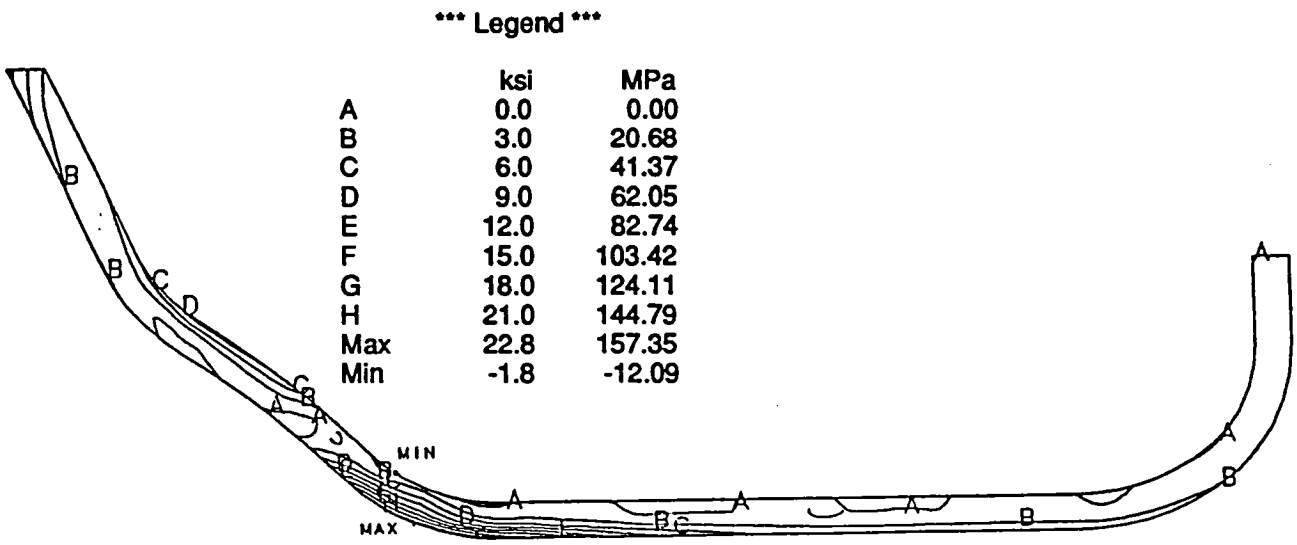


Stress

Probability of survival = 0.9978

TE92-3864

*Figure 1-11. Temperature and maximum principal stress distributions for NT230 valve seat under steady-state conditions.*

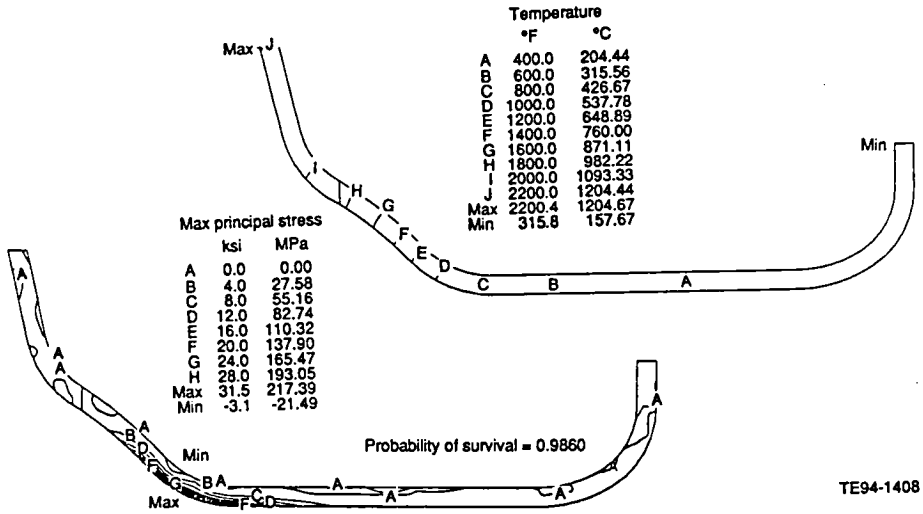


*Figure 1-12. Temperature and maximum principal stress distributions for NT230 valve seat under worst case transient conditions after 42 seconds.*

exit region of the inner liner, forcing the necessary external convection. Other changes not included in this analysis were made to further reduce metal temperatures in the region.

Predicted temperatures for the cast Stellite 31 dome region of the combustor are shown in Figure 1-15 with the corresponding deflected shape plot. Initially, the dome mount flange design was a solid ring, but high stresses resulted from the thermal gradient along the flange. Figure 1-16 shows the stress distribution for the original and modified configuration of the dome mount flange. The continuous flange was broken into six tabs that are allowed to slide at the mounting point to relieve thermal stress. Initially, the dome was a single-piece casting with three support struts joining two rings, but a high cross corner stress resulted in the struts. Figure 1-17 shows the stress distribution for the original single-piece casting as well as the modified two-piece casting with the struts free on one end. By allowing the two rings to move independently, the cross corner stress is eliminated. Also, the joint between the dome and the combustor inner liner was changed from a spherical seat to a piston ring to reduce the chance of binding. Figure 1-18 compares the initial and modified casting designs. During the transient, the stress levels in the two-piece dome exceeded the yield strength of Stellite 31 so the material was changed to IN713 for its higher strength.

Screening tests of prototype fuel nozzles for the poppet valve combustor were conducted by the fuel nozzle supplier. The main fuel nozzle must produce an annular spray since the shaft of the poppet valve passes through the center of the nozzle. Two concepts were tested, one with a full annular exit slot, the other with a ring of discrete holes. The discrete hole design yielded a more uniform circumferential spray pattern, so this design was adopted. A uniform spray distribution is required to obtain a uniform fuel/air distribution in the combustor fuel preparation zone. The design objective is a circumferential deviation in fuel flow from minimum to maximum of no greater than 15%. The initial prototype met this objective at high fuel flows, but not at low flows. To remedy this situation, an internal restrictor was added in the fuel circuit to more evenly distribute fuel. Figure 1-19 shows the poppet valve combustor main fuel nozzle spraying into the atmosphere at the maximum power steady-state operating condition.

All poppet valve combustor parts had been received or were on order at the end of 1992. The second low emissions combustor concept, the sliding pad combustor, was through the preliminary sizing stage by the end of 1992.

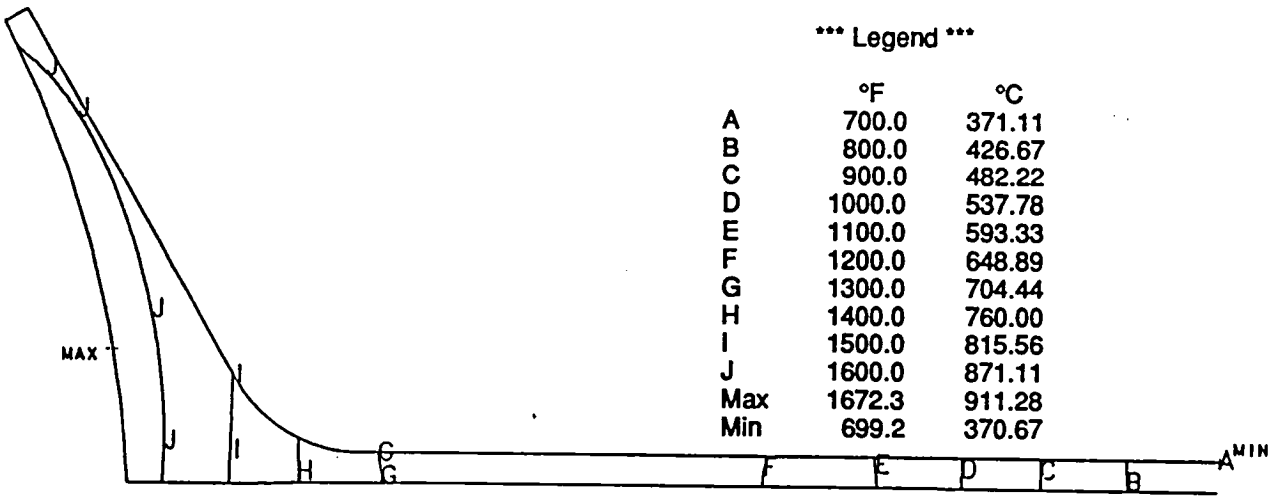


Temperature

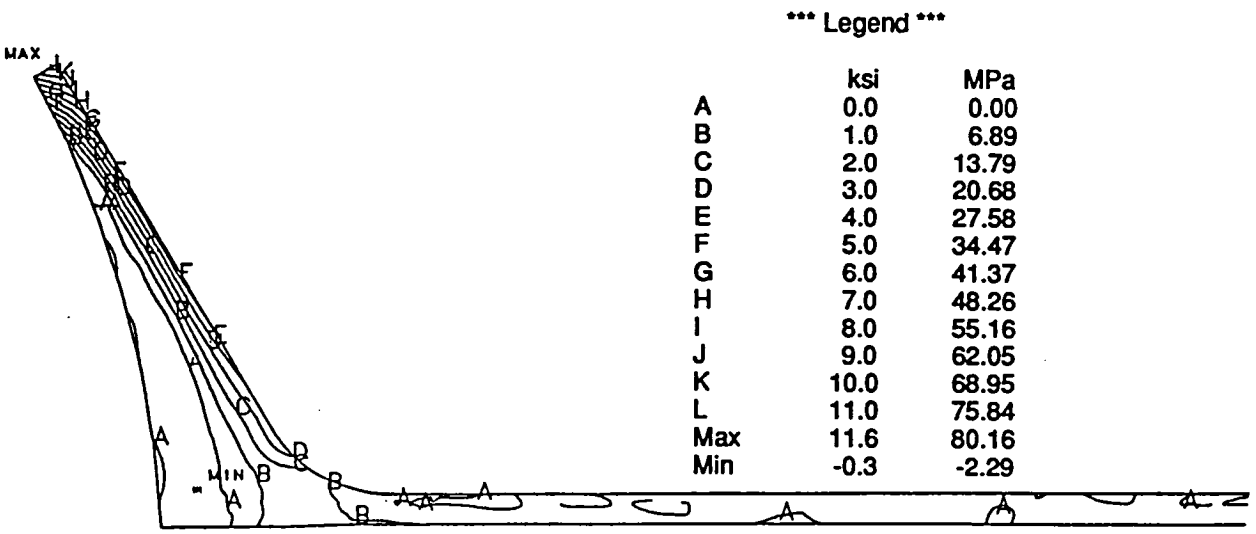


Stress

Probability of survival = 0.9978

TE92-3865

*Figure 1-13. Temperature and maximum principal stress distributions for NT154 valve under steady-state conditions.*

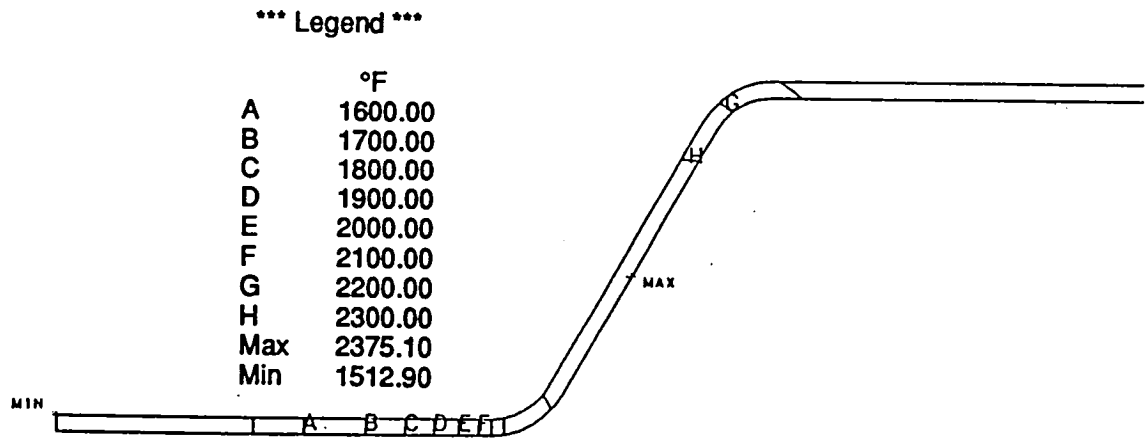


Without back side cooling

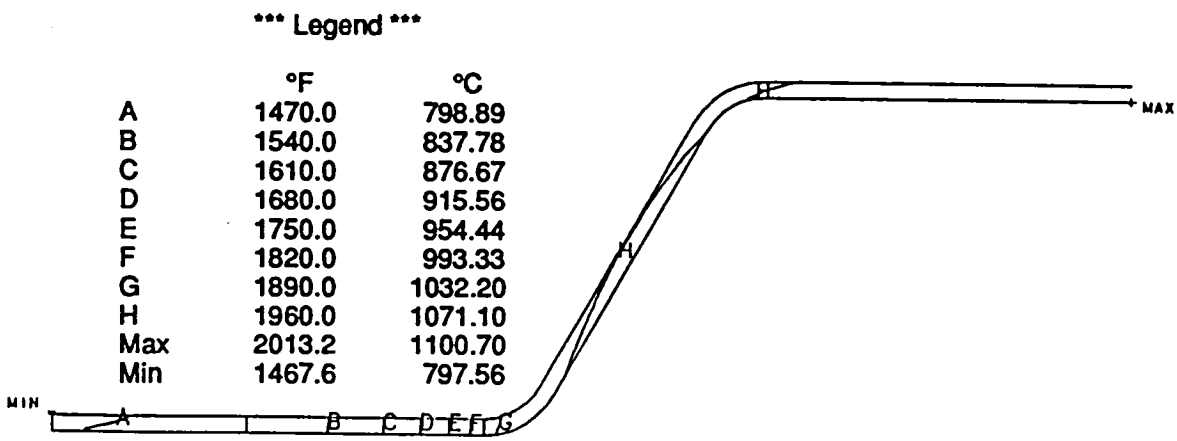


With back side cooling

TE92-3867

*Figure 1-14. Temperature distributions for the inner liner transition section under steady-state conditions with and without backside cooling.*

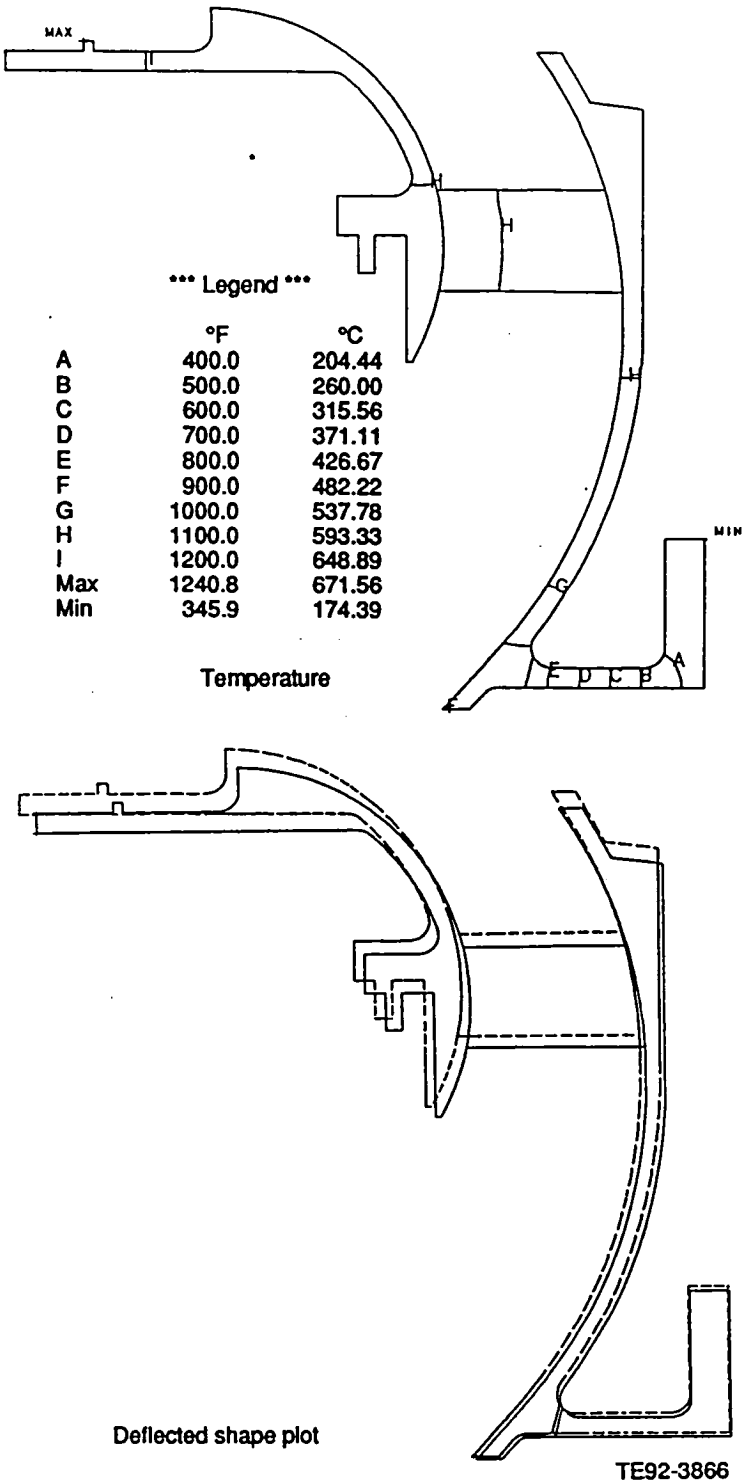


*Figure 1-15. Temperature and deflected shape plots for cast poppet valve combustor dome under steady-state conditions.*

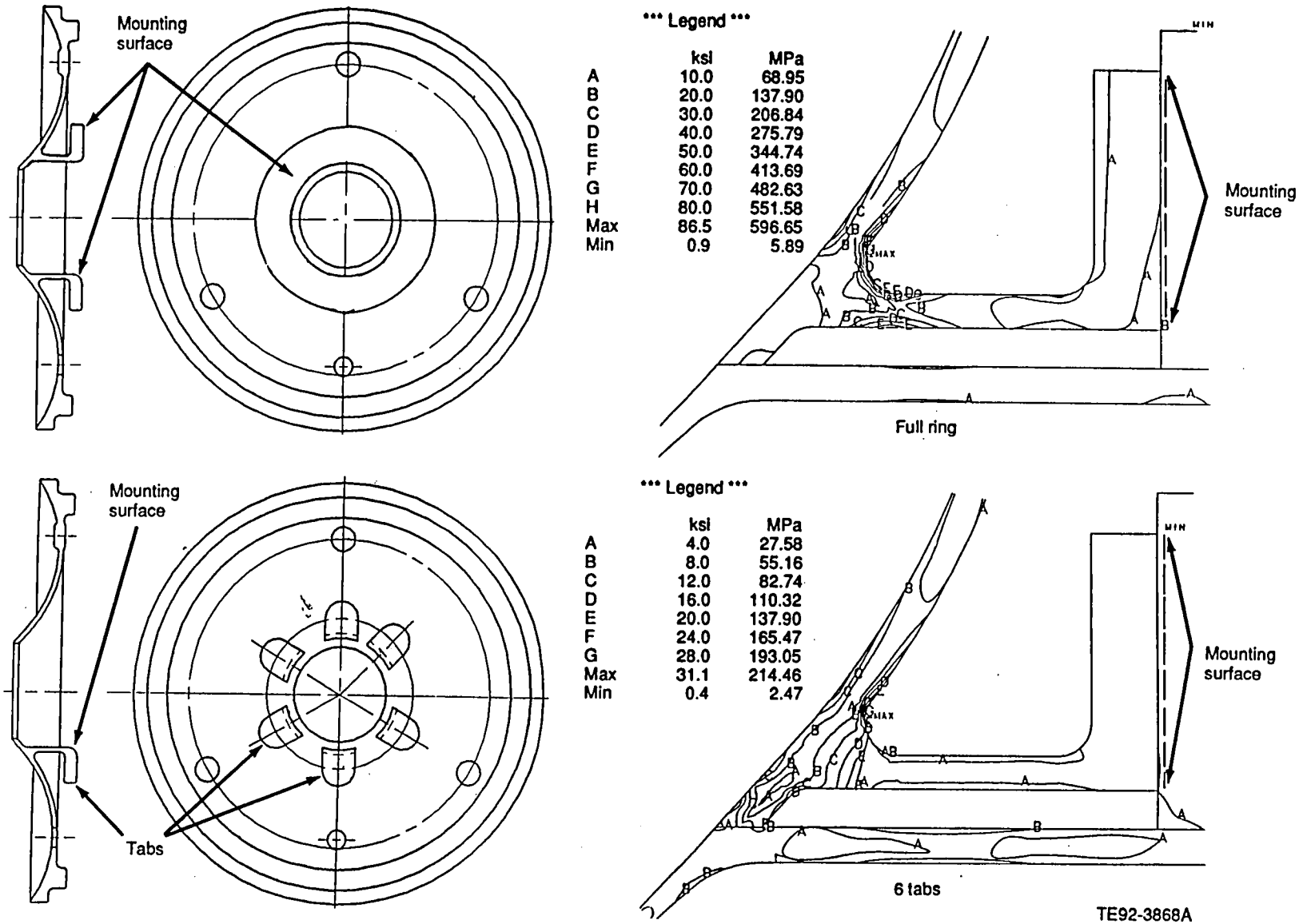


*Figure 1-16. Maximum principal stress distributions for initial and modified dome mount flange configurations under steady-state conditions.*

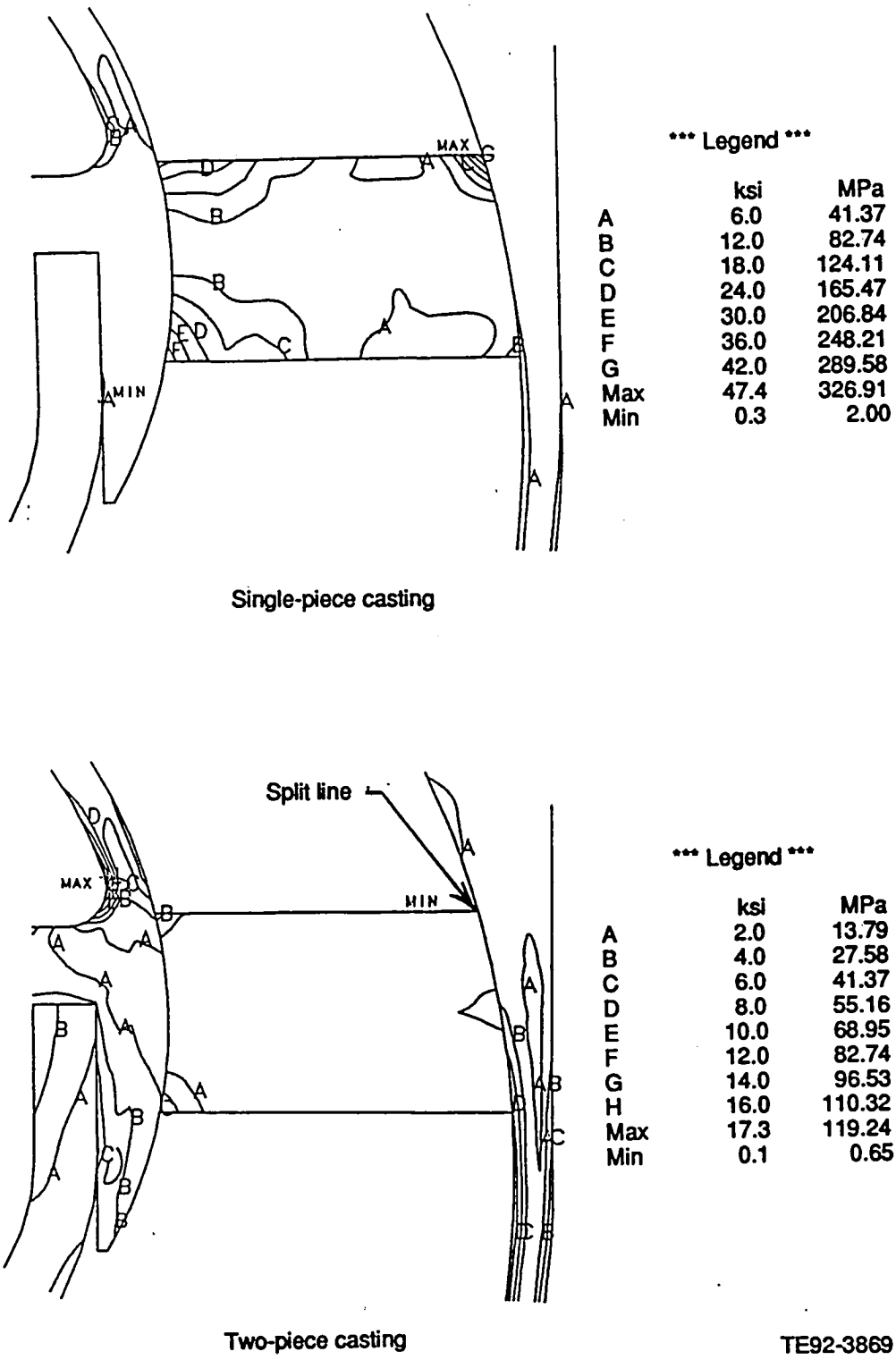


*Figure 1-17. Maximum principal stress distributions for initial and modified dome support strut configurations under steady-state conditions.*

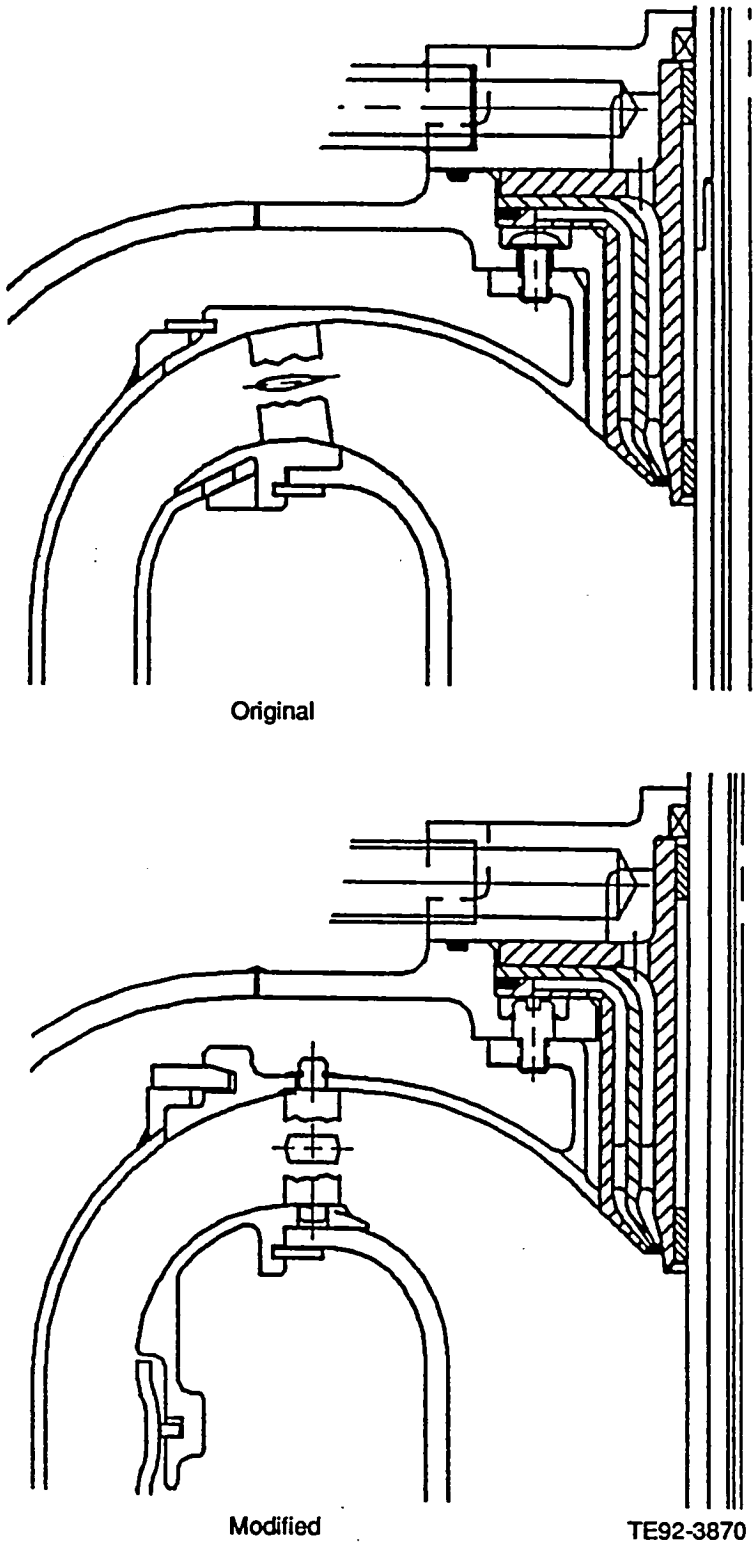


*Figure 1-18. Comparison of initial and modified poppet valve combustor dome designs.*

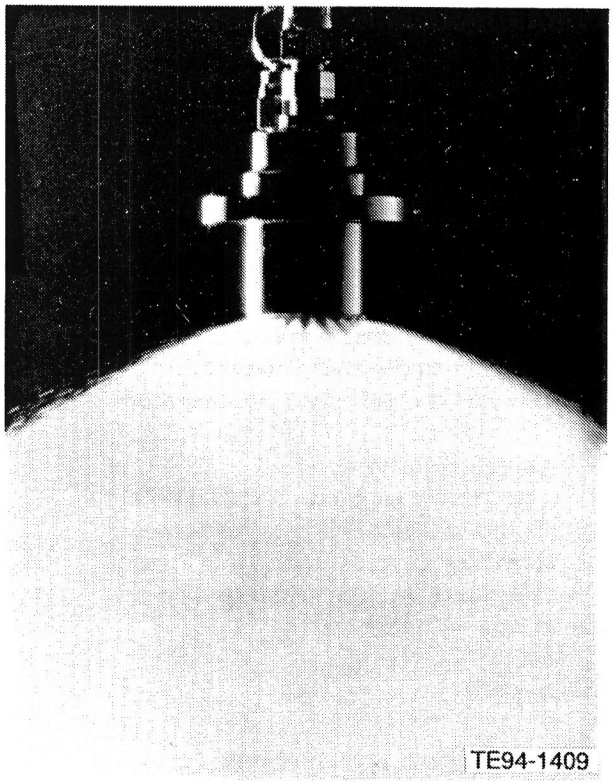


*Figure 1-19. Poppet valve combustor main fuel nozzle at maximum power flow condition.*

### 1.4.3 Alternate Flow Paths

#### Objective/Approach

The objective of this task is to carry out aerodynamic design and assessment of alternative flow paths. The flow paths are potential or existing design concept candidates for incorporation into the tested engine configuration.

#### Accomplishments/Results

- The AGT-5 alternate scroll total pressure loss and exit angle survey was completed.
- The plastic RPD-size alternate scroll was flow tested.
- The RPD-size gasifier rotors were also flow tested.

#### Discussion

A plastic model of the ceramic alternate scroll was manufactured using a rapid prototype system. The flow at the exit of the plastic model was surveyed and the circumferential span averaged exit angle was found to vary by 6 deg.

A plastic prototype of the RPD-size scroll was also fabricated using a rapid prototyping process. The scroll was instrumented with 36 surface static taps and ten exit total pressure holes. The scroll cross section static pressure was surveyed at four circumferential positions. At each position, seven static taps were used to span the cross section. The cross section static pressure was found to vary with radius; the static pressure increased with increasing radius, suggesting a free vortex velocity profile. This radial distribution of static pressure was found at all of the four surveyed cross sections.

The exit total pressure and exit angles were measured at three different mean exit Mach numbers: 0.77, 0.92, and 1.12. The exit angle of the flow was found to decrease with increasing expansion ratio. The averaged radial distribution of the exit angle is illustrated in Figure 1-20.

Several RPD-size ceramic gasifier rotors were flow tested. Initial air flow numbers verified that the rotor throats were smaller than design. During the manufacturing process, it appears that the trailing edge of the rotor slightly drooped, decreasing the rotor throat. Subsequent engine use of these rotors will require a larger tip diameter than designed. Due to the poor manufacturing quality of these ceramic rotors, all RPD-size ceramic rotors should

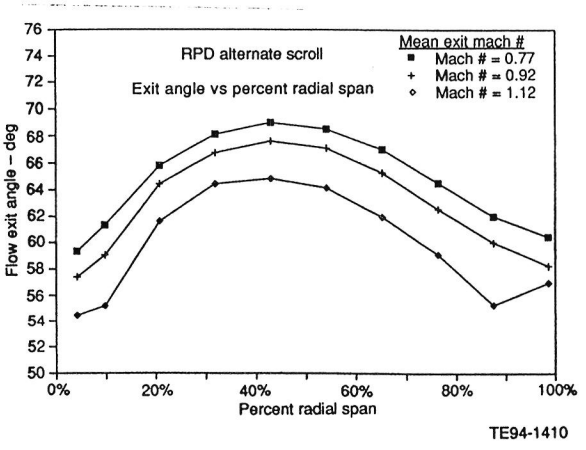


*Figure 1-20. RPD alternate scroll averaged radial distribution of exit angle.*

be flow tested and the tip diameter machined to match the designed engine air flow.

## 1.4.4 Engine System Integration

### Objective/Approach

The objective of engine control systems (control software and control hardware) for ATTAP is to integrate ceramic components and 1371°C (2500°F) temperature capabilities into the AGT-5 engine and associated rigs (lube and fuel systems, starter motors, etc).

### Accomplishments/Results

- EDM-800 controller program versions were consolidated into one program using conditional assembly.
- Magnetoresistive (MR) sensors were designed for air induction system mounting to measure N1.
- A burner variable geometry (BVG) actuator using a dc motor and remote closed-loop position control was selected for use in the engine configuration.
- Automatic setting of minimum fuel was established, derived from flameout tests.
- Start nozzle logic was completed and incorporated into the BVG program flowchart.

### Conclusion/Results

The controller program for the EDM-800 electronic engine control system consists of several different versions to accommodate various rigs, engines, and testing conditions. These were combined into one program which allows them to be compiled with different options prior to downloading to the EDM-800 controller.

An MR sensor is a three-wire sensor that can have a stronger signal output than a magnetic sensor or an optical sensor under conditions of wide gap, contamination, or high frequency. The MR sensor's small size allows packaging in locations that might otherwise be unsuitable.

The BVG requires a linear actuator to move the variable geometry parts. A suitable DC motor actuator has been identified and is available with a remote closed-loop position controller.

Minimum fuel values are difficult to set because of build-to-build differences and changes over time. The reason for minimum fuel values is to prevent flameout, especially during gasifier decelerations. A method of inferring flameout from existing sensors would allow the use of this parameter to determine whether an automatic adjustment of the minimum fuel is necessary. Unfortunately, there are no actual test runs showing engine states during flameout. Such data would be useful in calibrating the test parameter constants and making a preliminary judgment on the validity of this method.

The BVG system requires two fuel nozzles that need to be selectively enabled. The EDM-800 can perform this task according to the necessary conditions. A flow chart outlining this logic has been completed, and the next step is to translate it into software.

### Discussion

**Engine Control.** Since all the program versions now have one common source, any changes made to one program will automatically update all versions simultaneously. The ability to compile different versions and save the results separately makes it easy to run different engines or rigs by downloading the new program alone, rather than requiring the program to be recompiled (a process, which can take half an hour on slower computers like the VMS-1000).

Magnetoresistive sensors can have a higher output signals than other sensors, since they act like varying resistors in the circuit and the resistance is proportional to the gap between the sensor chip and the ferromagnetic material being sensed. A magnetic pickup, however, actually generates a voltage through a coil of wire as the ferromagnetic material moves toward it or away from it. The voltage in this case depends upon the speed with which the material moves and upon the air gap. The lower the speed, the lower the signal. An MR sensor is speed independent. The sensor is located in the air intake shroud and senses the edges of the compressor nut. This location was chosen for its low temperature environment and easy access. The greater allowable air gap between the sen-

sor tip and the nut allows mounting in this area where it is harder to hold a tight tolerance.

The remote closed-loop position controller of the BVG actuator frees the EDM-800 to perform other functions. The BVG actuator will be driven by a specialized remote closed-loop position feedback controller that will receive position commands from the EDM-800 and proceed to drive the actuator into position. Commands will be in the form of analog voltage levels between zero and five volts and will originate from a D/A converter in the EDM-800; this can save time and complexity when developing the BVG. The BVG requires a linear actuator to move the variable geometry parts. The actuator chosen uses a recirculating ball-type screw with a preloaded drive nut for zero backlash and can operate at a 133.45N (30 lbf) thrust with over a 60% duty cycle at 15.24 cm/sec (6 in./sec) linear speed. This meets or exceeds projected worse case requirements.

Automatic adjustment of minimum fuel as the engine runs requires rates of various temperature and speed changes during flameout to indicate an event has occurred and could allow the controller to take corrective actions for the next time. However, data from flameout events showing engine states and emissions are not available at the present time. Since a flameout causes excessive HC emissions, it is important to have a good estimate on the minimum fuel needed to prevent flameout. Even if build-to-build variations were eliminated in production, the changes over time as well as changes in T1 can affect the optimum values of minimum fuel. A self-correctable scheme would eliminate this problem. Furthermore, if a low cost, reliable flameout sensor were available, automatic adjustment of the minimum fuel would be a simple matter.

# II. CERAMIC COMPONENT DESIGN

## 2.1.2 Gasifier Turbine Static Structure

### Objective/Approach

This activity is focused on designing static structural ceramic components for the gasifier turbine that meet performance, mechanical strength, and probability of survival, as well as dimensional criteria for operation in the AGT-5 hot gasifier rigs and test-bed engines at reference powertrain design conditions. Efforts include the construction of 2-D and/or 3-D FEM models to calculate component temperatures, deflections, stress profiles, and resulting probabilities of survival.

### Accomplishments/Results

- A worst case radial temperature profile for the gasifier turbine vane was estimated.
- The estimated radial temperature profile was to used to predict vane cracking observed in hot rig testing.
- The estimated radial temperature profile was also used to evaluate possible materials for fabricating replacement vanes.
- For silicon nitride vanes, using the new currently estimated radial temperature profile in place of the originally assumed flat profile, the predicted stress levels increased by about 30% in the transient mode and about 150% at steady-state maximum power.
- Norton/TRW's NT154 and Kyocera's SN252 silicon nitride materials used for the vanes have acceptable predicted POS values with the worst case radial temperature profile.
- To achieve an acceptable predicted POS, the Norton/TRW vane must have machined material properties at the trailing edge.
- A finite element mesh and stress model of the alternate scroll assembly was constructed.
- A cold assembly structural analysis of the Norton/TRW advanced concept gasifier scroll assembly was completed using a detailed 2-D axisymmetric finite element model, incorporating a 20-bladed ceramic gasifier rotor and the associated metal shaft.
- Steady-state maximum power thermal and structural/POS analyses of the alternate scroll assembly were completed using the updated 2-D axisymmetric finite element model.
- The cold start transient thermal and structural/POS analyses of the alternate scroll assembly were completed using the updated 2-D axisymmetric finite element model.
- For the alternate scroll, component stresses are well below design limits, and POS exceeds the design goal.
- For the alternate scroll, ceramic component maximum power steady-state stresses are minimal and the corresponding ceramic assembly POS of 0.99999 far exceeds the design goal of 0.96359.
- For the alternate scroll assembly, metal component stresses are, for the most part, below design limits at the maximum power steady-state condition. Two exceptions are the zirconia-coated insulator and the gasifier stud shield. These metal components have local equivalent stresses, which exceed material yield strength at the maximum power steady-state condition.
- The alternate ceramic scroll assembly minimum POS of 0.895 occurs at 15 seconds into the cold start transient.
- The minimum transient POS for the alternate scroll is driven by stress in the NT230 SiC scroll turbine shroud.

### Discussion

**Turbine Vane.** The objective of the analysis was to determine the effect of a worse case radial temperature profile on the probability of survival of AGT-5 individual ceramic gasifier vanes. Results of analysis conducted on the same vane without a temperature profile were reported in the 1989 ATTAP Annual Report. To determine the effect of the temperature profile, the same finite element mesh and contact thermal boundary conditions were used here as in the previous analysis. Figure 2-1 shows the

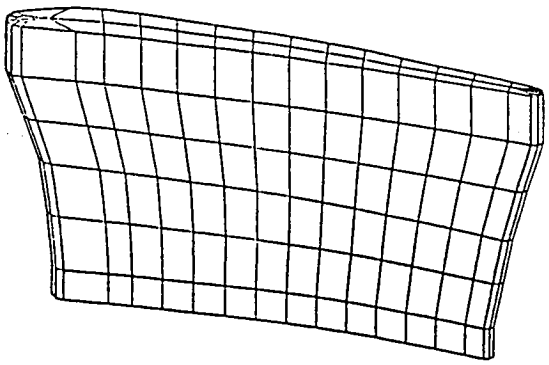

View of pressure surface

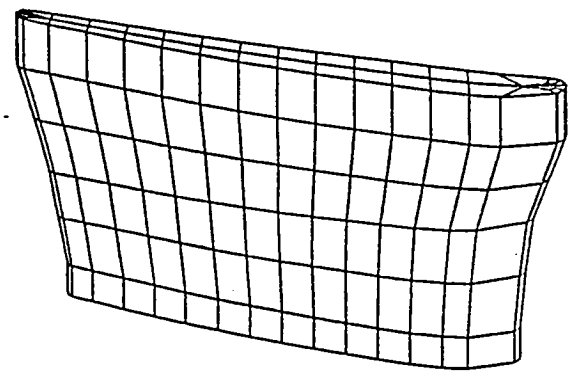

View of suction surface

TE94-1411

*Figure 2-1. Three-dimensional finite element mesh for ceramic gasifier vane.*

3-D mesh used in both analyses. This mesh is made of 20-noded solid elements. Figure 2-2 shows the boundary temperatures versus time used in the analysis. The bulk gas temperature in Figure 2-2 is the cycle temperature, not the average gas temperature of the radial temperature profile used in the analysis.

The radial temperature profile was created to account for both tangential and radial gas-path temperature gradients. From test data collected (as background data to ATTAP) on a metal AGT-5 engine, a 38°C (100°F) tangential gradient was estimated for the 1371°C (2500°F) cycle temperatures. The temperature profile used in the analysis had an average temperature at steady-state maximum power of 1427°C (2600°F) to analyze the worst case vane. A pattern factor of 0.2 was utilized. Using the definition of a pattern factor shown below, where temperatures are in degrees Farenheit, the

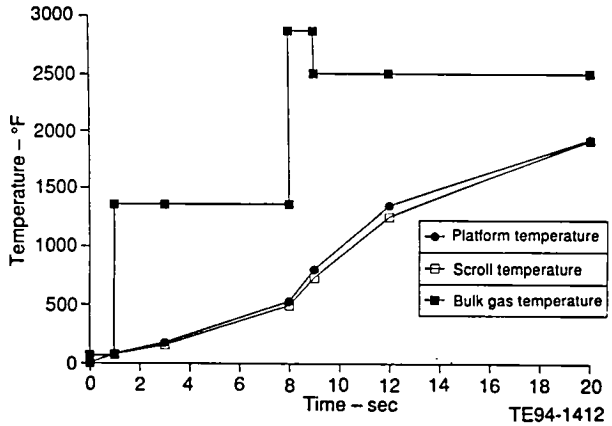


*Figure 2-2. Temperature boundary conditions used in the transient analysis.*

maximum temperature (T4max) of 1463°C (2666°F) was calculated for this analysis.

$$\text{Pattern factor} = \frac{T_{max} - T4_{ave}}{T4_{ave} - T3_{ave}} = 0.2$$

The temperature profile was created to satisfy the estimated maximum and average temperatures while maintaining a reasonable profile. The acceleration overshoot temperature profile was estimated in the same way. Under transient acceleration conditions an average of 1621°C (2950°F) and maximum of 1690°C (3075°F) are predicted. Figure 2-3 shows the estimated radial temperature profiles for maximum power and acceleration overshoot conditions.

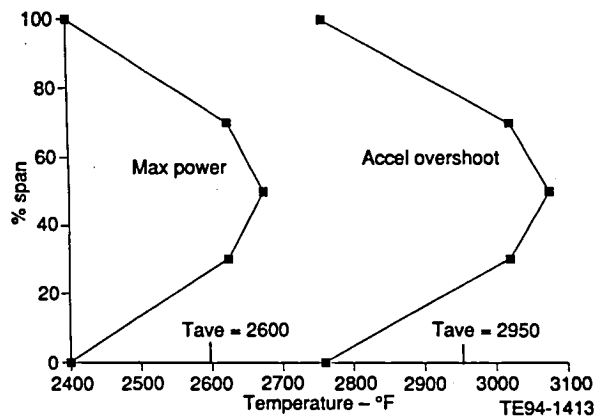


*Figure 2-3. Estimated radial temperature profile for the gasifier vane at maximum power and acceleration overshoot conditions.*

The vane temperatures predicted using the new temperature profiles are understandably higher than vane temperatures predicted using the original flat 1371°C (2500°F) temperature profile. With both sets of boundary conditions, the highest vane temperatures occur at steady-state maximum power, although maximum gas temperatures occur in the acceleration overshoot. The vane does not have time to fully respond to the overshoot condition in the acceleration exposure time. The overshoot does, however, increase the thermal gradients in the vane compared to a transient with no acceleration overshoot. Predicted stresses are higher using the new boundary conditions with the corresponding reductions in predicted probability of survival. Figures 2-4 and 2-5 show predicted temperature and stress profiles for the worst case transient and maximum power steady-state conditions. The plots shown are for Norton/ TRW's NT154 silicon nitride material, but all materials have the same basic temperature and stress distributions. In each vane, the maximum temperature point is also the maximum stress point. Table 2-I summarizes the results for each material using a flat 1371°C (2500°F) gas temperature distribution. Table 2-II summarizes the results for each material using the estimated radial temperature profile. The stresses are about 30% higher in the transient and about 150% higher at steady-state with the radial profile. The increased stresses are the result of the gas temperature profile forcing larger thermal gradients in the vane. Since the stresses are caused entirely by thermal loads, the materials with the highest coefficient of thermal expansion and lowest thermal conductivities have the highest stresses. α-SiC has the highest coefficient of thermal expansion and has the highest stress in the transient. α-SiC also has the highest thermal conductivity, so the temperature gradient at steady-state is low and the stresses are low. NT154, PY6, and SN252 are all silicon nitrides but have widely differing coefficients of thermal expansion so the maximum stress for each material varies.

PY6 and α-SiC vanes were fabricated early in ATTAP. All but one set of PY6 vanes have been consumed in test. The α-SiC vanes have not been tested to date but have a low probability of survival with the estimated pattern factor and have a lower FOD tolerance. To ensure there are enough vanes for engine and hot rig

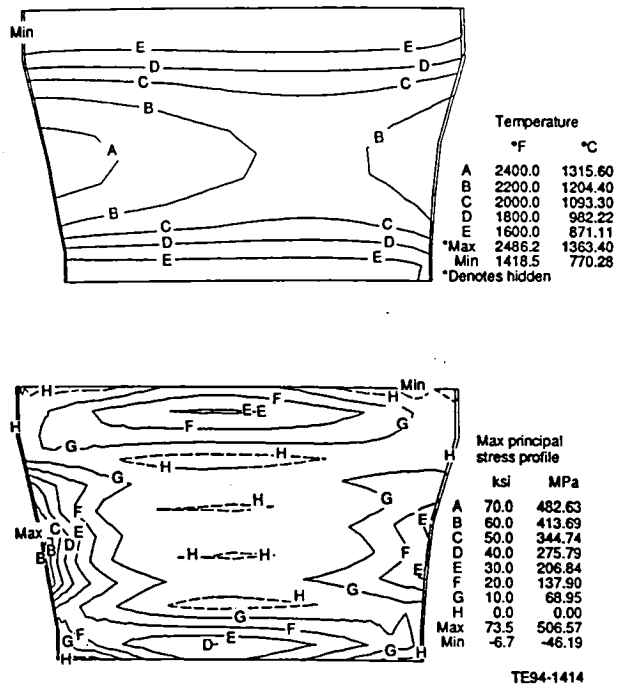


*Figure 2-4. Vane temperature and stress profile, NT154 $Si_3N_4$ worst case transient condition (trailing edge is to the left).*

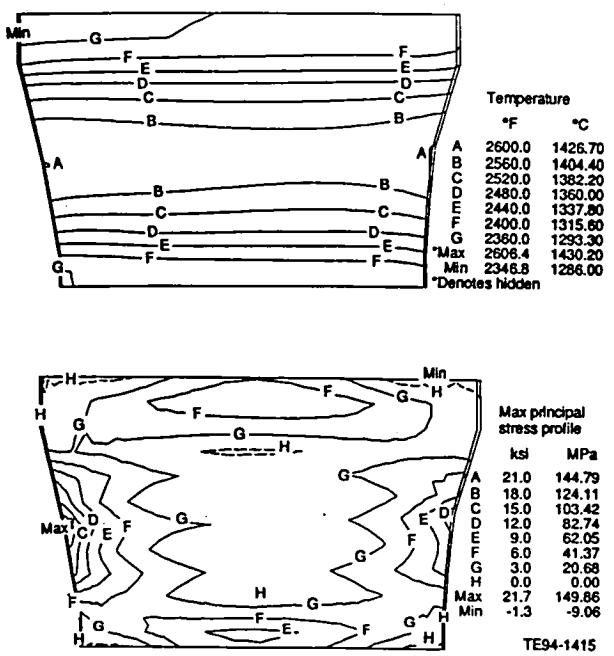


*Figure 2-5. Vane temperature and stress profile, NT154 $Si_3N_4$ maximum power steady-state condition (trailing edge is to the left).*

*Table 2-I.*
*Summary of vane analysis results without estimated radial gas temperature profile.*

| | Without profile | | | |
|---|---|---|---|---|
| | αSiC | PY6 | NT154 | SN252 |
| Engine acceleration transient | | | | |
| Time of minimum POS-sec | 14.0 | 11.6 | 11.0 | 11.0 |
| Max vane temperature-°C | 1252 | 1311 | 1260 | 1254 |
| (°F) | (2287) | (2392) | (2300) | (2290) |
| Max principal stress-Mpa | 401 | 339 | 386 | 254 |
| (ksi) | (58.2) | (49.1) | (56.0) | (36.9) |
| POS | 0.9951 | 0.9999 | 0.9965 | 1.0000 |
| POS w/ machined trailing edge | | | | 0.9972 |
| Max power steady-state | | | | |
| Max vane temperature-°C | 1357 | 1369 | 1362 | 1364 |
| (°F) | (2475) | (2496) | (2484) | (2487) |
| Max principal stress-Mpa | 59 | 57 | 58 | 40 |
| (ksi) | (8.6) | (8.2) | (8.4) | (5.8) |
| POS | 1.0000 | 1.0000 | 1.0000 | 1.0000 |

*Table 2-II.*
*Summary of vane analysis results with estimated radial gas temperature profile.*

| | With Profile | | | |
|---|---|---|---|---|
| | αSiC | PY6 | NT154 | SN252 |
| Engine acceleration transient | | | | |
| Time of minimum POS-sec | 11.0 | 11.0 | 11.0 | 11.0 |
| Max vane temperature-°C | 1252 | 1403 | 1363 | 1354 |
| (°F) | (2285) | (2557) | (2486) | (2469) |
| Max principal stress-Mpa | 583 | 459 | 507 | 332 |
| (ksi) | (84.5) | (66.6) | (73.5) | (48.1) |
| POS | 0.8093 | 0.9966 | 0.9699 | 1.0000 |
| POS w/ machined trailing edge | | | | 0.9923 |
| Max power steady-state | | | | |
| Max vane temperature-°C | 1404 | 1443 | 1430 | 1427 |
| (°F) | (2559) | (2630) | (2606) | (2600) |
| Max principal stress-Mpa | 95 | 157 | 150 | 99 |
| (ksi) | (13.8) | (22.8) | (21.7) | (14.3) |
| POS | 1.0000 | 1.0000 | 1.0000 | 1.0000 |

testing, additional NT154 and SN252 vanes have been fabricated but not tested.

**Gasifier Scroll.** A detailed 2-D axisymmetric finite element structural analysis has been completed for the Norton/TRW advanced concept gasifier scroll assembly. The objective of the analysis is to predict scroll assembly stresses, deflections, and ceramic component probabilities of survival at various operating conditions, which include cold assembly, maximum power steady-state, and the cold start transient. This included several iterations of the finite element model geometry. Achievements include updating of the finite element model by incorporating a 20-bladed ceramic gasifier rotor and metal shaft and completion of the cold assembly stress/POS analysis. The updated finite element model is illustrated in Figure 2-6. The gasifier rotor and shaft were added to the finite element model in support of an ongoing ceramic rotor failure investigation.

Assembly temperatures, stresses, and associated ceramic component probabilities of survival were generated for the maximum power steady-state operating condition utilizing the baseline scroll mount preload (0.012 in. gasket crush and 2850 lbf stud preload). Ceramic component steady-state temperatures and associated maximum principal stresses are illustrated in Figures 2-7 through 2-12 for the NT230 SiC scroll, NT154 $Si_3N_4$ tabbed mount ring, and NT154 $Si_3N_4$ seal ring, respectively. The ceramic component steady-state stresses are minimal (below 10 ksi), and the corresponding scroll assembly probability of survival is 0.99999. Recall that the initial scroll design assembly goal POS was 0.96359.

Metal component steady-state temperatures and stresses are, for the most part, below design limits. Two exceptions are the zirconia-coated insulator and the gasifier stud shield. Steady-state temperatures and corresponding equivalent stresses are illustrated in Figures 2-13 through 2-16 for the zirconia-coated Haynes 230 insulator and the Haynes 188 gasifier stud shield. Figures 2-17 and 2-18 illustrate corresponding maximum power steady-state stress ratios (stress ratio is defined as the local stress divided by the 0.2% yield strength) for the insulator and shield, respectively. Note that both components have predicted maximum stress ratios in excess of 1.0 (local yielding). Thermally induced compressive hoop stresses are the primary contributor to the localized high stress ratios in the zirconia-coated insulator. Elevated temperatures coupled with axial and radial bending stresses are the primary contributors to the localized high stress ratios in the Haynes 188 gasifier stud shield.

### 2.1.3 Gasifier Turbine Rotor

#### Objective/Approach

This activity is focused on designing structural ceramic rotors for the gasifier turbine that meet performance, mechanical strength, POS, and dimensional criteria for operating in the AGT-5 hot gasifier rig(s) and test-bed engine(s) at RPD conditions. Efforts include the analytic assessment of the structural reliability (statistical basis) of gasifier rotor designs considering various ceramic material systems. The rotor design reliability goal is 0.9797. Critical points in the engine operating cycle are analyzed, including 2500°F (1370°C) RIT maximum power steady-state and a cold start to maximum power transient.

#### Accomplishments/Results

- The Ceramics Process Systems (CPS) 26-bladed gasifier rotor was analyzed for possible rework to reduce high blade fillet stresses caused by a small blade fillet near the leading edge.
- Analysis shows that the probability of survival is not increased enough to warrant reworking parts.

#### Discussion

It became evident that a rework of the CPS 26-bladed gasifier rotor was needed after the first proof test. The rotor burst at 67,580 rpm, well below the proof test speed of 80,000 rpm. A post test inspection revealed that the fracture origin was in the blade fillet near the leading edge. The CPS 26-bladed rotors have a 0.05 mm fillet in this region, while the Norton/TRW and Kyocera rotors, which passed proof testing, have larger 1.5 mm fillet. The leading edge blade fillet region is the highest stress point in all

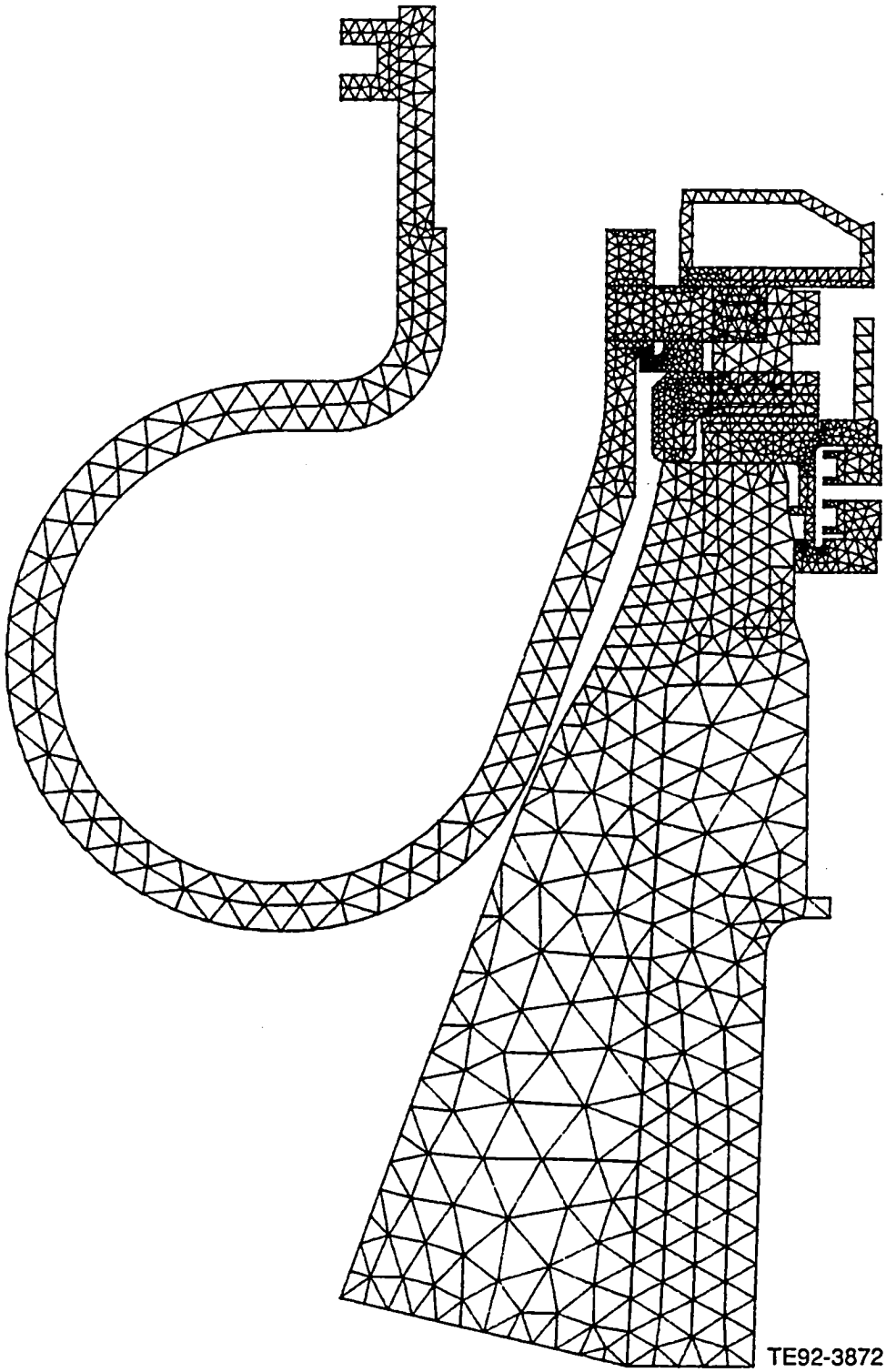


*Figure 2-6. Advanced concept scroll assembly finite element mesh.*

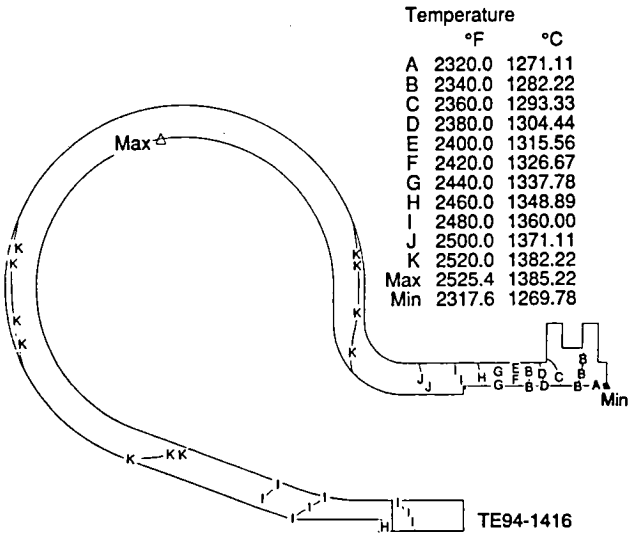


*Figure 2-7. NT230 SiC scroll temperatures for the maximum power steady-state condition.*

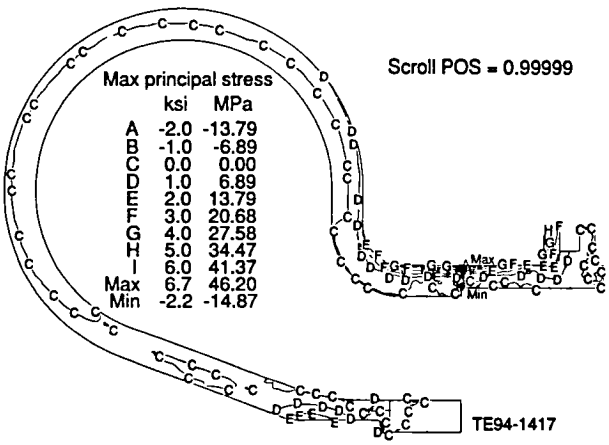


*Figure 2-8. NT230 SiC scroll maximum principal stresses and probability of survival for the maximum power steady-state condition.*

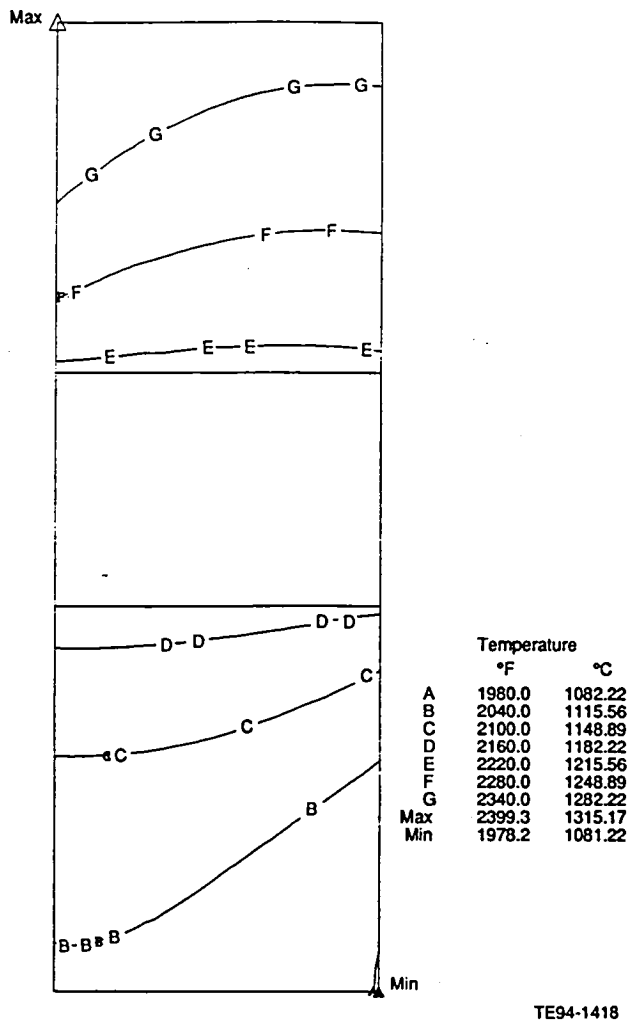


*Figure 2-9. NT154 $Si_3N_4$ tabbed mount ring temperatures for the maximum power steady-state condition.*

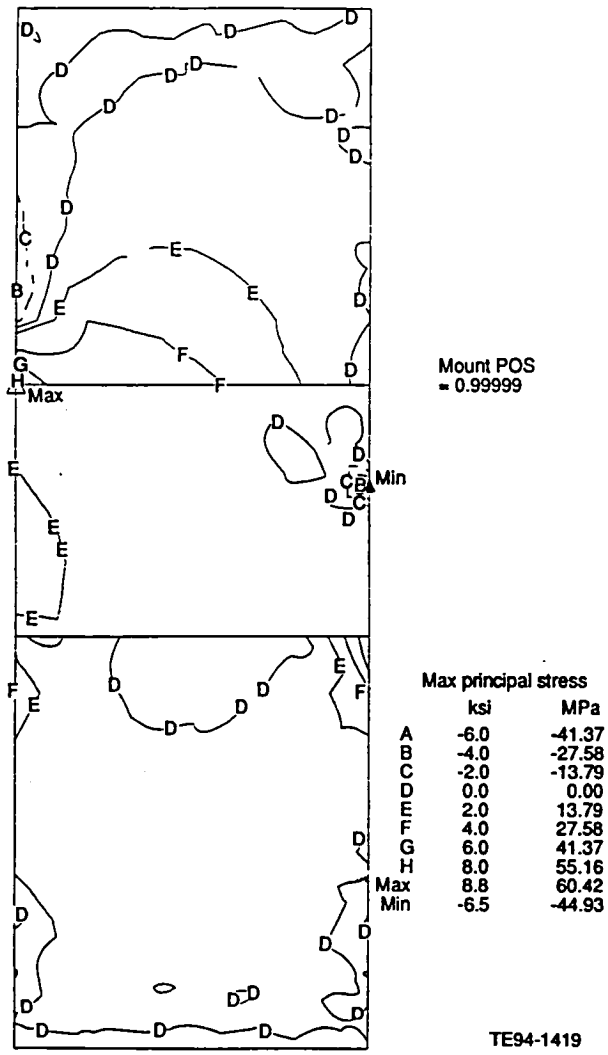


*Figure 2-10. NT154 $Si_3N_4$ tabbed mount ring maximum principal stresses and probability of survival for the maximum power steady-state condition.*

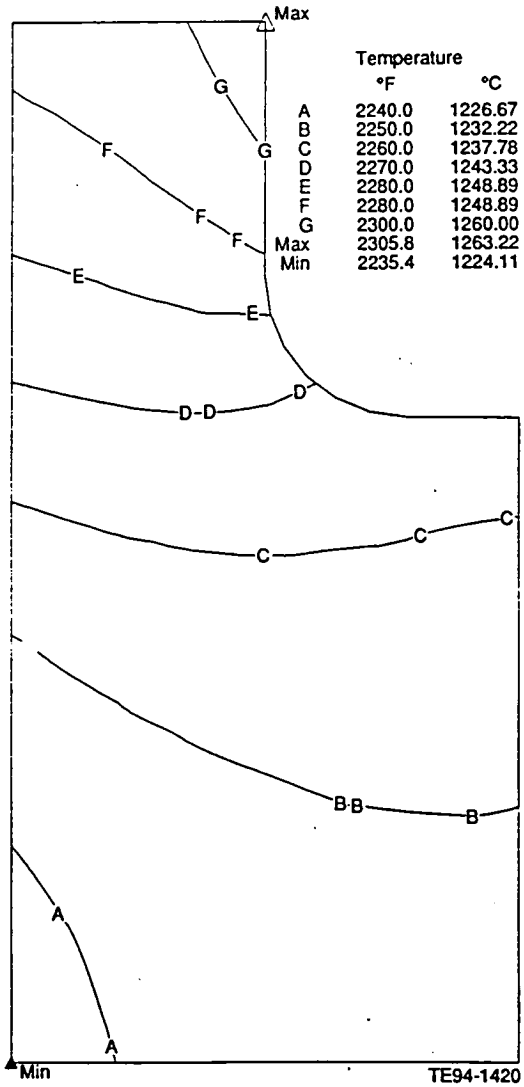


*Figure 2-11. NT154 $Si_3N_4$ seal ring temperatures for the maximum power steady-state condition.*

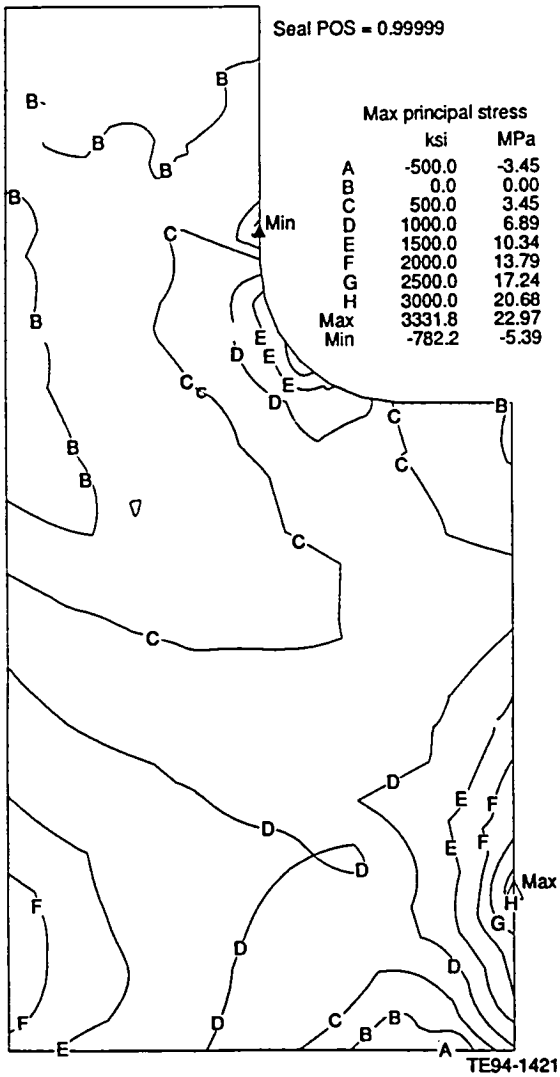


*Figure 2-12. NT154 $Si_3N_4$ seal ring maximum principal stresses and probability of survival for the maximum power steady-state condition.*

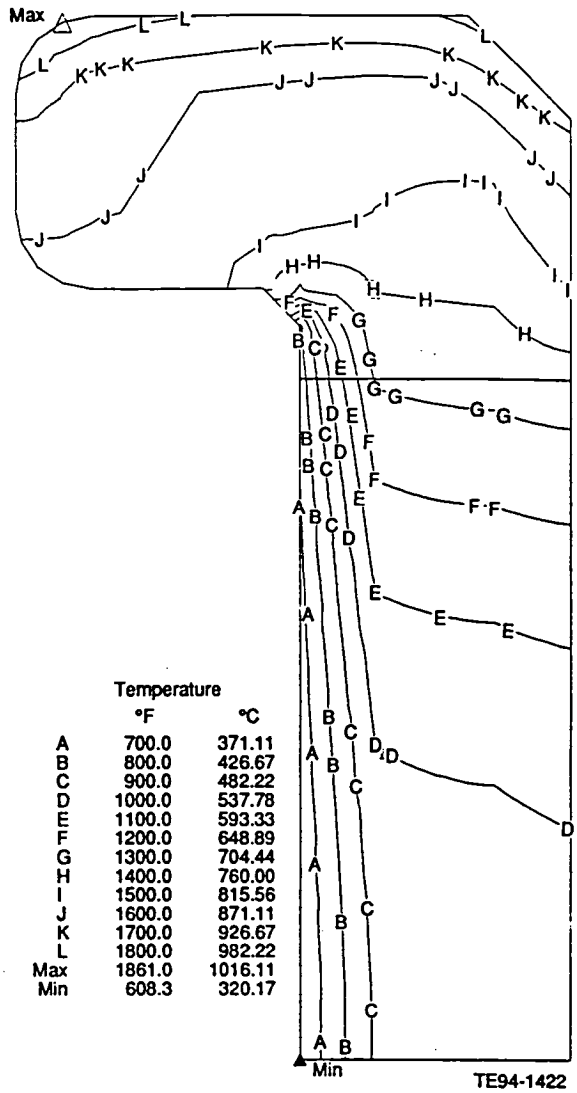


*Figure 2-13. Zirconia-coated Ha230 insulator temperatures for the maximum power steady-state condition.*

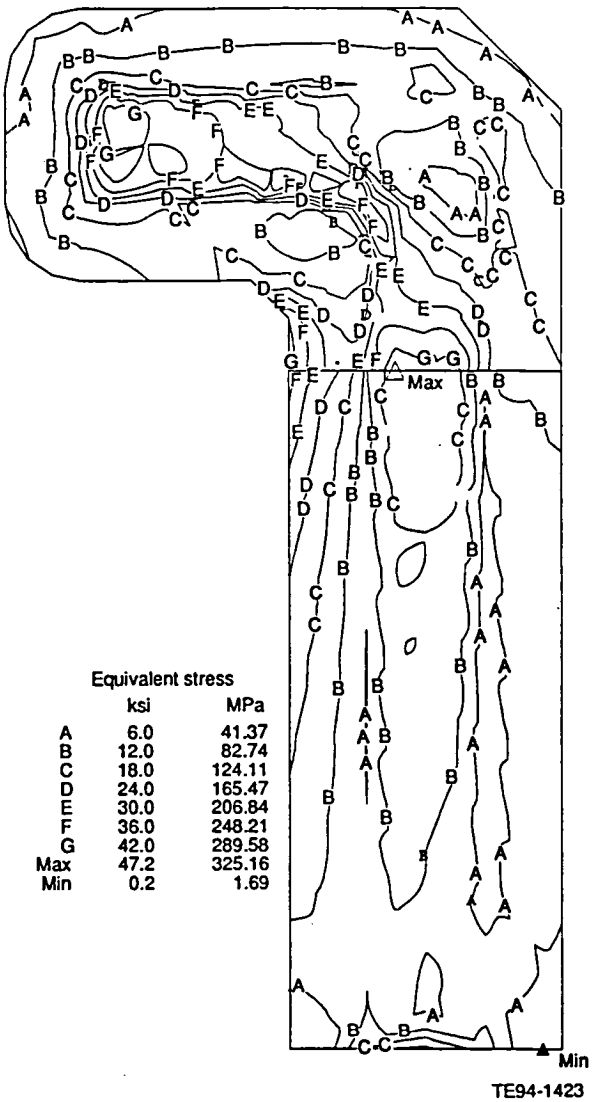


*Figure 2-14. Zirconia-coated Ha230 insulator equivalent stresses for the maximum power steady-state condition.*

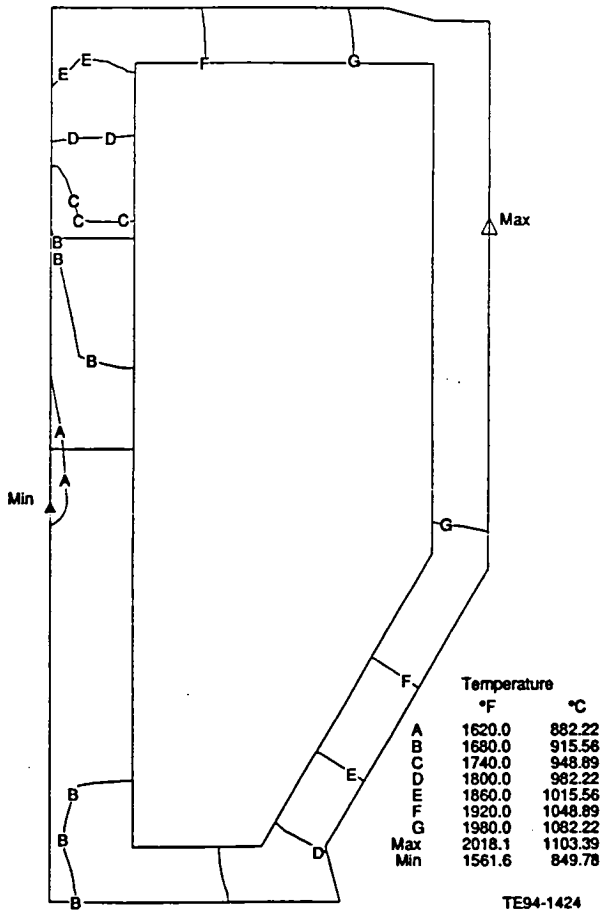


*Figure 2-15. Ha188 gasifier shield temperatures for the maximum power steady-state condition.*

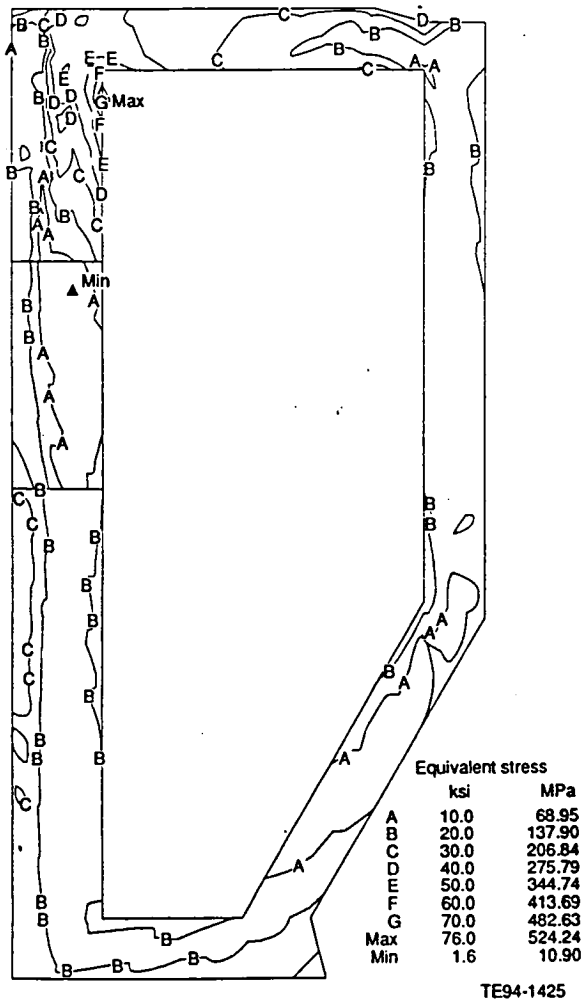


*Figure 2-16. Ha188 gasifier shield equivalent stresses for the maximum power steady-state condition.*

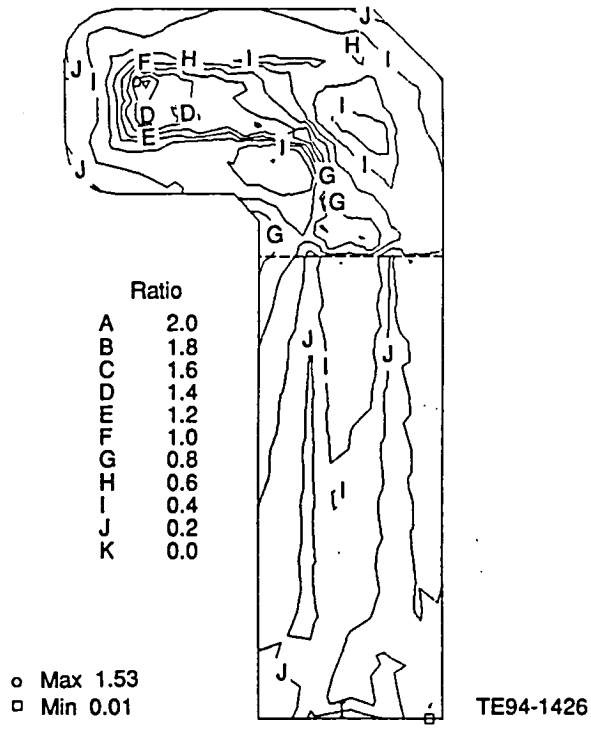


*Figure 2-17. Zirconia-coated Ha230 insulator stress ratios for the maximum power steady-state condition.*

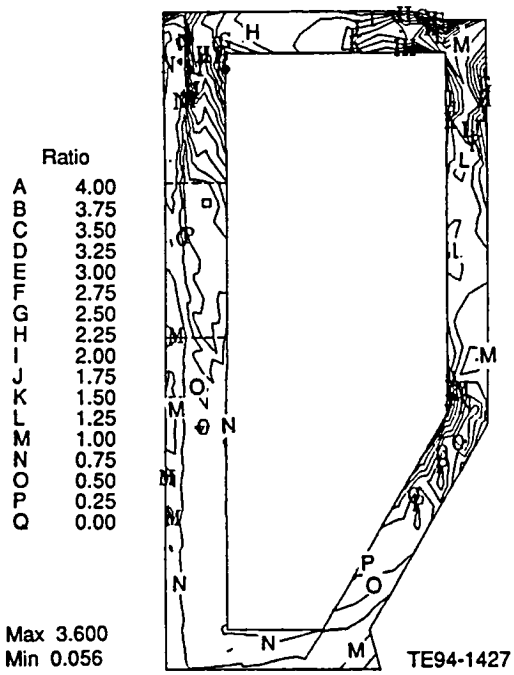


*Figure 2-18. Ha188 gasifier stud shield stress ratios for the maximum power steady-state condition.*

three rotors during cold spin testing and the sharp fillet on the CPS rotors makes the peak stress much higher.

The blade fillet is 0.05 mm only at the leading edge of the rim and transitions quickly to 1.5 mm. The stress concentration factor of a 1.5 mm fillet is 45% less than that of a 0.05 mm fillet in this region. The blade was cast with the smaller fillet, making it impossible to machine a larger fillet in place. The only promising method of reworking the finished part was to scallop the rim back further with a surface of revolution (Figure 2-19) to the point where the full 1.5 mm starts. This would eliminate the high stress concentration factor in the blade root but would increase the nominal stress by reducing the area and section properties of the blade root. To evaluate this rework, the nominal stress was calculated using a beam bending analysis approach that considers blade section properties and radial and bending CF loads. The stress concentration factor was found by use of a reference table. The probability of survival of each configuration was estimated using Weibull equations and experience gained from the 3-D analysis of the 15- and 20-bladed gasifier rotors. Probability of survival was calculated using as-cast material properties because the rework did not result in a machined surface for the blade fillet surface.

Table 2-III is a summary of results for the 0.05 mm fillet, the reworked rotor, and the standard 1.5 mm fillet rotor for the 80,000 rpm cold spin proof test. The last column of Table 2-III is the predicted POS of each geometry at the burst speed of 67,580 rpm. The predicted stress and resulting POS of the reworked rotor is an improvement but still does not result in an acceptable POS.

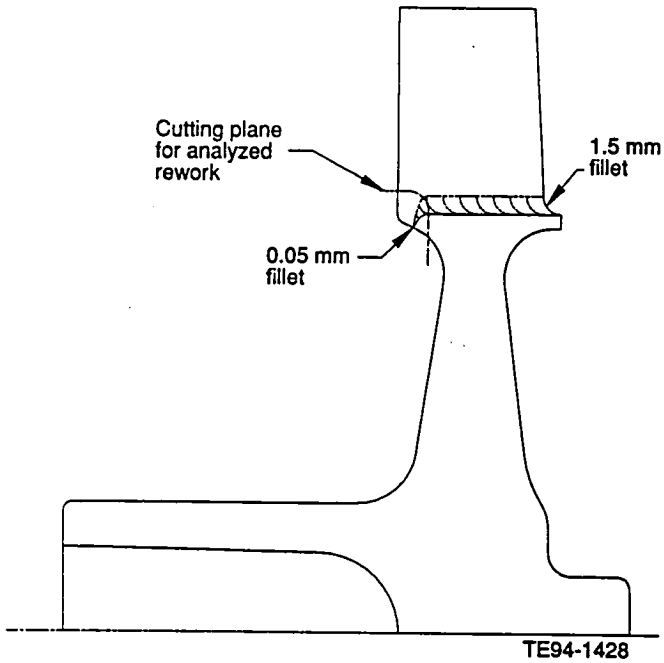


*Figure 2-19. Analyzed rework geometry of the CPS 26-bladed gasifier rotor.*

The spin test was encouraging because it proved the rotor disk was at least strong enough to reach the burst speed of previous tests. A rotor disk with gross defects would not have reached the target burst speed of 67,800 rpm. The current tool has been valuable for process development and will continue to be used for this purpose. The CPS rotors are not needed to continue rig and engine testing on the AGT-5 testbed, so a new tool will not be fabricated. The fact that the rotor burst does not indicate that the CPS material or process are inadequate for rotors.

*Table 2-III.*
*Summary of stress calculation results for the CPS 26-bladed gasifier rotor rework analysis.*

| | Nominal stress - Mpa | Stress concentration factor | Stress - Mpa | POS at 80,000 rpm (test speed) | POS at 67,580 rpm (burst speed) |
|---|---|---|---|---|---|
| 0.05 mm fillet | 234 | 2.88 | 675 ± 60 | 2.3E-20 | 0.10 |
| Reworked rotor | 380 | 1.59 | 606 ± 60 | 1.8E-8 | 0.40 |
| 1.5 mm fillet | | | 365 | 0.80 | 0.99 |

## 2.1.5 Power Turbine

### Objective/Approach

The objective of this design and development activity is to upgrade the AGT-5 from a 1038°C (1900°F) metal engine to a durable 1371°C (2500°F) structural ceramic component test-bed engine.

### Accomplishments/Results

- The ceramic power turbine shifted during running and became unbalanced due to relative movement between the first- and second-stage shafts.
- The first- and second-stage power turbine shafts were modified to obtain a tighter build clearance and allow less relative movement between the stages.
- A test apparatus was built to determine the optimum bolt torque.
- The necessary engine hardware and gearbox were assembled to simulate engine structural conditions.
- The power turbine shaft was modified to increase the engaged taper contact area.

### Discussion

The ceramic power turbine (Figure 2-20) was check balanced after initial cold spin testing and found to be out of balance. Runout measurements of the assembly seemed to indicate that the first-stage power turbine shaft had been bent. The first and second stages were uncoupled and runout measurements were taken of the first-stage shaft. Contrary to expectations the runout for the first-stage shaft was acceptable, indicating that the shaft had not been bent.

Further investigation into the runout problem showed the pilots between the first- and second-stage shaft to have unacceptably large clearances. It is theorized that during running, the second-stage shaft shifted off center, causing an unbalance. When runout measurements were taken, the shifted second-stage power turbine also moved the bearing surface, making it appear that the first-stage power turbine shaft had been bent.

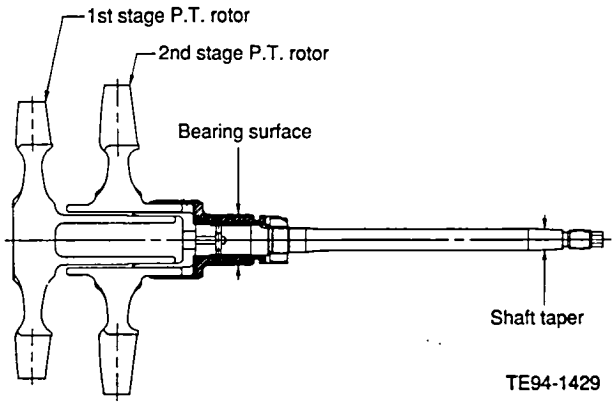


*Figure 2-20. Two-stage ceramic power turbine configuration.*

To reduce the possibility of future shifting of the second-stage shaft, the clearance between the first-and second-stage power turbine shafts was tightened and a test apparatus was built to determine the optimum bolt torque for the assembly. The clearance between the first- and second-stage power turbines was tightened by pressing a sleeve onto the second-stage shaft bore and requalifying the bore to have a ring fit to the first-stage shaft. To determine the optimum bolt torque for bolting the first- and second-stage shafts, a test apparatus was built that matched the dimensions of the power turbine shafts. Bolt stretch was measured for several applied torques. It was determined the optimum bolt torque for this assembly was 45 to 50 ft lbf.

To ensure that the structural modes of the power turbine spin rig would correspond to the structural modes of the engine, the spin rig containment housing was removed from the gearbox and engine hardware was installed. Next, the first- and second-stage ceramic power turbines were assembled and balanced. After assembly, runout measurements were taken at several critical locations on the shaft and the ceramic rotors. All runout measurements were found to be acceptable.

The ceramic power turbine is now ready for a second attempt at spin testing.

# III. MATERIALS CHARACTERIZATION AND CERAMIC COMPONENT FABRICATION

This section describes the ongoing ceramic material and component fabrication, characterization, and development activities that are a key focus of ATTAP. The ceramic materials subsection documents the results of characterization and qualification of candidate ceramic materials and components being developed for advanced gas turbine engine applications. This includes characterizations of material properties (microstructure, density, fracture strength, and fracture toughness), results of failure analyses of rig/engine tested components, and nondestructive evaluation results. The ceramic component fabrication subsection describes the ongoing ceramic component process development activities at the selected ceramic suppliers for the Allison/GM ATTAP effort, including Carborundum, Schuller, Corning, Ceramics Process Systems, and Norton/TRW Ceramics. Allison's approach to ceramic component technology development continues to be one of subcontracting process development to the domestic ceramic manufacturing community and working in an iterative development loop with those suppliers in the areas of component design, fabrication, characterization, and rig/engine data feedback. While basic ceramic materials development is not part of ATTAP, the program integrates material developments from DOE/Oak Ridge National Laboratory programs, supplier in-house activities, and other sources as they become available for component fabrication.

## 3.1 MATERIALS AND COMPONENT CHARACTERIZATION

### 3.1.1 Material Properties and Microstructure

#### Objective/Approach

The materials and component characterization efforts have focused on the testing and evaluation of candidate ceramic materials and components being developed for use in the AGT-5 automotive gas turbine engine. The primary objective of this task is to establish a data base of appropriate material characteristics to support the design, analysis, development, and testing of hot section ceramic components. A secondary objective is to evaluate new candidate ceramic materials and suppliers and to assess which, if any, should be used in subsequent component development. The material characterization activities have focused on microstructural, density, flexural strength, and fracture toughness evaluations of various candidate ceramic materials. Fracture surface analysis is also used to determine the nature and location of strength-controling flaws. In addition, tensile strength and time dependent strength characteristics are evaluated for select materials.

#### Accomplishments/Results

The ceramic materials characterized during this reporting period include the following:

- Norton/TRW Ceramics NT230 siliconized SiC
- Dow Chemical $Si_3N_4$ (Material C)
- Dow Chemical $Si_3N_4$ (Material D)
- Dow Chemical $Si_3N_4$ (Material E)
- DuPont/Lanxide $Al_2O_3$/SiC Particulate Ceramic Composite

#### Discussion

**Norton/TRW NT230 SiC.** Evaluation of the as-cast material strength characteristics of Norton/TRW Ceramics' NT230 silicon carbide material was conducted this reporting period. The test specimens were sectioned from billets fabricated by slip casting using process parameters similar to those established for fabrication of the turbine scrolls. The NT230 material is a reaction sintered SiC with approximately 5 to 15% free silicon. The average density of this material measured 3.121 g/cc (0.113 lb/in.$^3$).

Two distinct as-cast surfaces were evaluated for the NT230 material. The mold surface refers to the material formed in contact with the plaster mold used in the pressure slip casting process, while the drain surface refers to the material present on the I.D. of the cast piece that remains after the excess slip is removed from the NT230 SiC material are summarized in Table

3-I and presented graphically in Figure 3-1 along with the strengths obtained for a longitudinally ground tensile surface condition.

The NT230 specimens tested with the as-cast mold surface in tension had an average room temperature fracture strength of 185.61 MPa (26.92 ksi) with an associated Weibull modulus of 9.7. The surface condition of the mold surface test specimens is shown in Figure 3-2 (18x magnification). The typical strength-controlling defects were observed to be surface flaws and shallow depressions on the surface of the bars, as shown in Figure 3-3. The test specimens were occasionally observed to have a shell-type feature at the fracture origin, as shown in Figure 3-4. These shell-type fractures are typically a result of mechanical impact damage to the surface of the material. In addition to a chemical treatment, the NT230 SiC is also subjected to a "sand" blast operation to remove the excess free silicon from the surface. It is thought that the mechanical treatment is the source of the impact features and is being examined by Norton/TRW for possible improvements in material strength of component reliability. Specimens tested at 1000°C (1832°F) had an average strength of 289.16 MPa (41.97 ksi), with strengths of 216.42 MPa (31.39 ksi) at 1250°C (2282°F) and 226.84 MPa (32.90 ksi) measured at a temperature of 1370°C (2500°F). The primary fracture origins observed in the specimens tested at an elevated temperature were similar to those observed in the bars tested at ambient temperature, i.e. surface depressions and flaws.

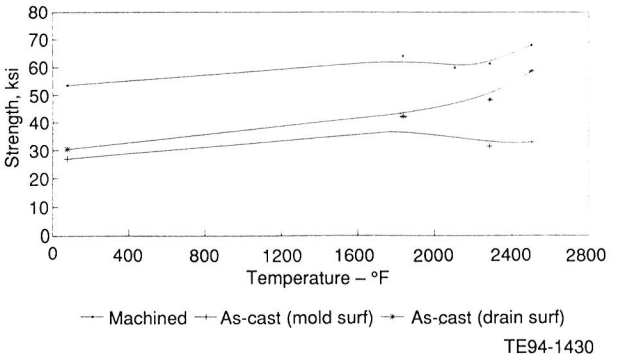


*Figure 3-1. Strength characteristics of Norton/TRW NT230 SiC.*


*Figure 3-2. Optical micrograph of as-cast NT230 SiC (mold surface). Magnification = 18x.*

*Table 3-I.*
*Strength characteristics of Norton/TRW NT230 siliconized SiC material.*

| Temperature, °C (°F) | Strength, MPa (ksi) | | |
|---|---|---|---|
| | Machined | Mold Surface | Drain Surface |
| 25 (77) | 369.21 (53.55) | 185.61 (26.92) | 209.39 (30.37) |
| 1000 (1832) | 440.71 (63.92) | 289.16 (41.97) | 290.96 (42.20) |
| 1250 (2282) | 422.44 (61.27) | 216.42 (31.39) | 332.88 (48.28) |
| 1370 (2500) | 468.49 (67.95) | 226.84 (32.90) | 404.72 (58.70) |

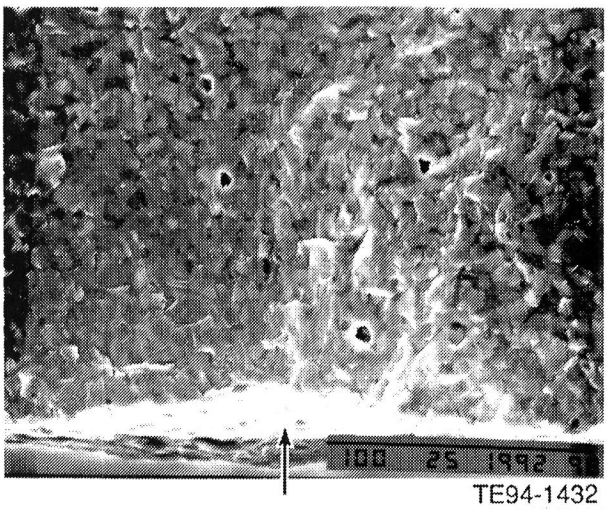


*Figure 3-3. Typical fracture origin (shallow surface depression) observed in as-cast NT230.*

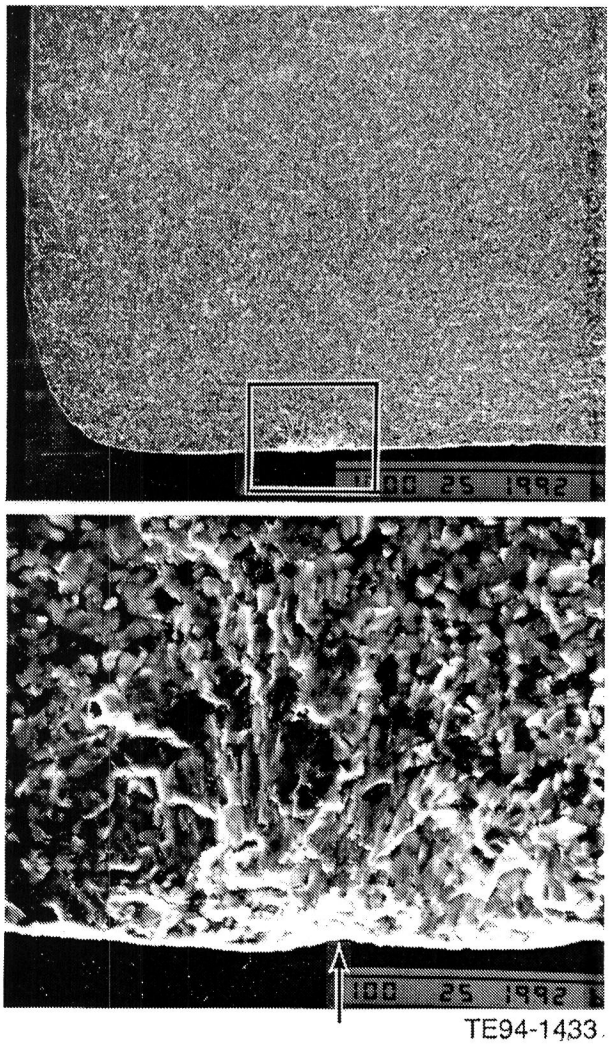


*Figure 3-4. Shell type fracture origin observed in as-cast NT230 SiC.*

NT230 specimens tested with the as-cast drain surface in tension had an average room temperature strength of 209.39 MPa (30.37 ksi) with a Weibull modulus of 9.4. Specimens tested at 1000°C (1832°F) had an average strength of 290.96 MPa (42.20 ksi), with a strength of 332.88 MPa (48.28 ksi) at 1250°C (2282°F) and 404.72 MPa (58.70 ksi) measured at a temperature of 1370°C (2500°F). The primary fracture origins observed in the specimens tested with the drain surface in tension were similar to those observed in the bars tested with the mold surface in tension, i.e. surface depressions and flaws.

Additional characterization activities were conducted on the NT230 SiC material to determine the effects of thermal exposure on material strength. Preliminary heat transfer analysis of the NT230 SiC combustor body in the diffusion flame combustor configuration indicated that maximum material temperatures of 1400°C to 1600°C (2552 - 2912°F) might be encountered during steady-state operation at maximum power. Data from Norton/TRW indicated that a significant reduction in strength of the NT230 occurs at temperatures above the melting point of silicon. The fast fracture strength decreases from 468.49 MPa (67.95 ksi) at a temperature of 1370°C (2500°F) to 241 MPa (35 ksi) at a temperature of 1427°F (2600°F). Due to the limitations of the flexure test facility at Allison, which is also limited to temperatures of approximately 1427°C (2600°F), it was decided to conduct additional testing of the NT230 material using high temperature furnaces and burner test rigs to evaluate the effects of thermal exposure on the material strength characteristics.

Initial characterization was performed by exposing the NT230 for 5 hr in static air in a furnace to a temperature of 1510°C (2750°F). The condition of the test specimens after removal from the furnace is shown in Figure 3-5. The material was basically unchanged with the exception of small (2.5 mm [0.1 in.]) silicon nodules that were observed on the specimen surface. Following the static thermal exposure, the test bars were broken at room temperature. The average room temperature fracture strength was 334.67 MPa (48.54 ksi), a slight reduction in strength compared to the room temperature strength of 369.21 MPa (53.55 ksi) measured for the baseline test bars. The typical fracture


*Figure 3-5. Norton/TRW NT230 SiC after static thermal exposure at 1510°C (2750°F) for 5 hr in air.*

origins were surface flaws, similar to those observed in all the NT230 specimens.

Following thermal exposure testing in a static air environment, additional specimens of NT230 SiC were tested after exposure in a burner test rig to more accurately simulate the conditions that exist in the ATTAP combustor body. The bars were exposed to hot gas flowing at Mach 0.3 at a temperature of 1540°C (2800°F) for a period of 5 hr. The fuel used for combustion was JP5. The condition of the material after thermal exposure is shown in Figure 3-6. Following the dynamic thermal exposure, the test bars were broken at room temperature. The average room temperature fracture strength was 307.16 MPa (44.55 ksi). The typical fracture origins were surface flaws, similar to those observed in all the NT230 specimens.

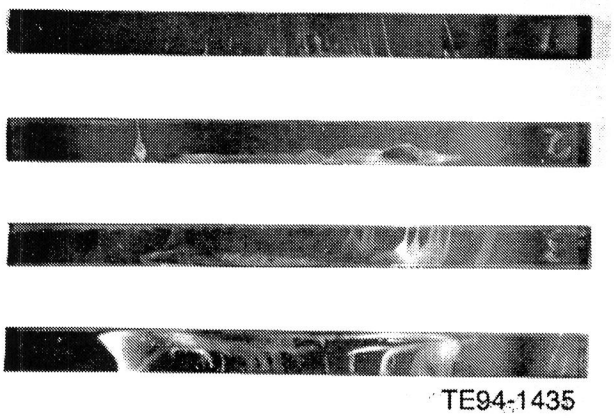


*Figure 3-6. NT230 SiC after exposure in burner rig at 1540°C (2800°F) for 5 hr in Mach 0.3 gas.*

**Dow Chemical Silicon Nitride.** Evaluation of the material strength characteristics was conducted for three Dow Chemical silicon nitrides (designated materials C, D, and E). The test specimens were sectioned from billets. The three silicon nitride materials received from Dow Chemical for evaluation were material C (hot pressed), material D (cold isostatic pressed (CIP'ed) and pressureless sintered), and material E (CIP and hot isostatic pressed [HIP'ed]). Material C is a high temperature creep resistant silicon nitride. Material D is a lower temperature silicon nitride composition tailored for low temperature strength, high fracture toughness, and densification by pressureless sintering. Material E is a high temperature silicon nitride with recrystallized grain boundary phases to improve the elevated temperature properties.

The strength characteristics of Dow Chemical silicon nitride material C were evaluated. Test specimens were sectioned from a billet fabricated by hot pressing. All specimens were evaluated with a longitudinally ground tensile surface condition. The average density of the material was 3.245 g/cc (0.117 lb/in.$^3$). The average room temperature fracture strength measured 804.13 MPa (116.63 ksi) with a Weibull modulus of 16.0. The typical fracture origins were small pores and iron-containing inclusions, as shown in Figure 3-7. The strength at a temperature of 1000°C (1832°F) averaged 481.25 MPa (69.80 ksi), with strengths of 515.52 MPa (74.77 ksi) at 1150°C (2102°F), 557.30 MPa (80.83 ksi) at 1250°C (2282°F), and 490.90 MPa (71.20 ksi) at a temperature of 1370°C (2500°F). The fracture origins of the specimens tested at elevated temperature were typically nondescript surface flaws.

The fracture toughness of the Dow Chemical silicon nitride material C measured 8.3 MPa-m (7.6 ksi-in.), as measured using the single-edged notched beam (SENB) method.

Material D is a lower temperature silicon nitride composition tailored for low temperature strength, high fracture toughness, and densification by pressureless sintering. The total amount of sintering additive in this material is 6%. In the current version of this material, no recrystallization of the grain boundary phase

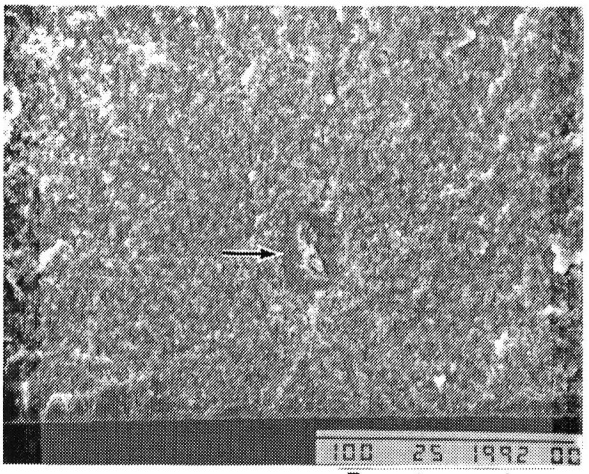


*Figure 3-7. Typical fracture origin (iron-containing inclusion) observed in Dow Chemical silicon nitride material C.*

is conducted, although Dow is studying various techniques to improve the refractoriness of this composition. The microstructure of this material, shown in Figure 3-8, consists of relatively long (10-50 micron) tabular β-$Si_3N_4$ grains with an aspect ratio of approximately 10 dispersed in a network of relatively equiaxed grains. The in-situ growth of the β-$Si_3N_4$ grains is responsible for the high fracture toughness of this material. The average density measured 3.229 g/cc (0.117 lb/in.$^3$).

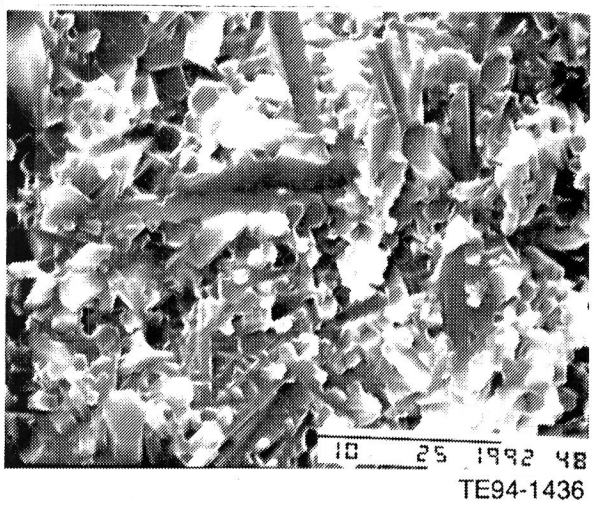


*Figure 3-8. Microstructure of Dow Chemical silicon nitride material D.*

Test specimens were sectioned from a billet fabricated by CIP. All specimens were evaluated with a longitudinally ground tensile surface condition. The average room temperature fracture strength measured 798.46 MPa (115.81 ksi) with a Weibull modulus of 13.6. The typical fracture origins were surface flaws and small surface and internal pores, as shown in Figure 3-9. The strength at a temperature of 1000°C (1832°F) averaged 484.92 MPa (70.33 ksi), with strengths of 408.24 MPa (59.21 ksi) at 1150°C (2102°F), 244.09 MPa (35.40 ksi) at 1250°C (2282°F), and 196.22 MPa (28.46 ksi) at a temperature of 1370°C (2500°F). The fracture origins of the specimens tested at an elevated temperature were nondescript surface flaws. The maximum allowable use temperature for this material would appear to be approximately 1000°C (1832°F) without optimization of the amorphous grain boundary phase. Both of the other Dow Chemical silicon nitride materials have superior elevated temperature strength characteristics, with maximum use temperatures approaching 1370°C (2500°F).

The fracture toughness of the Dow Chemical silicon nitride material D measured 7.8 MPa-m (7.1 ksi-in.), as measured using the SENB method. This high fracture toughness value is a result of the acicular β-$Si_3N_4$ grains, formed by in-situ conversion of the α-$Si_3N_4$ grains to β-$Si_3N_4$.

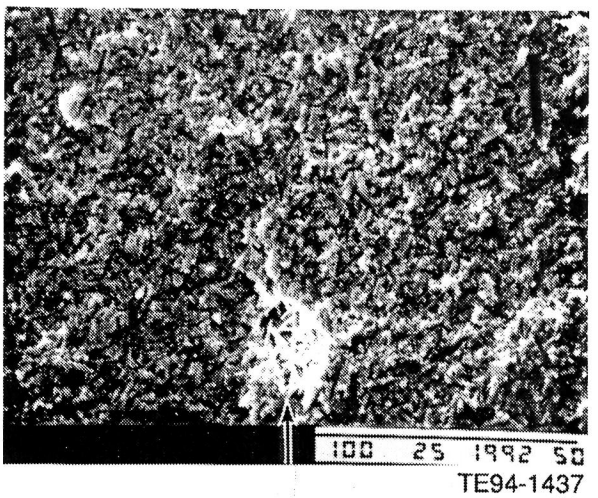


*Figure 3-9. Typical fracture origin (internal pore) observed in Dow Chemical silicon nitride material D.*

Evaluation of the strength characteristics of Dow Chemical silicon nitride material E was also conducted. Test specimens were sectioned from a billet fabricated by CIP followed by HIP'ing. All specimens were evaluated with a longitudinally ground tensile surface condition. The average density measured 3.206 g/cc (0.116 lb/in.$^3$). The average room temperature fracture strength measured 720.84 MPa (104.55 ksi) with a Weibull modulus of 10.2. The typical fracture origins were small pores and iron-containing inclusions, as shown in Figure 3-10. The strength at a temperature of 1000°C (1832°F) averaged 704.09 MPa (102.12 ksi), with strengths of 721.39 MPa (104.63 ksi) at 1150°C (2102°F), 697.33 MPa (101.33 ksi) at 1250°C (2282°F), and 480.70 MPa (69.72 ksi) at a temperature of 1370°C (2500°F). The fracture origins of the specimens tested at an elevated temperature were nondescript surface flaws. In addition, the material tested at 1370°C (2500°F) was observed to have a relatively thick oxide layer that formed on the tensile surface during the relatively short exposure of the strength testing.

The fracture toughness of the Dow Chemical silicon nitride material E measured 7.8 MPa-m (7.1 ksi-in.), as measured using the SENB method.

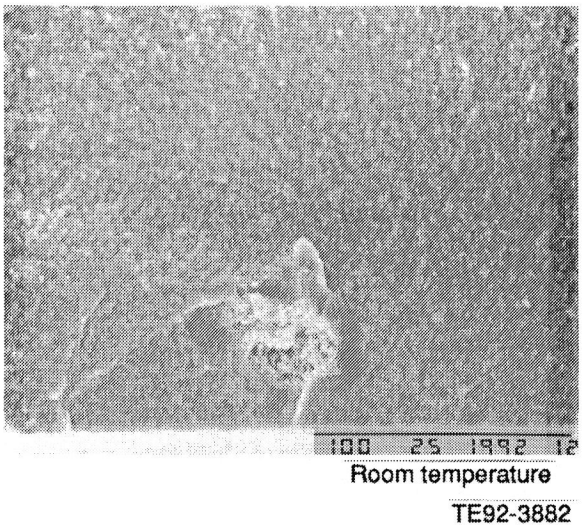


*Figure 3-10. Typical fracture origin (pore surrounded by iron-rich region) observed in Dow Chemical silicon nitride material E.*

Both silicon nitride materials C and E have strength and fracture toughness characteristics that would make them attractive for ATTAP ceramic components.

**DuPont/Lanxide $Al_2O_3$/SiC Particulate Ceramic Composite.** Evaluation of the material strength characteristics of DuPont/Lanxide alumina with SiC particulate reinforcement was conducted during this reporting period. This ceramic composite material was fabricated using the directed metal oxidation (DIMOX) process developed by Lanxide. The DIMOX process (Figure 3-11) uses DIMOX reactions of molten metals to grow ceramic matrices of the oxidation reaction products through preplaced filler or reinforcing materials. The material evaluated consisted of an aluminum oxide matrix with SiC particulate reinforcement in approximately a one-to-one ratio. The ceramic composite had about 10% residual aluminum and silicon metal in the open microchannels and locked inside the matrix of the ceramic. The specimens were "passivated" prior to testing, a procedure that involves an alumina wash and subsequent heat treatment to remove the residual metal to a depth of approximately 50 microns. This seals the microchannels and prepares the composite for use and testing to 1482°C (2700°F) with short term exposures to 1649°C (3000°F). The microstructure of the material is shown in Figure 3-12; the light gray larger areas are the SiC particles, while the dark regions correspond to alumina and the white areas to metallic aluminum.

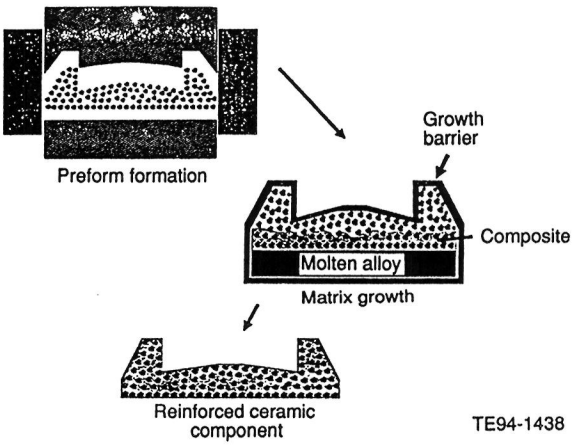


*Figure 3-11. DuPont/Lanxide directed metal oxidation process for composite material fabrication.*

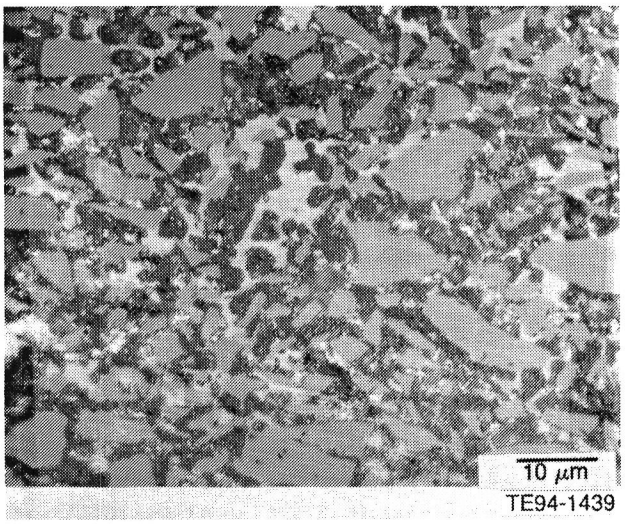


*Figure 3-12. Microstructure of DuPont/Lanxide alumina with SiC particulate reinforcement. Large light gray areas are SiC particles, dark regions are alumina, and light areas are aluminum.*

The results of mechanical characterization of the DuPont/Lanxide $Al_2O_3$/SiC particulate material are summarized in Table 3-II. All strength testing was conducted on specimens conforming to MIL-STD 1942 "B", with a machined surface in tension. The average room temperature strength was 404.82 MPa (58.71 ksi) with a Weibull modulus of 8.8. The typical fracture origins observed in the bars tested at room temperature were nondescript surface flaws. The second most common fracture origins found in the specimens were internal pores, as shown in Figure 3-13. The strength at a temperature of 1000°C (1832°F) averaged 280.82 MPa (40.73 ksi), with strengths of 293.65 MPa (42.59 ksi), 286.68 MPa (41.58 ksi), and 275.31 MPa (39.93 ksi) measured at temperatures of 1150°C

*Table 3-II.*
*Strength characteristics of DuPont/Lanxide $Al_2O_3$ with SiC particulate reinforcement.*

| Temperature, °C (°F) | Strength, MPa (ksi) |
|---|---|
| 25 (77) | 404.82 (58.71) |
| 1000 (1832) | 280.82 (40.73) |
| 1150 (2102) | 293.65 (42.59) |
| 1250 (2282) | 286.68 (41.58) |
| 1370 (2500) | 275.31 (39.93) |

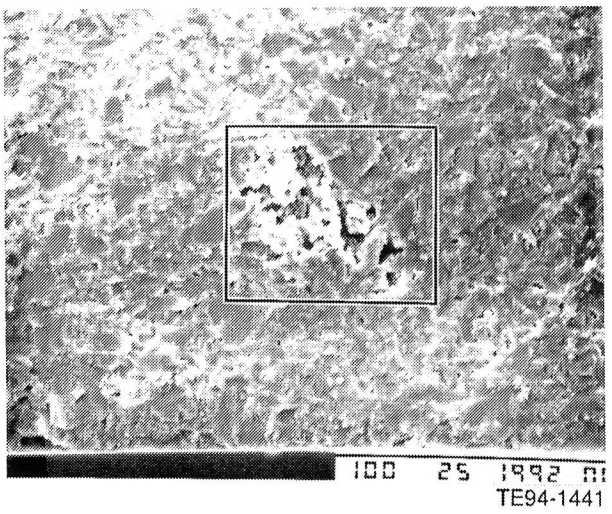


*Figure 3-13. Second most common fracture origin (internal pore) observed in DuPont/Lanxide $Al_2O_3$/SiC material.*

(2102°F), 1250°C (2282°F), and 1370°C (2500°F), respectively. The fracture origins were similar to those observed for the specimens tested at room temperature, i.e., surface flaws.

The room temperature fracture toughness of this material measured 6.3 MPa-m (5.7 ksi-in.) as determined by the SENB. The fracture toughness at a temperature of 1370°C (2500°F) measured 3.5 MPa-m (3.2 ksi-in).

### 3.1.3 Failure Analysis

#### Objective/Approach

Failure analysis details the results of fractographic analyses of ceramic components that experienced unscheduled damage during rig/engine testing and evaluation. Fractographic analysis is one of the most powerful tools used in the failure analysis of an engine or rig tested component. A careful study of the general and detailed features of the topography of a fracture by visual assessment and scanning electron microscopy provides a wealth of information concerning the failure origin and the failure mode(s). Analysis of hardware failures allows the separation of design features from material deficiencies, defects, or nonoptimum fabrication procedures and can suggest appropriate corrective measures.

## Accomplishments/Results

- Fractographic analysis of a Norton/TRW NT154 20-blade gasifier rotor (P/N 5-80598, S/N 5S) was conducted. The rotor had been run in the hot gasifier rig S/N 14, BU 7. The rotor failure originated at a deep cut created during the balance stock removal.
- Fractographic analyses of the Kyocera SN252 gasifier rotor (P/N 5-66946, S/N 5K12) and scroll (P/N 5-80553, S/N 0001-1) were conducted. The parts had been run in the durability test in hot rig S/N 14, BU 9.
- Failure analysis of the gasifier assembly C1, which contained a Kyocera SN252 15-blade rotor (P/N 5-66946, S/N 5K13), a Kyocera SN252 scroll (P/N 5-80553, S/N 2), and CBO SiC vanes (P/N 5-80556), was conducted. The assembly had been run in the hot rig S/N 12, BU 37. The gasifier assembly failed by foreign object damage (FOD) from the broken pieces of the combustor.
- Fractographic analysis of a CBO thick wall SiC combustor (P/N 5-80583, S/N FX79406) was conducted. The combustor had been tested in the hot rig S/N 12, BU 38 and 39. The failure originated at subsurface pores located at the inlet neck area.
- Fractographic analysis of the Norton/TRW NT154 20-blade gasifier rotor (P/N 5-80598, S/N 6F) was conducted. The rotor had been tested in the hot rig S/N 14, BU 22. The rotor was released from the shaft during the testing.
- Failure analysis of the gasifier assembly C1 was conducted. The assembly contained the Kyocera SN252 20-blade rotor (P/N 5-67200, S/N 5K21) and the Kyocera scroll (P/N 5-81154, S/N KX59815) and had been tested in the durability test.

## Discussion

**Hot Rig S/N 14, BU 7.** The gasifier assembly C3 composed of a Norton/TRW NT154 silicon nitride 20-blade rotor and Norton/TRW NT230 silicon carbide scroll was tested in the preparation for durability testing. The rotor burst at 0.4 hr at the peak condition of 1305°C TIT and 97.5% N1 speed. Inspection of the origin area showed that the fracture originated at the edge of the balance stock removal area where rough deep cuts existed, Figure 3-14. The failure origin was located at the aft side hub surface. Figure 3-15 shows the scanning electron microscope micrographs of the origin area. According to the fracture mirror size analysis, the fracture strength was 22 ksi, which was lower than the material's test bar strength of 76.5 ksi at 1000°C.

**Hot Rig S/N 14, BU 9.** The Kyocera SN252 gasifier assembly C1 (except for the GTE PY6 vanes) was tested for the durability schedule. Peak test condition was at 1372°C and 100% N1. The assembly was found broken after 186.1 durability hours. Figure 3-16 shows the post test condition of the gasifier assembly. The rotor fracture origin was at the forward hub face radius, as shown in Figure 3-17. The origin was

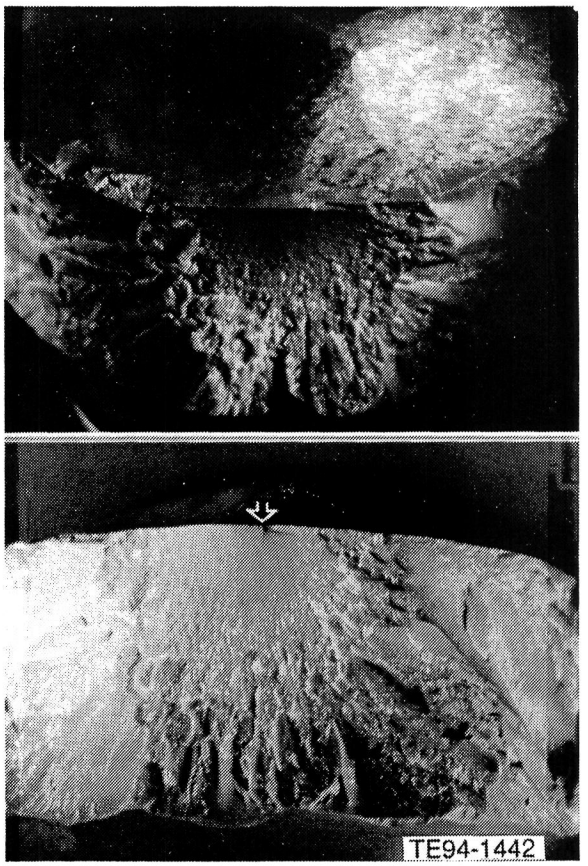


*Figure 3-14. Two views of the gasifier rotor's fracture origin.*

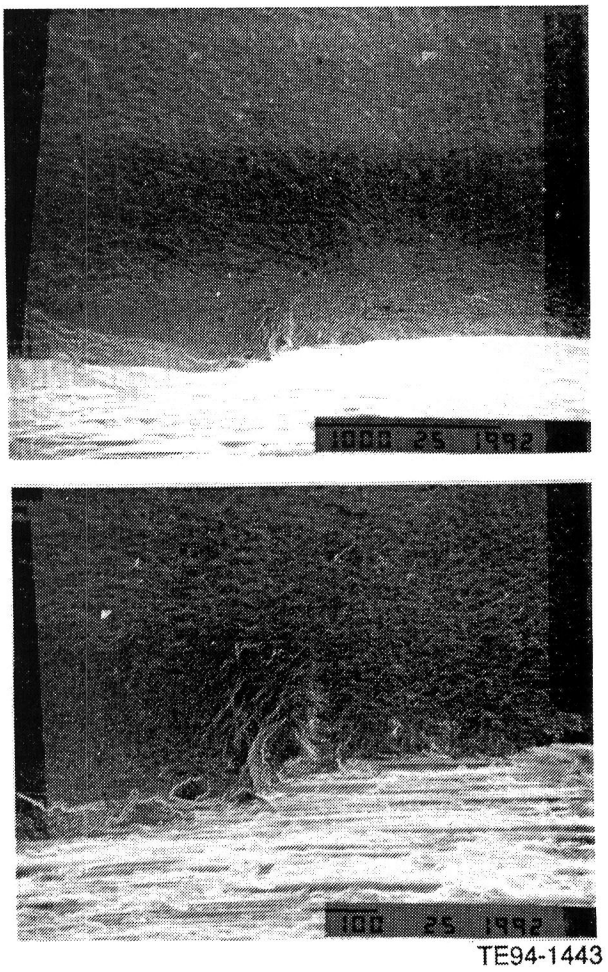


*Figure 3-15. Scanning electron microscope fractographs of the rotor origin area and adjacent hub face.*

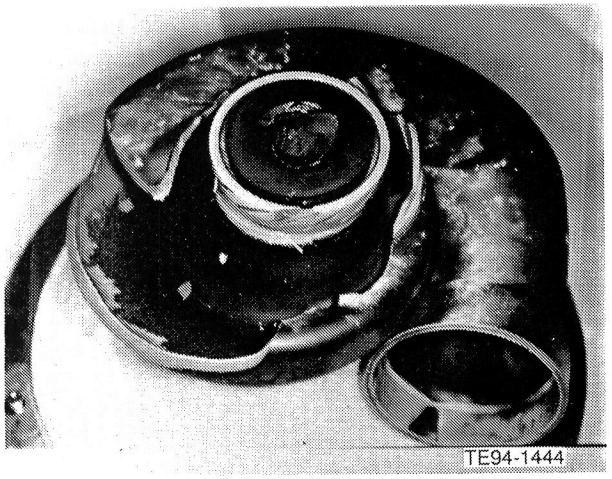


*Figure 3-16. Final condition of the remaining portion of the gasifier assembly.*

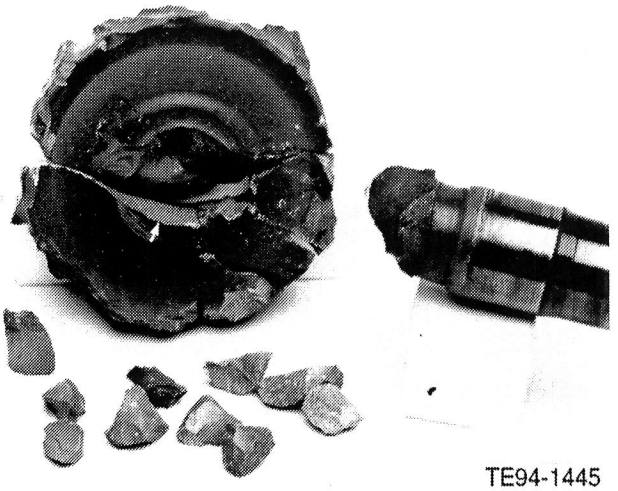


*Figure 3-17. Reconstructed rotor and stub shaft (the arrow points to the rotor fracture origin).*

a large and long grain of silicon nitride, Figure 3-18. The fracture strength calculated from the fracture mirror radius was 78 ksi, which agreed well with the material test bar strength of 73 ksi at 1000°C. The shroud and vane pocket region of this scroll were broken into small pieces; the primary fracture could not be located. The scroll had preexisting cracks at three vane pockets, but inspection showed that none of the preexisting cracks progressed and caused the failure. The fracture of the rotor, scroll, and other parts were secondary events. The exact cause of the assembly failure could not be determined.

**Hot Rig S/N 12, BU 37.** A set of new CBO silicon carbide gasifier vanes was tested with the Kyocera rotor and scroll by running the durability schedule. While the rig was on the third durability schedule (6.4 hr), it suffered a failure. The peak test temperature was 1371°C.

Post test inspection revealed the Lamilloy®* combustor body had a distressed area of roughly 2.5 x 2 in. with 2 coin-size holes caving in adjacent to a small dilution hole (Figure 3-19). Another odd shaped hole (1.5 x 0.5 in.) was located directly downstream near the big dilution hole. Figure 3-20 shows oxidation and melting occurred at the outside wall adjacent to

* Lamilloy is a registered trademark of General Motors Corporation.

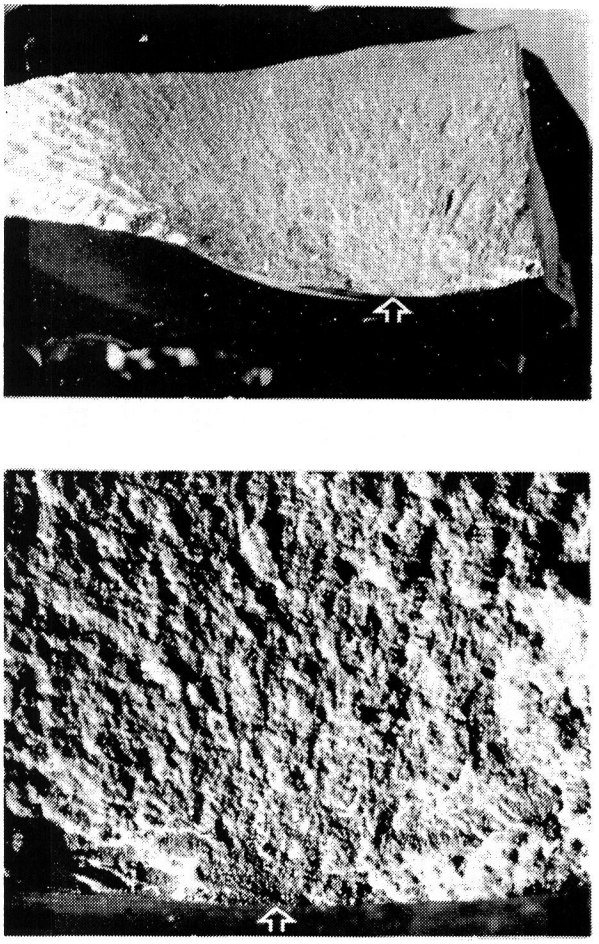

TE94-1446

*Figure 3-18. Rotor fracture origin.*

the distressed area. The oxidation was more severe on the inside wall than on the outside wall.

More than a dozen pieces of broken combustor wall were recovered at the regenerator cavities. Investigation showed that portions of the molten combustor body had splashed on gasifier components such as the scroll inlet (Figure 3-21), the leading edge of the rotor blades, and the convex side leading edge of the vane (Figure 3-22). It was concluded that melting and oxidation occurred at local spots on the Lamil-loy combustor body and the gasifier module was failed by FOD from the broken pieces of the combustor body.

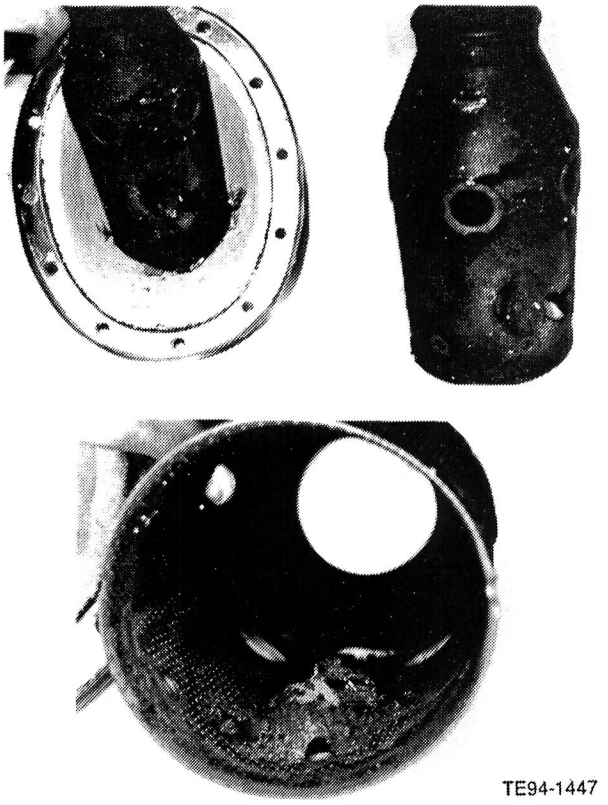

TE94-1447

*Figure 3-19. Post test condition of the combustor body.*

**Hot Rig S/N 12, BU 38 and 39.** The CBO SiC combustor with a 4 mm thick wall was proof tested in an all-metallic gasifier. The test condition was 1075°C TIT and 93% N1. Total part time was 1.2 hr.

Post test inspection revealed the combustor had cracked into multiple pieces (Figure 3-23). The primary fracture origin was located at the outside diameter of the neck of the inlet. The origin consisted of two elongated pores lying just 0.005 in. below the surface (Figure 3-24). The estimated fracture stress was less than 16.9 ksi.

**Hot Rig S/N 14, BU 22.** The Norton/TRW NT154 rotor and NT230 scroll were proof tested for the durability test. The C5 assembly failed after 0.3 hr at a speed of 65%.

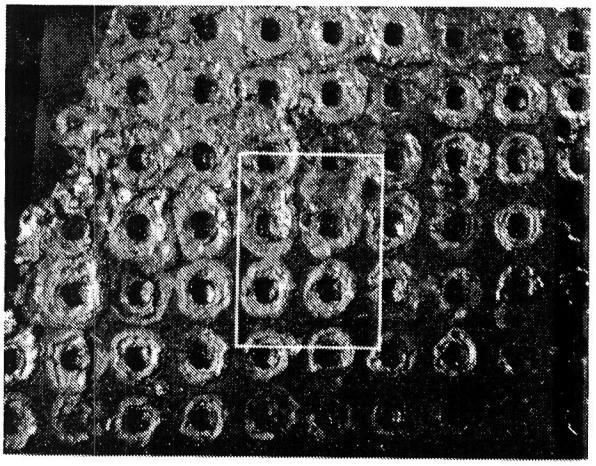

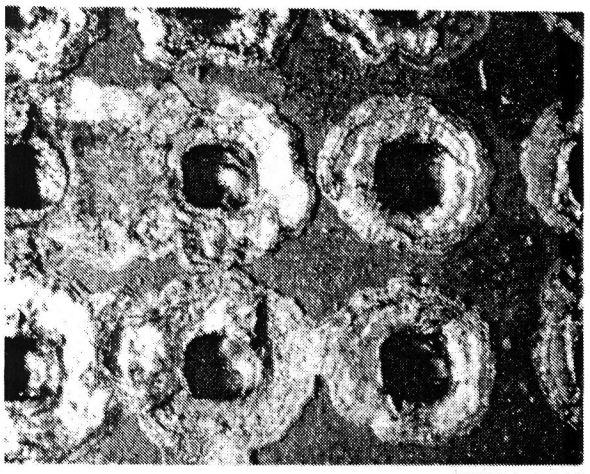

TE94-1448

*Figure 3-20. Outside surface of the combustor body near one coin-size hole.*

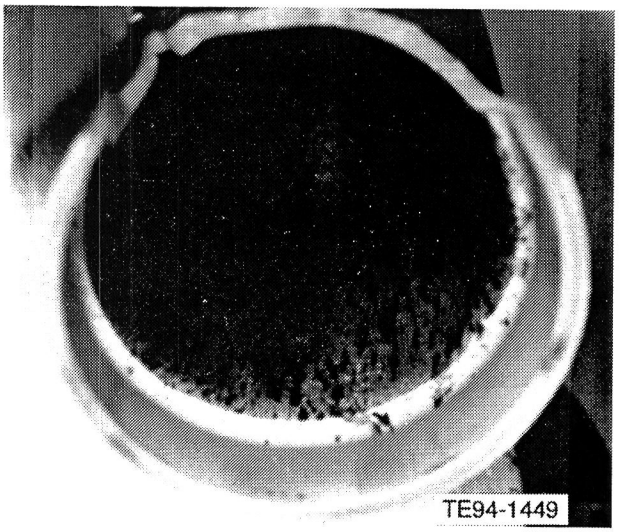

TE94-1449

*Figure 3-21. Condition of the inside surface of the scroll at the combustor outlet. The inside surface was splashed with molten metal from the combustor body.*

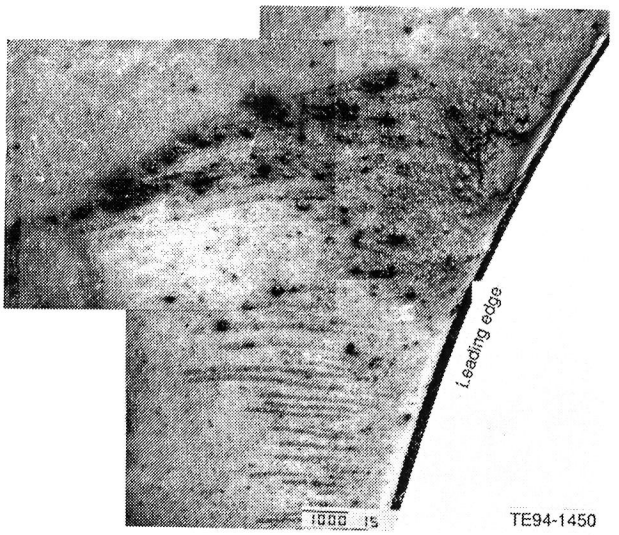


*Figure 3-22. Scanning electron micrograph of the convex side of a vane. Flow lines of deposits show the charging effect in the SEM.*

Inspection revealed that the rotor was released from the rotor shaft during the testing. The free flying rotor then broke the shroud and the cross key of the scroll. The impact also broke off all rotor blades (Figure 3-25) and the stub shaft.

**Hot Rig S/N 14, BU 24.** The durability testing of the gasifier assembly C1, composed of a Kyocera SN252 scroll and a Kyocera SN252 20-blade rotor, lasted 267.7 hr when the assembly failed. Post test inspection revealed the following:

- The impeller sagged and a gap existed between the impeller and the shroud.
- The impeller rubbed the shroud; the impeller was rubbed at the inducer tips at one side and the exducer tips at the other side; the rubbed tip smeared to both sides of the tip, which indicated the rub was a sudden impact action; the exducer rub mark on the shroud was heavy and located on one side.
- The rotor blades fractured at different heights indicative of secondary fractures; the rotor shaft was scored through 120 deg just outside the aft carbon seal by the seal carrier and through 60 deg at the aft end by the heat shield.


*Figure 3-23. Failed combustor showing crack propagation directions (small arrows). The origin is marked by the large arrow, and the numbers indicate the three inlet cracks.*

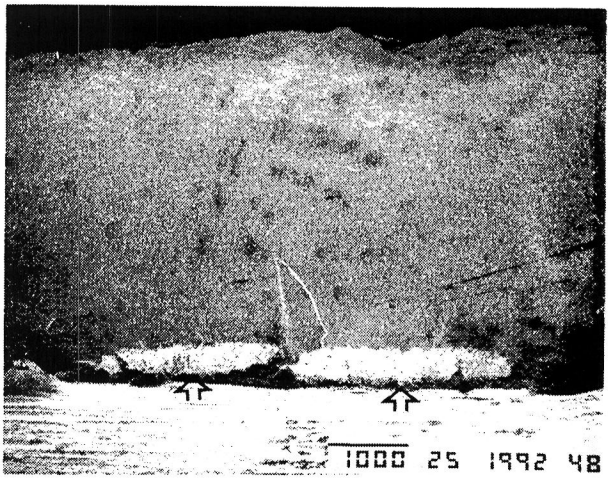


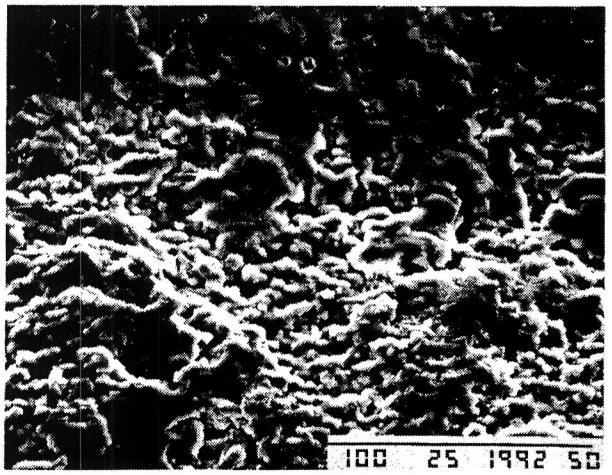


TE92-3885

*Figure 3-24. Scanning electron micrograph of the fracture origin area (hollow arrows).*

- The shroud section broke into large segments and stuck in the dummy power turbine nozzle as a whole; the scroll body came out in one piece; there were two heavy rub marks on the aft shroud; the heavier one was not observed after 202.8 hr of running.
- The shroud fracture surface was covered by the rotor material, indicating that shroud fracture preceeded the rotor impact.

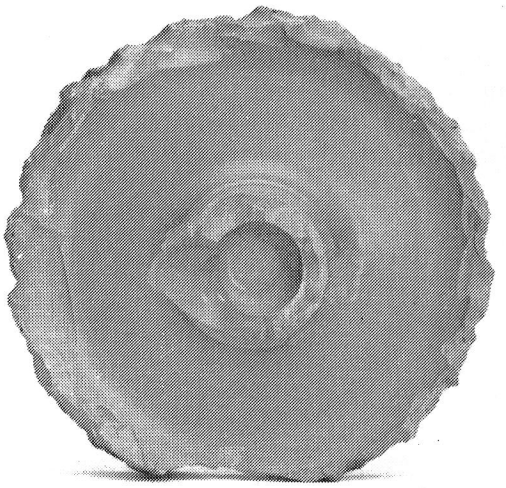

TE94-1451

*Figure 3-25. Final condition of the gasifier rotor (stub shaft side).*

- The end of the bolt at the 5 o'clock location in the aft-side view was sheared off and the adjacent bolts were twisted.
- A portion of the gasket was gone from the 3 o'clock to the 9 o'clock locations.

In summary, the rub or distress on the stationary components occurred at the lower half of the assembly and centered around 5 o'clock in the aft-side view. One scenario is that hot air in the seal carrier gasket area evaporated half the gasket and thermally distorted the carrier flange. The distress shifted the shroud and caused the shroud rub. The fracture of the shroud might have impacted the impeller and rubbed the compressor shroud.

## 3.2 CERAMIC COMPONENT PROCESS DEVELOPMENT AND FABRICATION

### 3.2.2 Schuller International

#### Objective/Approach

Efforts at Schuller are aimed at developing an injection-moldable insulation capable of low-cost high-volume production for automotive gas turbines. The approach is to modify the insulation material system for improved injection

molding properties while developing the injection molding process for both simple and complex engine components. In addition to the development of the molding process, several other developmental items are being addressed, including insulation/metal hardware bondability, erosion resistance, and nonrespirable materials.

## Accomplishments/Results

- High levels of cleaning and mechanical processing of the fiber are necessary for the optimization of molding characteristics.
- The insulation formulation established previously provides the best balance of molding and drying shrinkage.
- Injection molded insulation test samples have the same thermal conductivity as hand molded test samples.
- Shelf life limit of one of the raw materials was established.
- The wet insulation is best made by adding the liquid components consecutively with no delay between the adding of the different fluids.
- The injection molding material exhibited marginal drying shrinkage after three days.
- Both the simple and complex piece molding processes appear to be viable high volume injection molding candidates.
- The insulation formulation using a low level of fiber processing is ideal for hand molding.
- Increased levels of fiber processing produce injection moldings that exhibit satisfactory surface finish and low levels of drying shrinkage.
- The insulation formulation using a 600 level of fiber processing is best for injection molding.
- A cyclic durability test rig, including a burner system and insulation sample holder, was designed.
- The design of pilot-line molding with AEROQUIP was completed and trial molding equipment was procured.
- AEROQUIP is proceeding with the fabrication of the pilot-line gasifier housing molding.
- 35 kilograms of cleaned fiber have been processed at the 600 level for the pilot-line gasifier housing molding trial at AEROQUIP.
- Fiber emissions were measured by sampling the exhaust of an operating turbine.

## Discussion

Batches of insulation were prepared by using Level 3 fiber cleaning, followed by mechanical processing. This improves the moldability of the wet insulation. The insulation formulation component levels were varied and were evaluated for their impact on moldability and drying shrinkage. The previously established formulation yielded the optimum balance of moldability and acceptable drying shrinkage. The most significant impact on moldability was the total water content of the insulation formulation. Varied amounts of the other formulation components resulted in either excessive drying shrinkage or poorer moldability, as evidenced by increased stiffness of the mix or increased softness of the mix.

The thermal conductivity of test samples molded to simulate the rougher surface of injection molded insulation has been determined. The apparent thermal conductivity of these samples is plotted in Figure 3-26 and compared with previously tested samples. In Figure 3-26, the current material is identified as "ROUGH, 25 PCF" and the previously tested materials are identified as "SMOOTH SURFACE, 23 PCF" and "ROUGH SURFACE, 21 PCF." The thermal conductivities of the insulation of the three samples tested are within 15% of the same values within the normal operating range mean temperatures for the insulation.

The pH of four different lots of acid stabilized colloidal silica, still in hand at both MTC and GM/Allison, were determined (Figure 3-27). The pH appears to increase with time and exceeds the manufacturer's specification limit after 9 to 12 months. By monitoring the pH periodically, older material can be discarded so it will not be utilized to mix insulation. Past experience has led to the conclusion that out-of-specification colloidal silica results in higher than desired drying shrinkage and dewatering during molding.

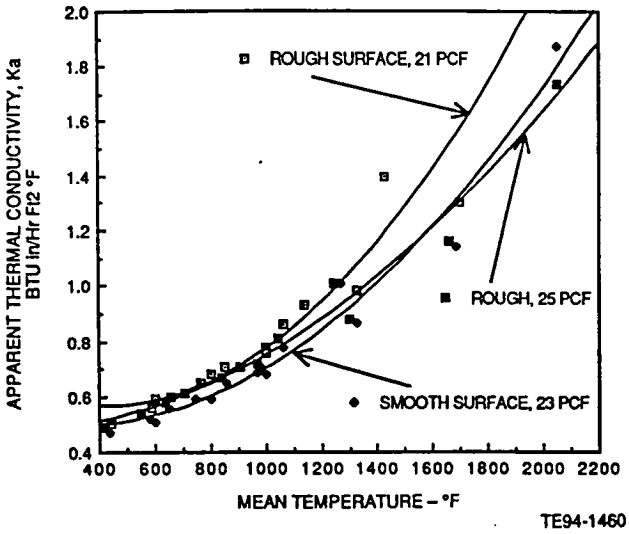


*Figure 3-26. Moldable high temperature insulation thermal conductivity.*

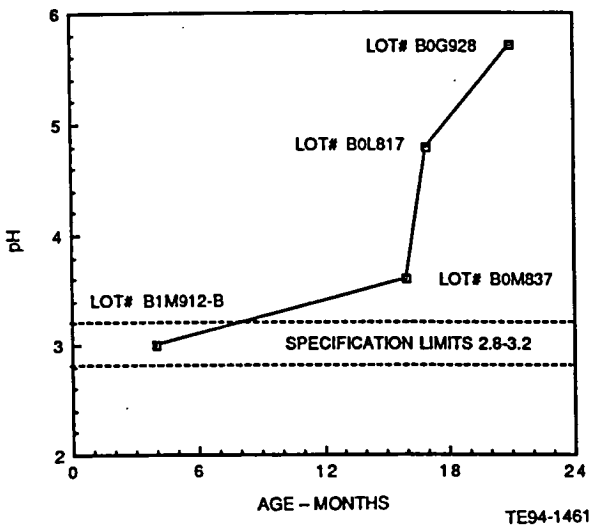


*Figure 3-27. Colloidal silica shelf life response.*

Small and large batches of insulation were prepared using the "NORMAL" or previously accepted mixing procedure with the liquid components added consecutively with no delay. The normal mixing procedure included a five minute "DELAY" between the addition of the liquid components. The "REVERSE" order of addition of the liquid components proceeded with no delay. The normalized drying shrinkage is shown in Figure 3-28 for each of the three mixing procedures. The drying shrinkage is below the maximum acceptable level for the

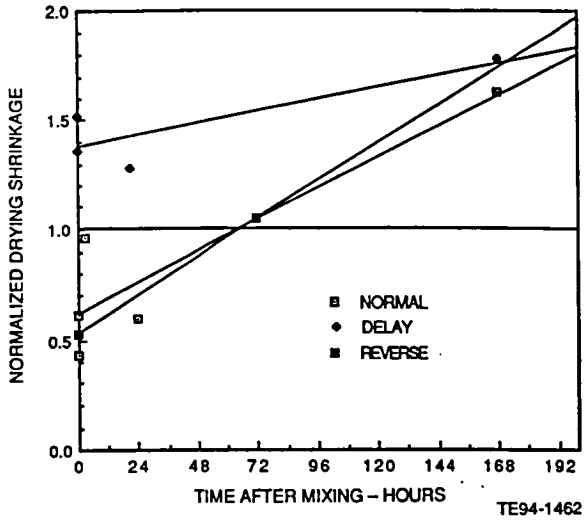


*Figure 3-28. Drying shrinkage after mixing.*

normal procedure and for all times for the delay mixing procedure. The reverse mixing procedure appeared to be less sensitive to mixing than the normal mixing procedure. The reverse mixing procedure has been established as the new standard procedure.

Large mixer batches of insulation were prepared using fiber at increasing levels of fiber processing to determine the best level of processing for hand molding. The drying shrinkage measurements of 6 in. x 1 in. x 1/2 in. bars and 6 in. x 2.7 in. x 1 in. blocks are shown in Figures 3-29 through 3-32 for fiber processing level ranging from 0 to 1500 and for increased fiber content at the lower fiber processing levels.

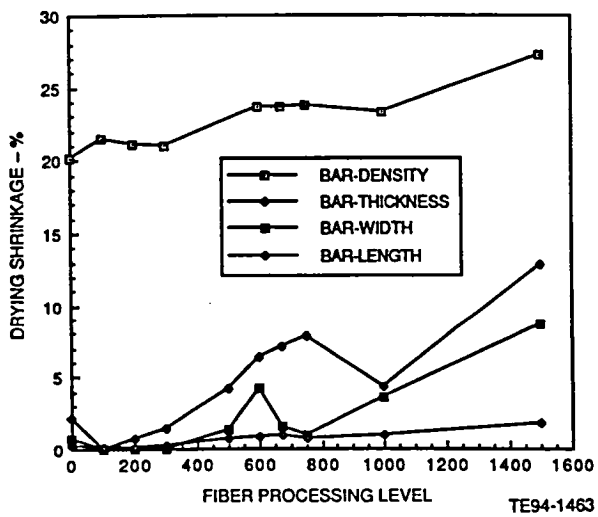


*Figure 3-29. Fiber processing 6 in. x 1 in. x 1/2 in. bar drying shrinkage.*

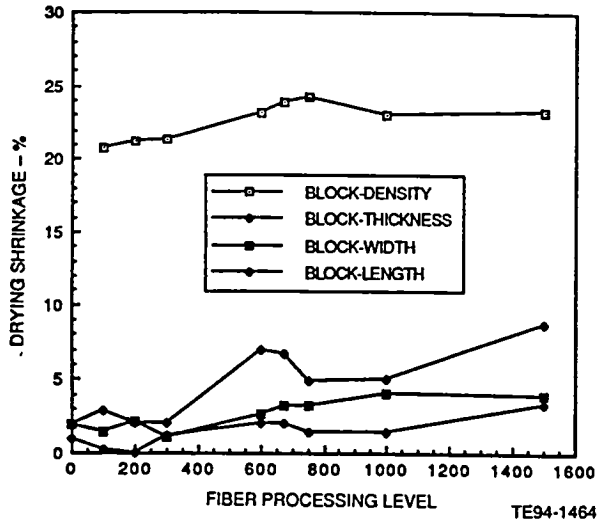


*Figure 3-30. Fiber processing 6 in. x 2.7 in. x 1 in. bar drying shrinkage.*

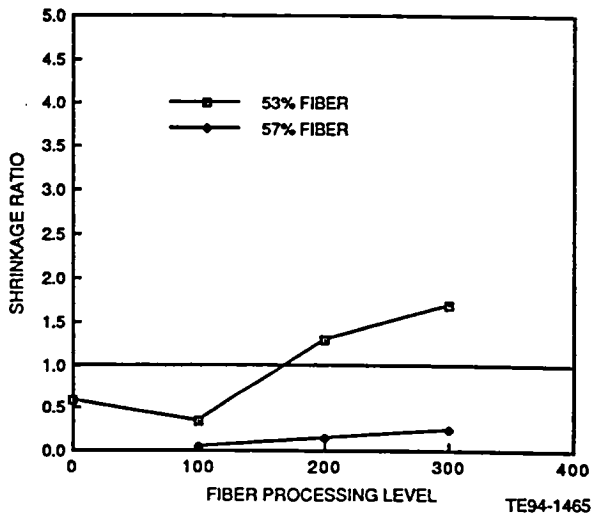


*Figure 3-31. Fiber processing for hand molding 6 in. x 1 in. x 1/2 in. bar mold drying shrinkage.*

The higher fiber processing levels indicate progressively shorter fiber lengths as a result of longer processing time and greater agitation. As the fiber processing level increased, the texture of the wet insulation became smoother, but the drying shrinkage also increased. The best balance of wet insulation smoothness and low drying shrinkage was at a fiber processing level of 200 and at 57% fiber.

Gasifier housings (simple piece) were molded using fiber processed at the higher levels (600 to 1500) prepared as shown above. The drying shrinkage was measured by comparing the dry

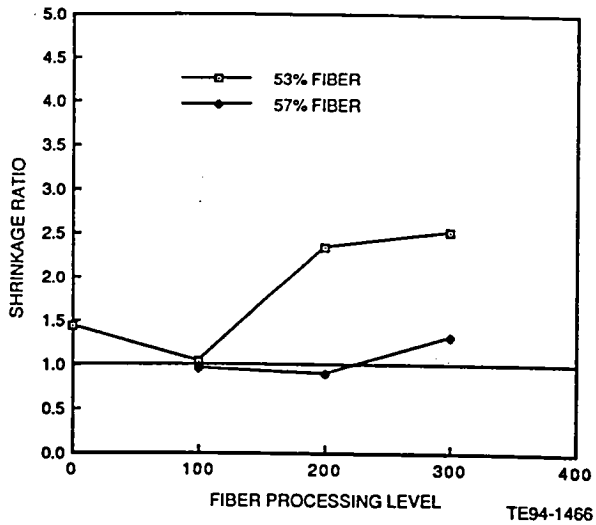


*Figure 3-32. Fiber processing for hand molding 6 in. x 2.7 in. x 1 in. block mold drying shrinkage.*

contour of the molded piece with the contour of a rigid plastic mold liner. The rigid mold liner was marked at 12 radial locations and at 5 elevations. The marked mold liner and the 1000 level fiber processing gasifier housing molding are shown in Figure 3-33.

After molding and drying, the distance from the mold liner to the dry insulation was measured at all locations. The average of the distances measured from the mold liner to the dry insulation for the fiber levels is shown in Table 3-III.

*Table 3-III.*
*Fiber processing level drying deviation.*

| Fiber processing level | Average drying deviation (in.) |
|---|---|
| 500 | 0.054 |
| 600 | 0.042 |
| 675 | 0.097 |
| 750 | 0.060 |
| 1000 | 0.076 |
| 1250 | 0.136 |
| 1500 | 0.167 |
| 1500 (10% less water) | 0.139 |
| 1500 (10% less water, more fiber) | 0.121 |
| 1500/200 (80%/20%) | 0.087 |

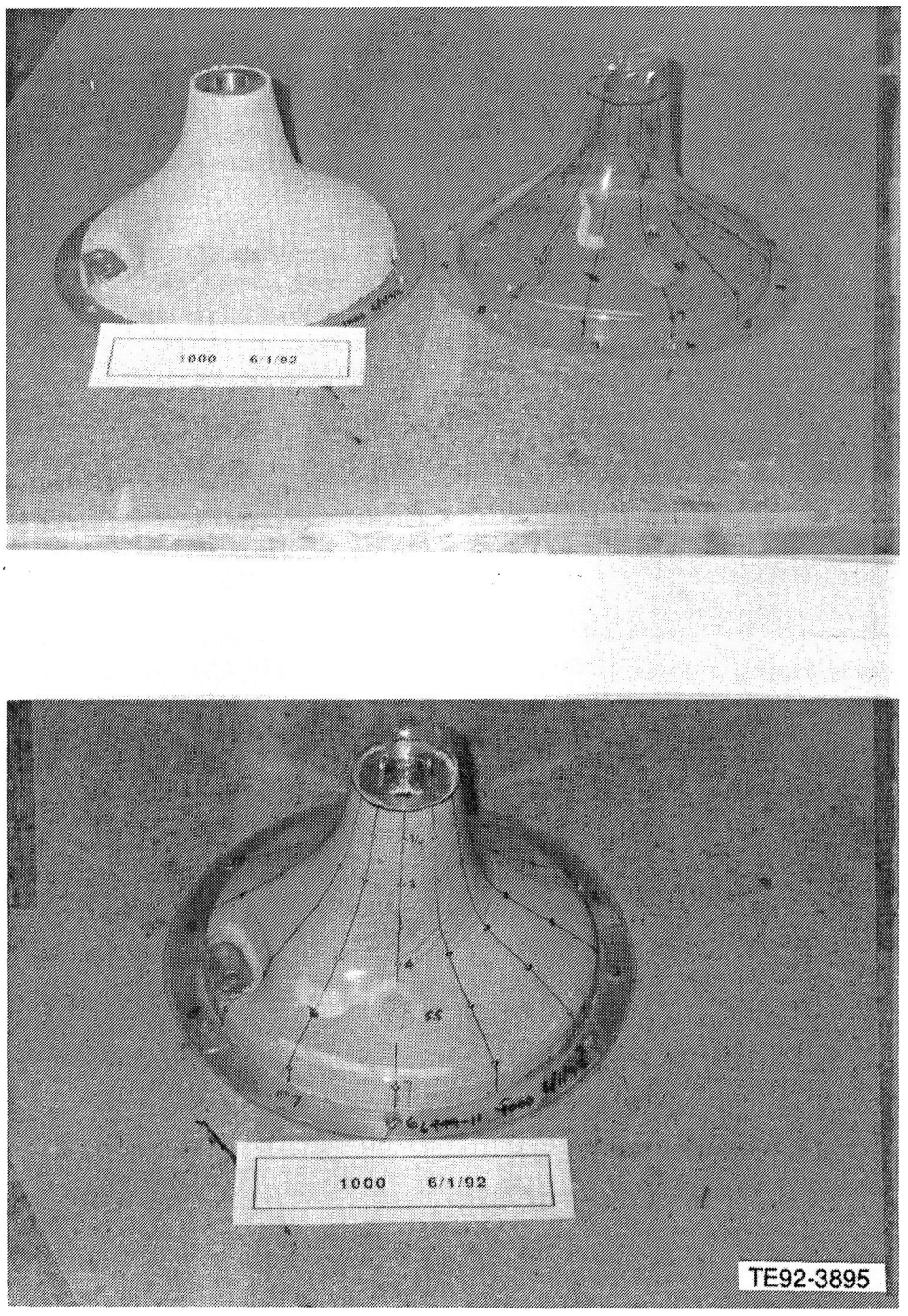


*Figure 3-33. Insulated gasifier housing and marked mold liner for 1000 level drying shrinkage measurement.*

The best drying shrinkage was at the 600 fiber processing level. Overall, the higher fiber processing levels resulted in better surface finish, but much higher drying shrinkage. Figures 3-34 and 3-35 show the 600 level and 1500 level moldings. The excessive shrinkage of the 1500 level molding resulted in the surface fissures shown. Modifications of the formulation at the 1500 fiber processing with less water, more fiber, and the addition of longer fiber (200 level) resulted in reduced drying shrinkage, but with less surface finish smoothness.

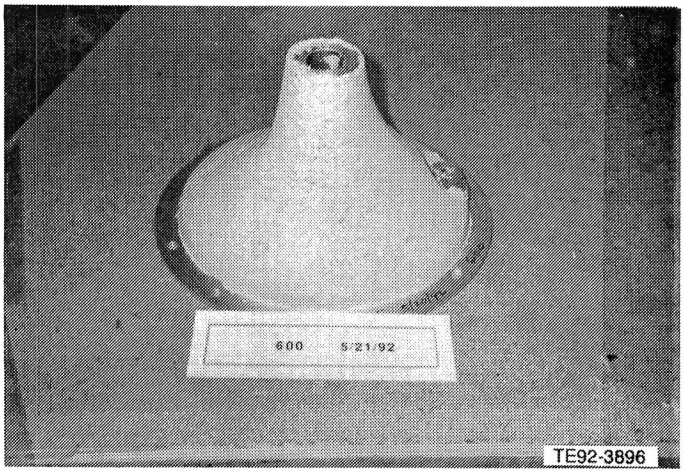


*Figure 3-34. Gasifier housing insulated at the 600 fiber processing level.*

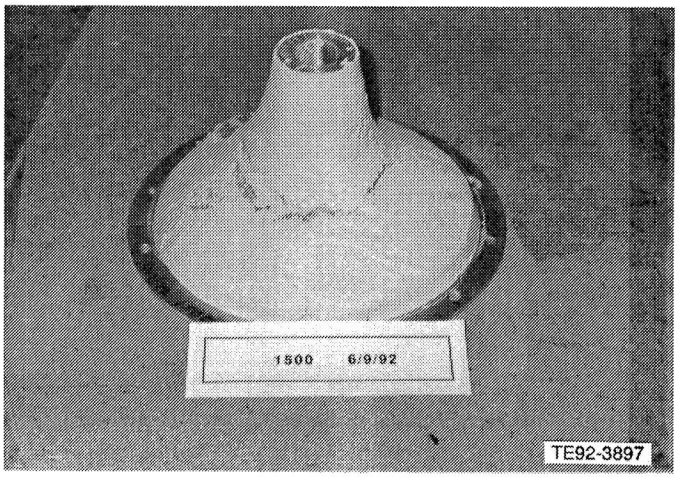


*Figure 3-35. Gasifier housing insulated at the 1500 fiber processing level.*

Larger mixer batches of insulation were prepared using fiber at various levels of fiber processing to determine the best level of processing for injection molding. Gasifier housings were injection molded to observe mold fill out, surface finish, and overall drying shrinkage. The 600 level fiber processing, with minor changes in total water content, resulted in the best combination of mold fill out and surface finish with acceptable drying shrinkage. Deviations from as-molded dimensions upon drying averaged less than 0.04 in. Mold fill out was complete with some "popcorning" or rough surface finish.

Molding of the simple piece gasifier housing has been demonstrated using plastic film mold liners for mold release. Molding of the simple piece turbine engine housing has been demonstrated using metal inserts that are near net shape.

AEROQUIP Corp. will complete the design, fabrication, and operation of a pilot-line molding operation for the molding of 25 gasifier housings. Sufficient quantities and the other raw materials are at Schuller and will be sent for the molding trial.

A burner system has been designed to expose the insulation to conditions expected in the operating engine. The burner will expose the insulation to about 980°C (1800°F) with an impingement velocity of about 250 ft/sec for 15 sec every 60 sec. The exposure is to last for 100,000 cycles or failure, whichever occurs first. The test design includes a high velocity natural gas burner, an air/fuel ratio control valve, air operated control solenoids, timers and counters, safety shutoffs, and a water-cooled insulation mounting fixture. Temperatures will be monitored during the exposure at the hot and cold surfaces of the insulation and in the water-cooled fixture. Observations of the exposed surface of the insulation will indicate the possible need for erosion resistant surface treatments. If needed, these surface treatments can be applied and tested with the system.

Engine exhaust sampling was conducted for normal engine operating conditions and for failure of insulation within the engine. Sampling was performed at GM/Allison by the Schuller Industrial Hygiene Laboratory. The failure of the insulation was simulated by injecting the

equivalent of one cubic inch of dry, crumbled insulation into the burner section of the engine. This simulates the ingestion of insulation as might occur if a piece were to become dislodged while the engine is operating at near-full power. The exhaust gases were sampled for a four hour period before failure and for a four hour period after failure.

### 3.2.4 Corning

#### Objective/Approach

The objective of this task is the development of the required materials and processing technology, leading to the development of a reliable, low cost, high performance, one-piece extruded ceramic regenerator disc capable of operating for full life in an automotive gas turbine environment at temperatures up to 1150°C (2100°F). The four families of ceramic materials to be investigated are alumino-silicate/lithium alumino-silicate (AS/LAS), magnesium alumino-silicate (MAS [Cordierite]), mullite aluminum titanate (MAT), and zirconium phosphate (NZP).

#### Accomplishments/Results

Corning has continued a major extruded ceramic regenerator development program, begun in late 1991, involving several materials, die concepts, and hub concepts.

- LAS
  - Adequate LAS life was predicted based on sulphur limits established in the 1993 U.S. diesel fuel regulations.
  - An additive providing 3x salt resistance was identified.
  - A technical data search revealed that salt was not a major cause of land based LAS failures in 1970s, as developed by Ford Motor Company.
- MAS
  - Reduced porosity and increased strength of regenerator material was achieved without significantly increased expansion
  - The current EX22 has the best combination of porosity and other properties
  - Adequate strength is demonstrated in cement-lined low cost hubs.
- NZP
  - Properties of several LoTEC NZPs were established.
- Extrusion dies
  - Small square, rectangular, and triangular cell dies were designed, fabricated, and tested.
  - 1500 lb of EX22 MAS and several 100 lb lots of LAS were extruded through a 280 mm (11 in.) (400 cpsi) die to refine the manufacturing process.
  - Experience gained was good enough to justify proceeding directly to development of a large 1100 cpsi die.

#### Discussion

In late 1991, a multiyear regenerator program was initiated with Corning, Inc., to develop a ceramic regenerator. The program consists of two components, materials development and processing development. As mentioned above, the four families of materials being investigated are AS/LAS, MAS, MAT, and NZP. The bulk material properties to be examined are the coefficient of thermal expansion (CTE), porosity, strength, chemical durability, and thermal shock resistance. Materials with promising bulk properties will be extruded into small samples and, after further evaluations, into full-size regenerator disks. The majority of processing development effort will focus on matrix extrusion and die technology. Other processing technologies to be investigated are center hub manufacturing and exterior skin coats.

**Material Development**

*MAS*. During this reporting period a series of material modifications were carried out to examine material porosity, CTE, and modulus of rupture (MOR) strength. Two base MAS materials were used, an original EX-22 MAS (EX-22-O) and a modified EX-22 (EX-22-M). The percentage of Cordierite-2 in the base material was increased in 5% increments from 5% to 50% Cordierite-2. The material properties were measured for each of the compositions.

As the percentage of Cordierite-2 was increased in the base material, the resultant material porosity decreased (Figure 3-36). The resultant material porosity at 5% Cordierite-2 was 23% porosity for the EX-22-O and 25.6% porosity for the EX-22-M. At 50% Cordierite-2, the material porosity had dropped to 13.1% for EX-22-O and 10.4% for EX-22-M.

The CTE increased with the addition of Cordierite-2 in the MAS materials (Figure 3-37). The CTE for the EX-22-O had two significant increases. At 15% Cordierite-2, the CTE increased from 3.2 to 4.6 x $10^{-7}$ m/m°C (1.8 to 2.6 x $10^{-7}$ in./in.°F) as shown in Figure 3-37. At 45% Cordierite-2, the CTE increased from 4.5 to 6.1 x $10^{-7}$ m/m°C (2.5 to 3.4 x $10^{-7}$ in./in.°F). The addition of Cordierite-2 to EX-22-O between 15% and 45% did not significantly affect the resultant material CTE. The CTE variation for the EX-22-M material did not significantly change between 5% Cordierite-2 and 25% Cordierite-2, but the resultant material CTE did vary widely at percentages of Cordierite-2 above 25%.

The MOR strength was measured for the EX-22-O material and was found to increase as the percentage of Cordierite-2 increased. The MOR data for EX-22-O is plotted against the CTE data in Figure 3-38. Increasing the percentage of Cordierite-2 in EX-22-O up to 40% significantly increased the MOR strength without significantly increasing the CTE of the resultant material.

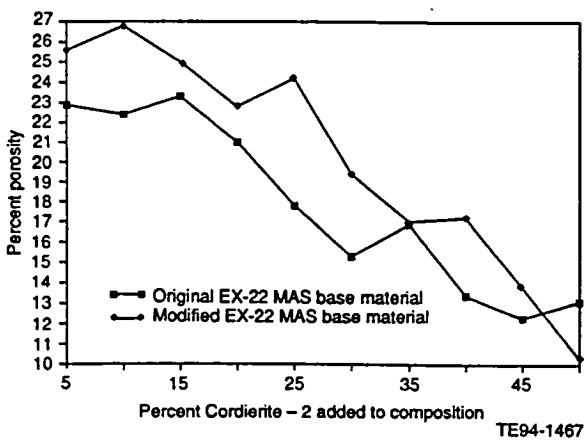


*Figure 3-36. Material porosity versus percent Cordierite-2 in MAS material.*

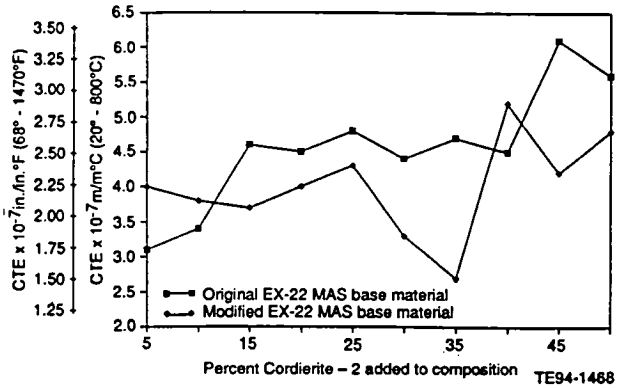


*Figure 3-37. Coefficient of thermal expansion versus percent Cordierite-2 in MAS material.*

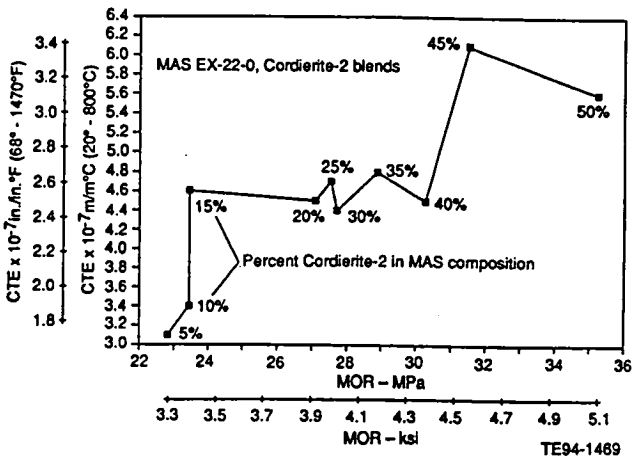


*Figure 3-38. Modulus of rupture strength versus coefficient of thermal expansion for MAS/Cordierite-2 blends.*

Two successful extrusions were made with the 10.4% porosity EX-22-M using a 76 mm (3 in.) diameter die with a cell count of 124 cells per square cm (cpsc) (800 cells per square inch (cpsi)). The fired material was found to have significant shrinkage during firing, and it was speculated that the excess shrinkage would produce problems during the firing of large extruded disks. At this point in the program, the low porosity MAS materials are the backup materials if higher strength materials are required. The primary MAS candidate is EX-22-M, with little or no Cordierite-2 added to the base material.

A series of through wall leakage tests were completed during this reporting period. The wall leakage for a MAS EX-22 matrix, with 54 cpsc (350 cpsi) and a wall thickness of 0.14mm

(0.0055 in.), was measured for a series of seal widths. The matrix sample was sealed at each end by rubber gaskets attached to a metal plate. Air was fed into the center and allowed to bleed out through the walls of the matrix. The leakage air flow rates were found to be quite low and well within regenerator design requirements. At equivalent engine conditions, the through wall leakage is 0.12% of engine air flow.

An LAS and an MAS extruded sample completed 10000 cycles on Allison's cyclic thermal exposure rig, following which the samples were cut up and the MOR was measured. As seen in previous tests, the regenerator material on the air inlet side had a significant loss in strength (Figure 3-39). Currently Corning and Allison are examining exposed samples in an attempt to understand the strength loss mechanism.

*AS/LAS.* The LAS materials were originally developed for the regenerator core but field experience by Ford Motor Company during the 1960s and 1970s found that sulfur and sodium significantly weakened the material. AS materials were developed to eliminate these chemical durability problems. Unfortunately, several of the processing steps in the conversion of an LAS regenerator core to an AS core are costly. Due to this manufacturing cost of AS and lower sulfur levels in current fuels, LAS is again being evaluated as a possible regenerator candidate. With the decreased levels of sulfur in diesel fuels, LAS chemical durability in the presence of sulfur should be sufficient. Figure 3-40 shows LAS regenerator core life as a function of fuel sulfur levels. Decreased 1993 diesel fuel sulphur limits will provide more than 10,000 hr of life where the life requirement for the regenerator for automotive use requires only 3500 hr (100,000 miles). Data points No. 3 and 4 are estimated core life for the 1993 diesel fuel sulfur limit and proposed gasoline regulation. It is concluded that at the 1993 fuel sulfur level, the life of a LAS regenerator disk will not be adversely affected by fuel sulfur levels.

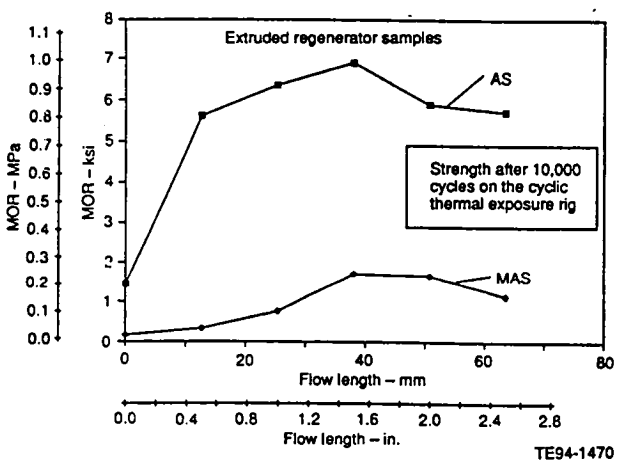


*Figure 3-39. Modulus of rupture strength following thermal cycling.*

Engine consumption of air bound salt and sodium contamination of the fuel are two sources of sodium contamination. Unfortunately, data on intake air salt concentration and sodium fuel concentration are limited. Corning's review of all relevant internal Corning memos, proprietary research reports, some Ford Motor Company memos, and three Ford ERDA reports (a progress report from 1975, and final reports from 1976 and 1980) revealed that sulphur was determined to have caused more problems than sodium. Ford therefore concluded that sodium was not a major cause of land based LAS regenerator failures in the 1970s. Ford never experienced field failures attributable to road salt.

Failures due to sodium salt in marine use were recognized by Corning. A sodium concentration of 0.007 ppm in the inlet air based on worst case General Motors Bermuda seashore data was considered as a requirement. Diesel fuel occasionally has been found to be contaminated with as much as 1 ppm sodium, equivalent to about 0.017 ppm sodium in the inlet air or 0.043 ppm NaCl in the inlet air. No data on road

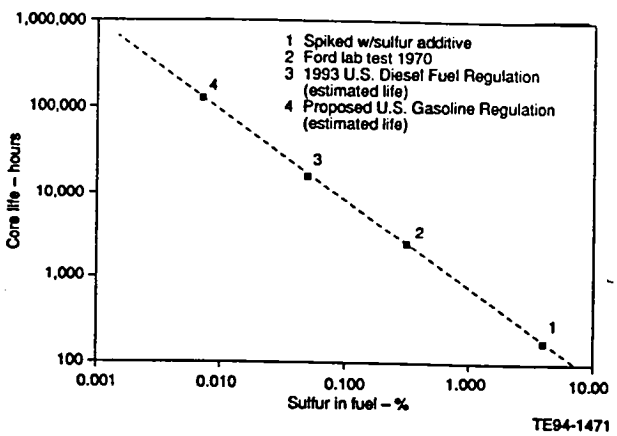


*Figure 3-40. Regenerator core life versus fuel sulfur content.*

salt concentrations have been found. Ford Motor Company ran ten accelerated NaCl injection tests to failure with powdered salt injected into inlet air. The average of these ten failures occurred at 111 hr with a salt-to-inlet air concentration of 1.6 ppm. Assuming an inverse relationship of hours to ppm, the average failure would project a life of 4260 hr with a continuous salt ingestion of 0.042 ppm in inlet air, equivalent to the worst case of 1 ppm sodium found in fuel, a wholly unlikely occurrence. Virtually no possibility exists for land based LAS failure due to seashore salt or salt contaminated fuel, while road salt caused failure is not unknown but occurs infrequently. Nevertheless, Corning has been trying to improve LAS salt resistance. Tests showed that LAS continues to absorb sodium on successive thermal cycles. Salt resistance tests were performed on 27 varied ratios of LAS. All suffered a significant increase in thermal expansion. One of several LAS additives improved salt resistance by a factor of three. Allison plans to run actual LAS regenerator salt resistance tests in an engine test rig.

A number of LAS compositions were developed during this reporting period. The objective of the composition work was to produce a sodium resistant LAS material. Two material approaches were undertaken to achieve greater chemical durability. In the first material approach, the composition LAS ratios were varied, 27 cellular samples were extruded, and the samples were exposed to a salt bath. The salt bath consisted of the following steps:

1. measure sample CTE
2. soak in salt water at 90°C (194°F) for 1 hr
3. dry
4. heat to 800°C (1470°F) for 48 hr
5. rinse
6. dry
7. measure sample CTE

A significant increase in the CTE was found for each of the 27 compositions. The second material approach introduced different additives into the LAS composition. The additive samples were also extruded and exposed to the salt bath. One of the additives was found to produce a minimal increase in the CTE after exposure to salt. The CTE after exposure to this additive composition was $5.7 \times 10^{-7}$ m/m°C, 20°C to 1000°C ($3.2 \times 10^{-7}$ in./in.°F, 68°F to 1832°F.)

LAS is normally produced from separate, pure, costly ingredients. The use of minerals would result in a considerable cost saving. Experiments were initiated to develop LAS directly from minerals rather than refined chemicals. The initial trial of production of LAS from low cost mineral sources was not promising. Alternative low cost chemicals are also being pursued.

Corning melted and ball milled 16,000 lb of LAS to produce a broad band of particle sizes appropriate for extrusion experiments. Progress was made in developing a firing schedule for large LAS extrusions from an 11 in., 400 cpsi die. Progress was also made in reducing the binder for LAS extrusions to reduce cost and firing shrinkage, which lead to distortion.

*NZP.* A literature study was conducted for NZP materials to understand the general material family and to anticipate problems that could occur during material evaluation. Virtually all of the literature contained only studies of the X-ray crystallographic thermal expansions and their relationship to bulk thermal expansion. Very little strength, chemical durability, melting, thermal cycling, or thermal expansion hysteresis data were found in the literature.

During the reporting period, three NZP compositions were received from LoTEC, Inc., in the form of powders. The powders were extruded at Corning and the dried rods were returned to LoTEC for firing. The fired material was returned and property measurements were made. The LoTEC material designations for the three materials were B1, B3, and C1.

Considerable hysteresis in the thermal expansion curve was found after one heating and cooling cycle. All three samples were found to be 150 ppm to 250 ppm shorter after the initial heating cycle. Each sample was then thermally cycled to 1000°C (1832°F), 100 times and the CTE was measured. The resulting CTE data, showing actual expansion curves before cycling and after cycling 100 times to 1000°C, are illustrated in Figures 3-41, 3-42, and 3-43.

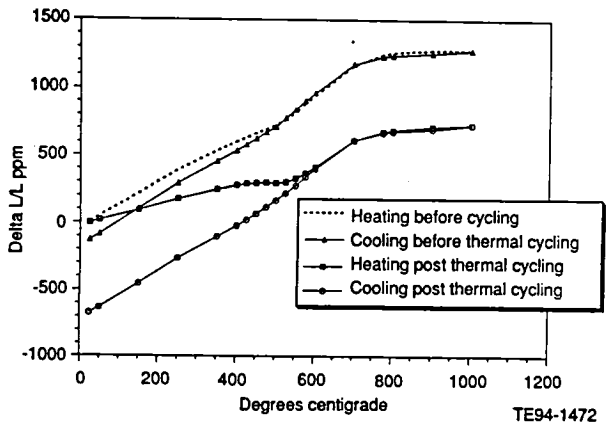


*Figure 3-41. Coefficient of thermal expansion for B1 NZP before and after thermal cycling.*

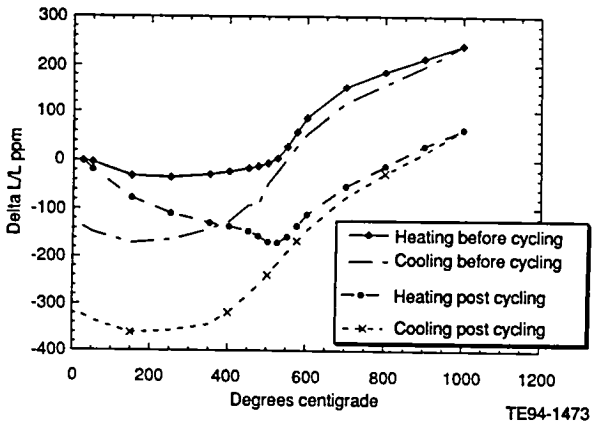


*Figure 3-42. Coefficient of thermal expansion for B3 NZP before and after thermal cycling.*

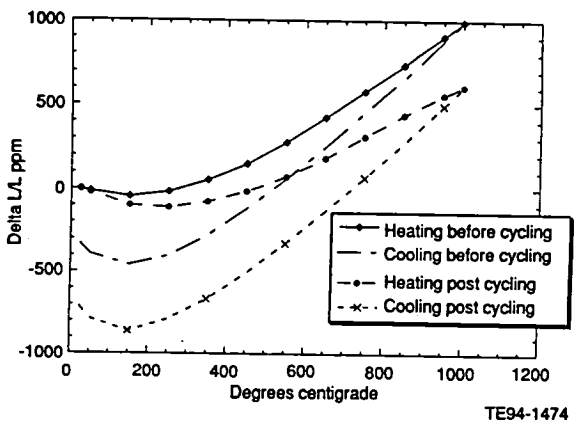


*Figure 3-43. Coefficient of thermal expansion for C1 NZP before and after thermal cycling.*

The CTE and shrinkage after one heating cycle were measured on the three samples of NZP supplied by LoTEC as shown in Table 3-IV.

Shrinkage after the first heating for the C1 material was found to change with time; the 700 ppm shrinkage in the Table 3-IV was an initial value that relaxed with time to 250 ppm. The program goal is to hold dimensional changes from either thermal or chemical exposure to 300 ppm.

NZP strength loss after thermal cycling was also examined. The NZP materials showed a strength gain after thermal cycles unlike most ceramics which show strength loss. NZP samples were cycled from room temperature to 1000°C (1832°F), with strength measured after 100 and 380 cycles. As shown in Table 3-V, NZP material strength was found to slightly increase with thermal cycles.

*Table 3-IV.*
*Coefficient of thermal expansion and shrinkage after one heating cycle.*

| LoTEC designation | CTE (RT-800°C) | Shrinkage after first heating |
|---|---|---|
| NZP-B1 | $16.3 \times 10^{-7}$°C | 120 ppm |
| NZP-B3 | $2.4 \times 10^{-7}$°C | 140 ppm |
| NZP-C1 | $5.0 \times 10^{-7}$°C | 700 ppm |

*Table 3-V.*
*NZP MOR strength measurements after thermal cycling.*

| Material designation | Original | 100 cycles | 380 cycles |
|---|---|---|---|
| B1 | 15,560 kpa (2240 psi) | 18,900 kpa (2750 psi) | * |
| B3 | 14,500 kpa (2100 psi) | 16,900 kpa (2450 psi) | 19,100 kpa (2770 psi) |
| C1 | 28,640 kpa (4150 psi) | 31,800 kpa (4610 psi) | 35,260 kpa (5110 psi) |

* test not completed by end of reporting period

Two chemical durability tests were conducted on the NZP samples. Material test samples were dipped in a saltwater bath (NaCl) and then heated to 800°C (1470°F) for 48 hr. Additional material samples were dipped in a solution of 50% sulfuric acid for 3 hr and heated to 800°C (1470°F) for 48 hr. Table 3-VI shows the sample growth for each of the materials, and LAS data have also been included for a comparison.

The data suggests that these NZP materials will have chemical durability problems. It should be noted that MAS fares poorly in liquid sulfuric acid but is not effected by sulfuric acid vapor.

As a result of the chemical exposure tests, an expanded chemical durability test was initiated in late 1992. The test program consisted of six reagents at three different temperatures. The LoTEC company will supply the material samples for the test, which is outlined in Table 3-VII.

*Table 3-VI.*
*Chemical sensitivity of NZP materials.*

| Material | Sodium exposure | Sulfuric acid exposure |
|---|---|---|
| B1 | +122 ppm | -382 ppm |
| B3 | +372 ppm | -188 ppm |
| C1 | -484 ppm | Dissolved |
| LAS | +450 ppm | +41 ppm |

## Process Development

Several MAS 62 cpsc (400 cpsi) regenerator cores were produced from the EX-20 material. Two cores were constructed with present manufacturing techniques and are ready for engine evaluation. Two additional regenerator cores were constructed to demonstrate cost reduction manufacturing technologies. The solid hub used on the present regenerator was eliminated and exterior machining steps were reduced.

A large extrusion run was successfully made at Corning's Erwin Development facility during this reporting period. 680 kg (1500 lb) of MAS EX-22 material was extruded through a 280 mm (11 in.) diameter die with a cell count of 64 cpsc (415 cpsi). The extrusion trial had the two objectives of shaking down the process for low porosity MAS materials and manufacturing EX-22 matrix material for test; 29 of the extrusion samples were saved. Eight samples were fired in the production batch kiln and two were fired in the production continuous kiln. The finished matrix had the material properties shown in Table 3-VIII.

A 76 mm (3 in.) diameter 174 rectangular cpsc (1100 cpsi) die was constructed and EX-22 material was successfully extruded. Processed and fired were 9 kg (20 lb) of batch material, yielding 4 "logs" 230 mm (9 in.) long.

*Table 3-VII.*
*NZP material test matrix.*

| Acids | Water | Bases |
|---|---|---|
| Sulfuric | | Potassium hydroxide |
| Nitric | | Sodium hydroxide |
| Hydrochloric | | |
| Acetic | | |
| Analyze for Ba, Ca, Sr, P | Analyze for Ba, Ca, Sr, P | Analyze for Na, K, P |
| Three concentrations | | Three concentrations |
| Three temperatures | Three temperatures | Three temperatures |

*Table 3-VIII.*
*Material properties of EX-22 matrix material.*

| | |
|---|---|
| Axial CTE - 2.8 x 10-7 m/m°C (1.6 x 10-7in./in.°F) | 20°C-800°C (68°F-1720°F) |
| Radial CTE - 5.6 x 10-7m/m°C (3.1 x 10-7in./in.°F | 20°C-800°C (68°F-1720°F) |
| Matrix MOR - 3436 kpa (498 psi) | |
| Porosity - 24 % | |

With the successful completion of the two extrusion runs, which verified both the ability to extrude a large diameter matrix of MAS material and the ability to extrude a high cell count matrix of MAS material, Corning has elected to begin construction of a large diameter, 174 rectangular cpsc (1100 cpsi) die. The stress modeling of the die predicted that the concept will work. The die is expect to be completed during the second quarter of 1993.

Small square, triangular, and rectangular dies with high cell count and thin walls were designed and manufactured and trial extrusions were made to determine the most feasible die concept. Small dies with 1100-1420 cpsi were made and trial extrusions made as shown in Table 3-IX.

Two triangular cell die construction techniques were investigated. Both dies had diameters of 25 mm (1 in.) but both were unable to extrude the desired matrix. A square cell die, with 203 cpsc (1313 cpsi) and wall thickness of 0.18 mm (0.0071 in.) was produced by modifying an existing die. Samples were successfully extruded from the die. A square dielet with 220 cpsc (1420 cpsi) and 0.12 mm (0.0046 in.) wall thickness is being designed and manufactured. A third triangular cell die concept is also being designed and manufactured. The triangular die will have 198 cpsc (1280 cpsi) and a wall thickness of 0.1 mm (0.004 in.).

*Table 3-IX.*
*Trial extrusions.*

| | | |
|---|---|---|
| -1125 cpsi | rectangular | good extrusion |
| -high cpsi | triangular | poor extrusion |
| -high cpsi | triangular | poor extrusion |
| -1313 cpsi | square | good extrusion |
| -1420 cpsi | square | — |
| -1280 cpsi | triangle | — |

A low cost regenerator hub concept was evaluated. The present glued-in solid hub is replaced with a hub I.D. coating of ceramic. The ceramic is a room temperature cure product and does not require a second firing step. Corning produced 18 regenerator samples with a 76 mm (3 in.) O.D. Eleven of the samples had a hub I.D. of 25 mm (1.0 in.) and seven core samples had a hub I.D. of 38 mm (1.5 in.). Table 3-X shows the strength of the hub samples, measured with a fixture that matched the engine regenerator support bushing. All the hub tests exceeded the required design engine load of 300 N (67 lbf).

To supply the glass powder for extruding LAS materials, 7000 kg (16,000 lbm) of LAS glass were melted and ball milled. Previous LAS glass had been milled using a fluid energy system. The wrapping process required a very narrow band of particle size, which the fluid energy system produced. The extrusion process required a broad distribution of particle size, a requirement which the ball milling process was developed to meet.

The 150 mm (6 in.) diameter and 280 mm (11 in.) diameter extrusions of LAS were successful. Several hundred pounds of LAS material were extruded using a die with 62 cpsc (400 cpsi). Using a schedule similar to that used for wrapped LAS regenerator cores, 150 mm (6 in.) diameter 62 cpsc (400 cpsi) LAS samples were successfully fired. The firing process is presently being developed for the large diameter LAS 62 cpsc (400 cpsi) extruded cores.

Combined experience with the large and small dies convinced Corning that a large, high cell

*Table 3-X.*
*Hub sample strength.*

| Sample hub I.D. | Mean hub strength |
|---|---|
| 25 mm (1.0 in.) | 2290 N (515 lbf) |
| 38 mm (1.5 in.) | 3270 N (735 lbf) |

count, thin cell wall die had good probability of success. The previous selection of 1100 cpsi, 2:1 rectangular cells with 5 mil walls was confirmed. A vendor for large dies began machining experiments on candidate die materials.

### 3.2.6 Ceramics Process Systems

#### Objective/Approach

A development program with CPS is being conducted to address the fabrication of gasifier turbine rotors utilizing CM200 and SRS201 sialon materials. Quickset injection molding was selected as the fabrication process, and the initial program plan, directed towards a 20-blade rotor configuration, was redirected to address a 26-blade rotor design. The rotor program consisted of the three major phases of injection molding including tool fabrication, rotor processing development, and deliverable rotor fabrication.

#### Accomplishments/Results

- Design and fabrication of a 26-blade rotor tool for Quickset injection molding was completed.
- Injection-molded 26-blade rotors had good surface quality and strength characteristics, similar to material properties taken from billets.
- Dimensional accuracy of rotors was excellent.
- Material development and optimization of duophase sialon material efforts continued.

#### Discussion

The primary efforts addressing rotor development were directed toward the fabrication and processing of 26-blade rotors. Due to ongoing difficulties with the purity and strength characteristics of components fabricated with CM200 sialon powder, initial rotor molding and processing activities were conducted using SRS201 sialon material. The SRS201 material was a pressureless sintered duophase sialon material developed on CPS internal funding. This material was identical to the CM200 sialon in chemical composition, but used Ube $Si_3N_4$ powder in conjunction with CPS processed sintering additives.

Over 200 rotors were Quickset injection molded with the 26-blade tool for rotor forming process development. The external quality of the SRS201 sialon rotors was significantly improved relative to prior prototype rotors and the vane platforms. In particular, the flow textures were significantly reduced by tailoring the injection rate profile and the molding parameters. As a result of these modifications, only minor surface pits were occasionally observed. These surface pits were a function of slip turbulence, which occurred as the slip entered the mold, and were predominately observed on hub surfaces and rarely on blade surfaces. This defect type will be eliminated by optimizing the injection rate profile to minimize slip turbulence.

Two SRS201 sialon rotors, S/N 297 and 302, were selected for cold spin testing based on the results of visual and X-radiography inspections and sintered density. After machining of the rotor blade tips, shaft, and hub ring, the rotors were returned to CPS to improve the blending of the shaft to the rotor hub surface. After machining, both rotors were annealed at 1000°C (1832°F) for 12 hr to heal any machining damage. After remachining, rotors S/N 297 and 302 were remeasured using CMM. Similar to the initial measurements, the hub profiles were measured to confirm that the parts were within specification after machining. In addition, the blade contours at sections D and E were measured for blades 6, 7, and 8 for both rotors.

Figures 3-44 and 3-45 show the nominal and measured hub and shaft profiles for rotors S/N 297 and 302, respectively, at each of the three "P" blades. The nominal profiles are indicated by the connected lines and the measured data are indicated by the open circles. The differences between the nominal and measured profiles on the shaft, top hub (shaft side), bottom hub, and bottom hub flat are indicated on each profile section and are listed in Table 3-XI.

The measured tolerances of the top and bottom hub profiles were unchanged at -0.08 mm (0.003 in.) to +0.10 mm (0.004 in.) since these profiles were not machined.

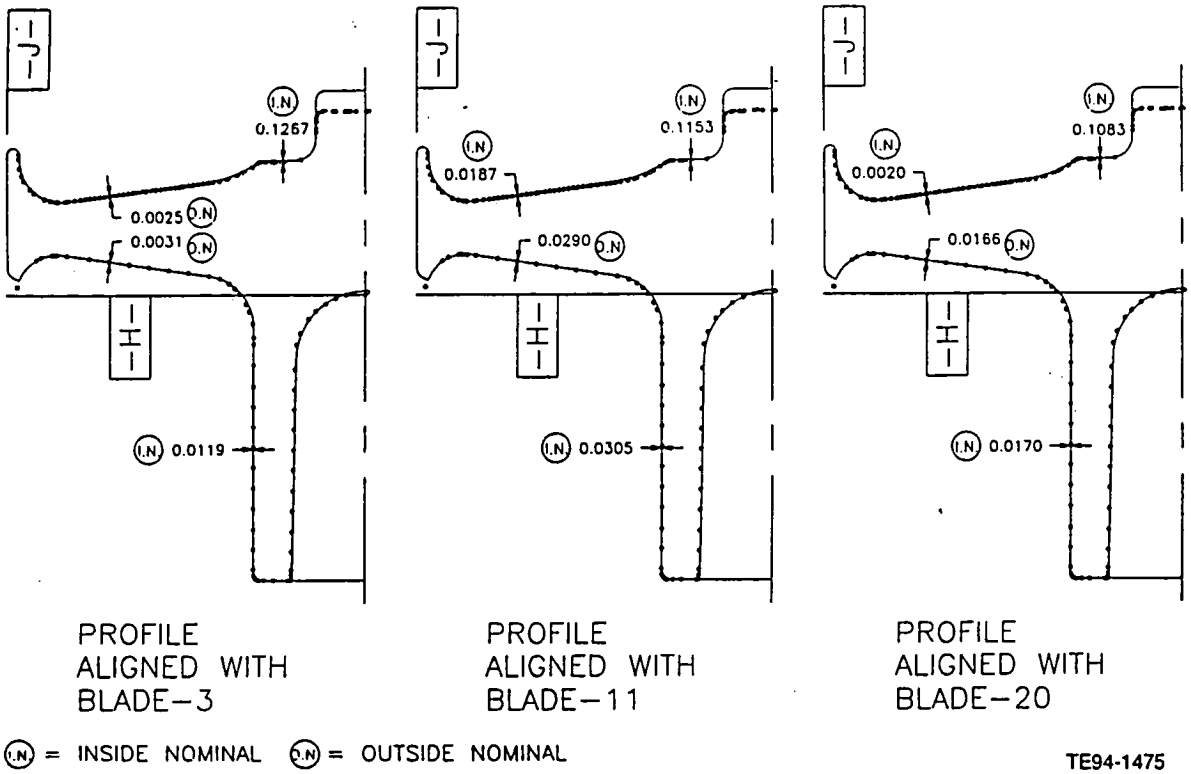


*Figure 3-44. Hub and shaft profiles for CPS SRS201 sialon rotor SN 297.*

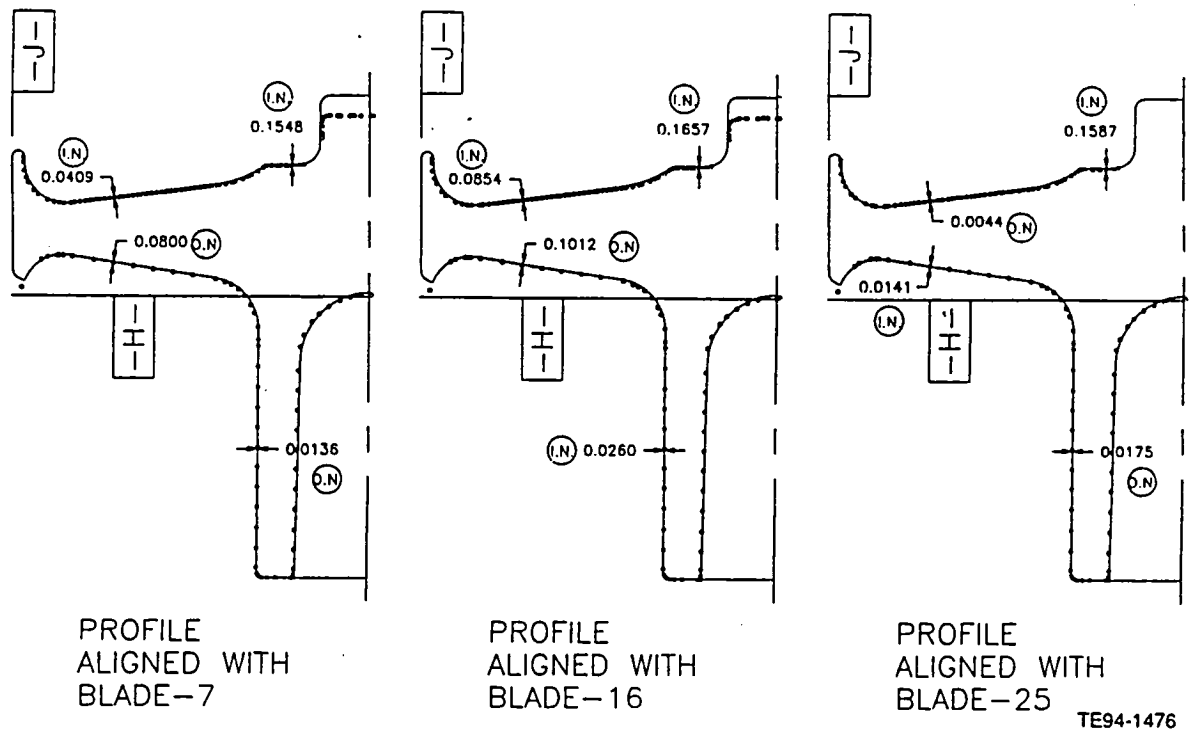


*Figure 3-45. Hub and shaft profiles for CPS SRS201 sialon rotor SN 302.*

*Table 3-XI.*
*Differences between nominal and measured dimensions in CPS gasifier turbine rotors.*

| Rotor S/N 297 | Shaft | Top hub | Bottom hub |
|---|---|---|---|
| Blade 3 | + 0.3868 (0.0152) | - 0.0217 (0.0009) | + 0.0150 (0.0006) |
| Blade 11 | + 0.3760 (0.0148) | + 0.0001 (0.0000) | + 0.0005 (0.0000) |
| Blade 20 | + 0.3196 (0.0126) | + 0.0215 (0.0008) | - 0.0361 (0.0014) |
| **Rotor S/N 302** | **Shaft** | **Top hub** | **Bottom hub** |
| Blade 7 | + 0.3698 (0.0146) | + 0.0300 (0.0012) | - 0.0312 (0.0012) |
| Blade 16 | + 0.3589 (0.0141) | + 0.0861 (0.0034) | - 0.0665 (0.0026) |
| Blade 25 | + 0.3413 (0.0134) | + 0.0519 (0.0020) | - 0.0541 (0.0021) |

Both rotors were nondestructive inspected with microfocus X-ray (MFXR) equipment. Rotor S/N 302 had no internal defects and was judged acceptable for cold spin testing. Hoever, a small crack in the hub region was discovered in rotor S/N 297 with the microfocus X-ray. The hub crack was not detected in prior conventional X-ray inspections. The crack was located underneath the shaft, midway between the shaft bottom and the hub surface. The rotor was rejected for cold spin testing due to this defect.

Rotor S/N 302 was submitted to The Balancing Company (BALCO) for proof spin testing. Following the cold spin test procedures established by Allison at BALCO, the rotor was attached to a metal shaft with epoxy. Only a small amount of material was removed from the metal shaft during balancing, with no material removed from the ceramic rotor, in an effort to minimize surface damage.

Rotor failure occurred during cold spin testing at a speed of 67,580 rpm, prior to the target proof spin speed of 80,000 rpm. Both Allison and CPS inspected the rotor fragments and the burst photograph. It was determined that the primary failure origin was located on the top hub surface near the base of the airfoil leading edge. The rotor fragment with the fracture origin was not found and was presumed to have been destroyed in the rotor burst. Based on prior inspections by CPS, no surface defect had been observed in the vicinity of the failure.

Failure of the rotor from this region at a speed lower than the proof spin level was not unexpected. Difficulties encountered in the translation of the 3-D rotor coordinates to the injection molding tool resulted in a blade fillet radius in which the airfoil leading edge transition to the rotor hub was much smaller than designed. Preliminary analysis by Allison of the CPS rotor configuration predicted excessively high stresses during spin testing.

Preliminary strength testing was conducted at CPS on MIL-STD 1942 "B" size test bars sectioned from both thick Quickset injection molded SRS201 sialon billets and specimens obtained from SRS201 gasifier turbine rotors. In each case, the test bars were not annealed prior to fracture. These results are summarized in Tables 3-XII and 3-XIII. Additional testing is planned to determine if there is an actual difference in strength in the SRS201 material between specimens sectioned from thick billets and rotors at elevated temperatures.

Initial room temperature flexural strength characteristics were generated at CPS for test specimens with an as-fired surface condition. The average strength measured for a total of six test specimens was 392 MPa (56.9 ksi). These test bars were machined from billets where the tensile surface of the sample was left as-molded, with no annealing. The fracture origins for all test bars were small surface pits. Additional test bars will be machined from billets in which the quality of the as-molded surface finish is emphasized.

A study is underway to identify a temperature cycle to anneal machined rotors. Test specimens

*Table 3-XII.*
*Strength characteristics of CPS SRS201 sialon test bars machined from thick billets with no post-machining annealing.*

| Temperature °C (°F) | Strength MPa (ksi) | No. bars | Weibull modulus |
|---|---|---|---|
| 25 (77) | 790 (114.6) | 25 | 10 |
| 1200 (2192) | 648 (94.0) | 10 | 12 |
| 1300 (2372) | 601 (87.2) | 10 | 15 |
| 1370 (2500) | 485 (70.3) | 15 | 22 |

*Table 3-XIII.*
*Strength characteristics of CPS SRS201 sialon test bars machined from gasifier turbine rotors with no post-machining annealing.*

| Temperature °C (°F) | Strength MPa (ksi) | No. bars | Weibull modulus |
|---|---|---|---|
| 25 (77) | 799 (115.9) | 15 | 9 |
| 1200 (2192) | 648 (94.0) | 5 | |
| 1300 (2372) | 536 (77.7) | 5 | |
| 1370 (2500) | 448 (65.0) | 5 | |

were transversely machined from thick billets in order to maximize machining damage, whereas the standard practice for test specimens is to longitudinally machine bars to minimize machining damage. Without annealing, the room temperature flexural strength for a sample of ten transversely machined specimens averaged 680 Mpa (98.6 ksi), which was significantly below the average strength of 790 MPa (114.6 ksi) typically measured for longitudinally ground test bars.

The most promising annealing condition currently identified is 1000°C (1832°F) for 12 hr in an air-fired furnace. The room temperature flexural strength for a sample of five transversely machined test bars measured 873 MPa (126.6 ksi). Note that this strength is significantly higher than that measured for both the transversely ground specimens and the standard longitudinally ground material. Additional testing will be conducted to establish the reproducibility of the preliminary results and to determine the effects of annealing on as-fired surface conditions. In addition, elevated temperature strength testing will be conducted on specimens with longitudinally ground, transversely ground, and as-fired surface conditions to determine the effects of annealing.

### 3.2.9 Norton/TRW Ceramics

#### Objective/Approach

The ceramic component development efforts being conducted with Norton/TRW Ceramics (NTC) are directed towards two AGT-5 components: the gasifier turbine rotor and the turbine scroll. The turbine rotor activity is being directed towards fabrication of both 20- and 26-bladed configuration parts. Pressure slip casting is being used for component production for both NT154 and NT164 silicon nitrides. The turbine scroll efforts are focused on pressure slip casting of reaction sintered NT230 SiC. Extensive development and optimization of the automated high pressure casting process, including slip optimization, plastic mold formulation, and casting trials are being conducted.

## Accomplishments/Results

- Process parameters were established for fabrication of NT154 and NT164 $Si_3N_4$ turbine rotors.
- 20- and 26-blade configuration rotors were fabricated and delivered for rig/engine evaluation.
- NT230 SiC slip and plastic mold formulation were optimized for automated pressure slip casting.
- Four NT230 SiC scrolls were delivered to Allison for rig/engine test activities.

## Discussion

**Gasifier Turbine Rotors.** In 1989-90, NTC developed and produced a number of 20-blade NT154 silicon nitride gasifier turbine rotors for Allison. Four of these components met the dimensional and structural requirements and were qualified for rig and engine testing by passing the proof spin test. One of these rotors, S/N 5S, successfully completed in excess of 200 hr of cyclic durability rig testing. The rotors, however, required extensive machining on the hub surfaces and had several linear indications on the airfoils. As a follow-on effort to the initial rotor program, a subsequent rotor development effort was initiated with Norton/TRW in 1991. This program involved development and fabrication of both 20- and 26-blade rotor configurations, with rotors being produced using both NT154 and NT164 silicon nitride materials.

Under the prior rotor development program conducted with Allison, NTC developed pressure slip casting as the forming method for fabrication of AGT-5 axial turbine rotors. NTC's pressure slip casting techniques involve several additional steps beyond the casting operation to optimize the process for axial turbine rotors, the most notable being the use of freezing to provide additional strength in the green rotors. NTC utilized this process under the prior program to prepare rotors that met the dimensional, mechanical, and spin test requirements. However, the as-cast components contained excessive stock in certain areas, particularly the shaft and hub regions. The excess stock was allowed in the initial rotor castings to reduce the complexity of the tooling and to minimize problems during the pressure casting operation. Because of the additional stock, the casting times for rotors were long (approximately 15 hr). A third generation rotor casting design was developed in 1991 and 1992 to improve the rotor castings and to eliminate the possibility of slip starvation within the blades. Compared to the original mold design, the benefits of the third generation casting mold were many. Casting times were reduced from 15 hr to 3 hr. Machining stock was minimized on the shaft and disk faces to approximately 1.25 mm (0.050 in.), with the shaft hole cast to net shape. Due to the piston action of the mold, the design is transferrable to an automated pressure casting machine with relatively minor modification. This mold design was utilized for casting of both the 20- and 26-blade AGT-5 rotors.

In preparation for casting of the 20-blade NT154 rotors, NTC fabricated two production rotor casting molds. Approximately 1 mm (0.040 in.) of additional stock was added to the shaft side of the hub face to provide adequate machining stock. Dense blank fabrication was then initiated, with a total of 16 rotors cast. After casting, 12 rotors passed visual inspection and were processed through drying, binder burnout, and presintering. MFXR inspection revealed radial cracking along the shaft axis in 8 of the 12 rotors. Upon review of the process, it was determined that modifications to the shaft hole base were required to minimize drying stresses.

A total of 14 additional rotors were cast using this modified shaft plug design. After casting, nine rotors passed visual inspection and were further processed. MFXR inspection of these rotors revealed no radial cracking. A total of 13 rotors were expedited through HIP densification and crystallization. During premachining inspection, however, only four of these rotors were of acceptable quality for finish machining. Fluorescent penetrant inspection (FPI) revealed minor cracking on the other nine rotors that was either not detected during green state MFXR or had initiated during HIP'ing. Cracks were detected in two areas: the shaft O.D. to hub transition area and the blade trailing edge to hub area (Figure 3-46). Both types of cracks were attributed to stresses on the component during the mold removal process. During removal of the mold, the as-cast rotor was stressed as porous and nonporous mold sections

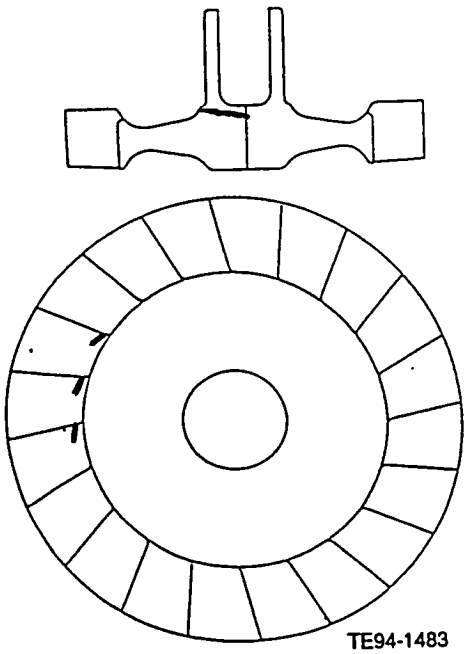


*Figure 3-46. Persistent component defects for rotors (blade tears and shaft cracks).*

were removed from around the rotor. During removal of the plaster shaft sections, the end of the shaft was stressed by a bending moment, generating minor cracking at the shaft end. Although not detectable by X-ray after presintering, these minor cracks manifested themselves during the glass encapsulation HIP'ing process. Likewise, as the mold inserts were removed from between the blades, the twisting/pulling motion exerted a relatively high stress at the blade-to-hub transition area, occasionally resulting in cracking.

In order to ensure that a minimum of three engine quality rotors would be delivered to Allison, an additional eight rotors were processed. Prior to casting, the demolding procedures were improved to reduce the stresses applied to the as-cast component. Seven of the eight rotors cast were successfully removed from the mold with no observable cracks. The seven rotors were presintered, MFXR inspected, HIP densified, and inspected prior to machining. Five of the seven rotors passed visual and FPI examinations. The remaining two rotors were rejected during FPI due to minor cracks at the trailing edge of the blades. The five qualified rotors were then expedited to finish machining.

In parallel with the rotor processing efforts, NTC also developed appropriate machining procedures for finish machining of rotors. Norton used the machining procedures previously developed during the 1990-91 rotor program as a starting point. The machining cycle time for the 1990-91 effort was more than 40 hr per rotor, due to a combination of the excessive stock removal required from the hub faces and shaft, conservative feed rates, and multiple machining setup requirements. Under the 1992 effort, NTC developed procedures that greatly reduced the machining cycle time to less than 5 hr per rotor. Using this machining process, a total of nine rotors were finish machined and inspected. Only three of the nine rotors passed FPI inspection after machining and were spin tested. The majority of the rotors were rejected during FPI due to shallow (<0.5 mm [0.020 in.]) glass-filled cracks on the shaft side of the disk face. Norton determined that the casting seam between two sections of the mold left a small, but sharp, V-shaped groove in the component. This groove was apparently sharp enough to cause surface cracking at its tip in the green state. During HIP densification, encapsulant glass was able to penetrate this crack to a depth of 1.25 mm (0.050 in.) into the rotor. During hub face machining, approximately 1 mm (0.040 in.) of material was removed leaving very shallow glass-filled surface cracks. Norton implemented a corrective action in subsequent rotors to remove this groove prior to HIP'ing. The five rejected rotors were reworked by additional machining of the hub face. Four of the rotors cleaned up using this machining profile and were sent for proof spin testing.

A total of seven finish machined rotors were spin tested at Balco. The spin test results are summarized in Table 3-XIV. Only two of the seven rotors were balanced and successfully proof spin tested to the design goal of 80,000 rpm. Two of the rotors were damaged during handling in the balancing operation, but because the damage to these rotors was limited to a single airfoil per piece, the rotors were hand finished and spin tested to failure. Both rotors burst at speeds above the proof speed, failing at 88,000 and 90,000 rpm, respectively. The remaining three rotors all failed from defects in the blade and hub areas. These rotors were of known lesser quality and were only spun after the better quality rotors were damaged.

*Table 3-XIV.*
*NT154/NT164 AGT-5 gasifier rotor spin test results.*

| Task no. | Rotor i.d. | Rotor type* | Spin-test speed** | Rotor status*** |
|---|---|---|---|---|
| 3.2 | 1538-75 | 20b-NT154 | 80 krpm | passed - delivered |
| 3.2 | 1541-88 | 20b-NT154 | 80 krpm | passed - delivered |
| 3.2 | 85-4 | 20b-NT154 | 88 krpm | passed - burst test |
| 3.2 | 90-3 | 20b-NT154 | 92 krpm | passed - burst test |
| 3.2 | 1538-88 | 20b-NT154 | 78 krpm | failed - hub flaw |
| 3.2 | 1540-88 | 20b-NT154 | 30 krpm | failed - blade flaw |
| 3.2 | 1541-75 | 20b-NT154 | 30 krpm | failed - blade flaw |
| 3.3 | 116X-1 | 20b-NT164 | 80 krpm | passed - delivered |
| 3.3 | 117X-1 | 20b-NT164 | 80 krpm | passed - delivered |
| 3.3 | 119X-1 | 20b-NT164 | 80 krpm | passed - delivered |
| 3.3 | 122X-1 | 20b-NT164 | 80 krpm | passed - delivered |
| 3.3 | 130X-1 | 20b-NT164 | 80 krpm | passed - delivered |
| 3.5 | 15-45-92 | 26b-NT154 | 80 krpm | passed - delivered |
| 3.5 | 15-62-92 | 26b-NT154 | 80 krpm | passed - delivered |
| 3.5 | 15-61-92 | 26b-NT154 | 80 krpm | passed - delivered |
| 3.5 | 15-58-92 | 26b-NT154 | 80 krpm | passed - delivered |
| 3.5 | 15-63-92 | 26b-NT154 | 80 krpm | passed - delivered |
| 3.5 | 15-65-92 | 26b-NT154 | 80 krpm | passed - delivered |
| 3.5 | 15-56-92 | 26b-NT154 | 80 krpm | passed - delivered |
| 3.5 | 15-60-74 | 26b-NT154 | 80 krpm | passed - display |
| 3.5 | 15-43-92 | 26b-NT154 | 75 krpm | failed - hub flaw |

*20b = 20 bladed AGT-5 rotor; 26b = 26 blade AGT-5 rotor
**Proof test speed = 80- krpm
***17 of 21 rotors passed proof test

Following the activities on the 20-blade NT154 rotors, efforts were initiated on fabrication of 20-blade NT164 rotors. Initial rotor processing was conducted to establish a fabrication process for the NT164 material and to determine conditions required for dimensional accuracy. Using this process and drawing heavily on the experience gained in the NT154 rotor activities, fabrication of near-net shape NT164 rotor blanks was initiated. Particular attention was paid to resolution of the persistent component defects that were experienced with the prior rotors. A total of 19 rotors were cast; 15 of the rotors passed visual inspection after casting and the remaining four rotors were rejected due to casting defects such as blade breakage and shaft cracking. The 15 acceptable rotors were dried, presintered, and passed MFXR inspection. Of the 15 rotors, 7 were hand finished at all casting seams and then HIP densified; the remaining 8 rotors were held in reserve to conserve funding. Five of the seven densified rotors passed premachining FPI and visual inspections and were finish machined. All five finish machined rotors passed FPI inspection and were sent to spin testing. All five of the rotors passed the proof spin test goal speed of 80,000 rpm and were delivered to Allison for rig/engine testing.

Efforts were also conducted on fabrication of NT154 rotors of a new design, featuring 26 airfoils. A stainless steel casting pattern was designed and fabricated for use in mold fabrication. The initial rotor casting mold design was identical to that used for production of the en-

gine quality 20-blade rotors. Following initial casting activities to identify dimensional accuracy and casting behavior, fabrication of near-net shape 26-blade rotors was conducted. A total of 34 rotors were cast in this effort, and 18 of these rotors passed postcasting inspection and were dried, presintered, inspected, and qualified for densification. The 16 components rejected were due to blade breakage during mold stripping from the blade trailing edges. The 18 acceptable rotors were hand finished at all seams and HIP densified; 10 of the 18 rotors were successfully HIP'ed and sent to finish machining. The eight rejected rotors were disqualified due to cracks related to the HIP loading arrangement and latent casting defects not previously identified in pre-HIP inspections. All ten acceptable quality rotors were successfully machined and subsequently spin tested; eight of the ten rotors spin tested attained the design proof speed of 80,000 rpm. One of the two remaining rotors was damaged during balancing and the other failed at 75,000 in the hub region. The eight proof spin tested rotors were delivered to Allison for test and evaluation.

**Turbine Scrolls.** A program for development and fabrication of AGT-5 scrolls is also being conducted at Norton/TRW. The material selected for this effort is NT230 SiC, a reaction-sintered SiC with a bimodal distribution of silicon carbide grains in a matrix of metallic silicon. Compositionally, NT230 SiC contains approximately 10% silicon, along with extremely low levels of trace impurities. By modification of the grain size distribution and selective changes to the fabrication process, NTC was able to essentially double the strength of existing siliconized SiC compositions. The material is also ideally suited for scroll fabrication due to the minimal shrinkage (1-2%) upon densification. Four major tasks are being conducted on the scroll development program, including automated pressure slip casting development, scroll component production, process proof demonstration, and component cost analysis.

The automated pressure slip casting task is directed at developing semiautomated forming procedures for scroll components. NTC selected pressure slip casting as the preferred forming method for scrolls, and to facilitate performance of this work, NTC acquired a semiautomated pressure casting machine and porous mold technology. Activity in this area has been focused on development of the automated pressure casting process to advanced ceramics, involving slip system development, porous plastic mold development, and automated pressure slip casting development.

Initial work with porous plastic mold technology suggested that slip characteristics were a critical element in successful casting. It was found that slip formulation, which cast readily at low pressure (<550 Pa [80 psi]) in plaster molds, did not necessarily produce good castings at high pressures in plastic molds. A study of appropriate parameters contributing to successful high pressure casting of Si-SiC was planned and conducted. Screening tests were performed first in an effort to isolate appropriate factors including solids concentration, pH, and various additives. Of these factors, it was found that both solids content and pH had beneficial effects on casting. Slips containing a flocculent resulted in high viscosities and cast bodies with unacceptable water content. Certain binders were found to decrease viscosity and enhance green strength and mold release behavior. Based on these tests, an L14 fractional factorial designed experiment was conducted. A low solids content, high binder content, casting additive-free formulation was selected from benchtop casting trials as the optimal NT230 slip for use with porous plastic molds. However, when evaluated on the Dorst automated pressure slip casting machine, the slip formulation did not result in enhanced shape retention and castability when compared to the standard NT230 mix. It became evident from the Dorst casting trials that further slip formulation development should focus on significant enhancements to castability and shape retention, as opposed to seeking marginal benefits from optimizing the current slip system.

Optimization of the slip formulation was directed toward development and characterization of various slip additives. The additives were evaluated regarding their improvement in the strength and fracture toughness of as-cast components. For the slips with additives, the wet green strength of as-cast scrolls was significantly greater than standard mix NT230 components. The additive appears to enhance the Weibull modulus of NT230 SiC with a marginal increase in fracture toughness with no impact on

strength. Based on the positive results from the scroll casting trials, the NT230 slip formulation for casting scrolls on the Dorst equipment was fixed using the casting additive.

Activities were also conducted on development and characterization of various porous plastic mold materials, plastic formulations, and mold fabrication processing conditions. Norton selected the Dorst/Laufen porous plastic material over a similar Japanese material for development and testing efforts. The microstructure of the standard Dorst/Laufen composition was examined to determine whether changes in raw materials or fabrication methods might effect casting behavior. A factorial experiment consisting of 12 experimental trials addressing 3 formulation variables was designed and conducted, but none of the 12 trials produced a casting with acceptable mold release and shape retention. Observations from the L12 experiment led to the screening of additional porous plastic mold variables. One mold formulation factor was discovered to dominate casting behavior. Acceptable mold release and shape retention was obtained in benchtop casting evaluations with the modified plastic mold composition. Based on a number of additional experimental test matrices and casting trials, plastic mold formulation and processing conditions were standardized for the balance of the scroll casting activities.

Using the standard NT230 slip system and optimized plastic mold formulation and processing conditions, initial screening trials were completed on the Dorst automated pressure slip casting equipment. The sample component cast was a 50.8 mm (2 in.) diameter by 88.9 mm (3.5 in.) closed-end tube, formed by using a two-piece clamshell-type porous plastic mold. Preliminary trials resulted in identification of appropriate vacuum assist and air back pressure cycles to sufficiently dewater the porous plastic. It was observed that high pressure extended duration air back pressure treatments resulted in fabrication of drain cast tubes that exhibited acceptable shape retention without tearing upon mold separation. Casting pressures were varied from 1.03 MPa (150 psi) to 2.76 MPa (400 psi). NT230 tubes with wall thicknesses ranging from 2.54 mm (0.10 in.) to 14.73 mm (0.580 in.) were successfully cast by varying pressure and casting time. The casting time for producing a 4 mm (0.16 in.) wall thickness was approximately three minutes over the range of pressures evaluated. The tubes were processed through siliconization for characterization of the dense material microstructure and mechanical properties. Siliconized densities ranged from 3.01 to 3.04 g/cc (0.109 to 0.110 $lb/in.^3$), which is slightly lower than the typical process range of 3.05 to 3.10 g/cc (0.110 to 0.112 $lb/in.^3$) for pressure slip cast NT230 material. The slightly lower siliconized density observed for the Dorst-formed material may be due to a high volume percent of free silicon metal originating from a lower silicon carbide particle packing efficiency. Flexural test specimens were machined from representative tubes cast on the Dorst machine. An average strength of 333 MPa (48.3 ksi) was obtained at room temperature, with an average strength of 420 MPa (60.9 ksi) recorded at a temperature of 1370°C (2500°F). These strengths are representative of the typical values obtained for NT230 SiC.

An iterative approach was employed in developing and optimizing a porous plastic mold design for AGT-5 scrolls. Three mold design iterations were evaluated first in porous plastic in benchtop casting trials followed by scroll castings using porous plastic molds of the same design on the Dorst machine. Fabrication of the first iteration porous plastic scroll mold was completed in June. The first iteration design was a seven-piece mold utilizing a four-stage demolding cycle on the Dorst machine. Several scroll casting cycles were attempted using a casting pressure of 1.65 MPa (240 psi) for 200 seconds in which the nominal 4 mm (0.16 in.) wall thickness was achieved. The as-cast scrolls had a high moisture content, lower wet green strength, and relatively poor surface quality compared to components cast in porous plaster molds. A scroll cast on the Dorst machine is shown in Figure 3-47. The mold design was modified to use a nonporous insert on the plug face to prevent casting off of the center surface. Four scroll casting trials were completed using this design on the Dorst machine. Difficulties similar to those observed with the first mold design were encountered, although they were less severe. Design and fabrication of a third iteration scroll mold was initiated in an attempt to facilitate demolding of scroll castings with acceptable in-mold drying shrinkage.

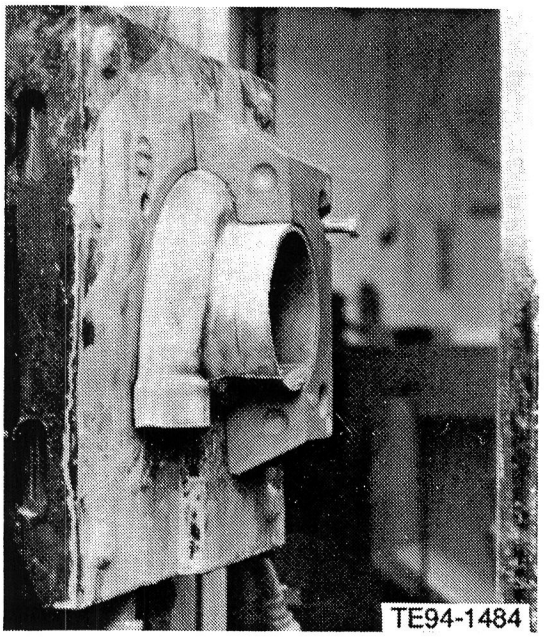


*Figure 3-47. AGT-5 scroll casting on Dorst machine.*

Scrolls were successfully cast and demolded without cracking or tearing in the scroll neck area; however, cracks were present on the inside wall of the scroll body. The surface finish and mold release characteristics of the scrolls appeared to improve with shorter mold conditioning treatments between casting cycles.

Concurrent with the slip and plastic mold development activities, Norton conducted work on fabrication of NT230 AGT-5 scrolls to satisfy rig/engine test requirements. The scroll design for this effort was finalized in December 1991, with scroll casting patterns and tooling delivered in February 1992. A first iteration porous plaster mold was designed and fabricated utilizing six mold segments and two endcaps with two internal cores. The initial scroll castings cracked during demolding due to several mold segments that were observed to lock up on the casting. This problem was eliminated in subsequent trials after the casting pattern and setup boards were modified to incorporate additional draft angles. Additional casting trials were performed to identify an optimal post-drain drying time and to finalize the design of the internal core piece. Two persistent forming problems were identified from these casting trials: cracking in the scroll I.D. and tearing on the shroud O.D. adjacent to the scroll inlet.

The cracking in the scroll I.D. was thought to be due to either shrinkage onto the internal plaster cores or misalignment of the core during demolding. It was observed that scrolls cast and demolded in a crack-free condition eventually cracked around the I.D. during drying. After performing an extensive screening of potential solutions, a casting additive was selected for use as a reinforcement material to the standard NT230 slip. This additive was successful, with a number of scrolls cast which remained crack-free after drying.

Additional casting trials were performed to identify the cause of the shroud O.D. tear. It was confirmed that drying of the scroll while it was still in the mold causes the component to shrink, and eventually tear, when the shrinkage is constrained by the mold. Shorter in-mold post-drain drying times verified elimination of the shroud O.D. tear, but tears and breakage were created in other areas of the scroll during demolding of the insufficiently dried castings. The tearing was eliminated by forming the shroud ring in a secondary casting operation. Two scrolls fabricated with the secondary bonding procedure were siliconized and evaluated. Representative sections of the siliconized joint are shown in Figure 3-48, showing a thin line of silicon metal rich material at the joint. Additional specimens were prepared for mechanical property evaluation. The average room temperature strength of the joined specimens was 262 MPa (38 ksi), with a strength of 400 MPa (58 ksi) at a temperature of 1370°C

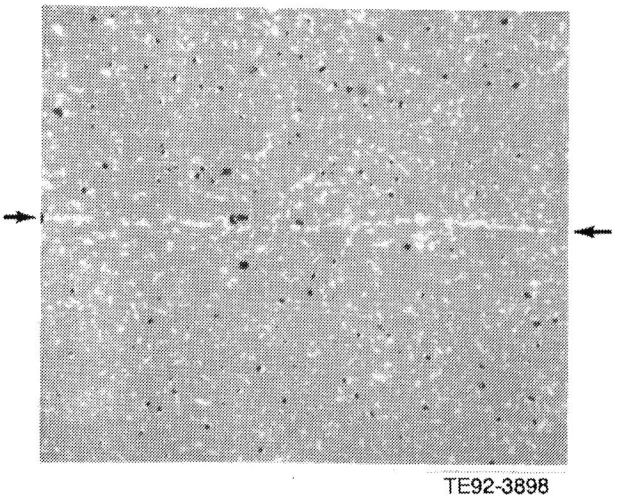


*Figure 3-48. Microstructure of Norton/TRW NT230 SiC shroud ring joint.*

(2500°F). This represents a decrease in strength of 25% and 9%, respectively, relative to baseline NT230 SiC.

A total of five batches of AGT-5 scrolls were cast in accordance with the scroll manufacturing specifications developed in the component preproduction efforts. The overall casting yield for the five batches was 78% (28/36). The predominant reason for rejection at this step was silicon-filled cracks. Even so, the 78% yield represents the highest yield after casting of any scroll component observed to date. Additional components were rejected during machining and at final inspection, resulting in an overall process yield of 17% (5/30). A total of four finish machined scrolls were delivered to Allison to support rig and engine testing and evaluation. Four additional acceptable quality scrolls were processed through siliconization and are candidates for final machining if required.

# IV. COMPONENT RIG DEVELOPMENT AND TEST

## 4.1.3.1 Rotor/Shafting System Rig Development

### Objective/Approach

The objective of this activity is to develop a rotor/shafting system rig capable of evaluating seals, bearings, rotor shaft dynamics, and lubrication systems as necessary to evolve the AGT-5 hot gasifier rig and engine to high temperature test-beds. In addition, the rig is to be capable of room temperature high speed proof testing of candidate ceramic turbine rotors prior to AGT-5 hot gasifier rig or test-bed engine evaluation.

### Accomplishments/Results

- Accelerometers were installed and a preliminary finite element rotor dynamics analysis of the AGT-5 gasifier rotor was completed utilizing a variety of rotor and compressor configurations.
- Vertical and lateral case accelerometer data for the AGT-5 hot gasifier rig during steady-state and transient operation was obtained.
- Specifications were completed for a layout drawing of an instrumented gasifier housing that incorporates shaft proximity probes and housing accelerometers.
- An AGT-5 gasifier housing was instrumented with lateral and vertical shaft proximity probes and accelerometers for use in an "all-ceramic" gasifier test.
- A data recording system was acquired for continuous monitoring of the shaft dynamics instrumentation.
- Two test runs were performed on an instrumented AGT-5 "all-ceramic" gasifier assembly (lateral and vertical shaft proximity probes and housing accelerometers).
- Approximately 18 minutes of steady-state and slow acceleration shaft dynamics data was recorded prior to a failure of the ceramic gasifier assembly (test data were subsequently reduced and analyzed).
- Critical speed analysis predicts that all rotor combinations have similar dynamic characteristics.
- Stability analysis predicts unstable rotor responses near 28,000 and 50,000 rpm.
- Preliminary analysis of hot rig case accelerometer test data has verified the existence of nonsynchronous rotor responses.
- Preliminary designs for bearing squeeze film dampers have been generated and will be incorporated in the event that measured gasifier rotor responses exceed allowable values.
- Initial testing of the instrumented "all ceramic" gasifier assembly revealed a severe rotor unbalance that would otherwise have gone undiscovered.
- The first attempt to run an instrumented assembly failed due to improper sealing of T3 air at the gasifier housing/compressor diffuser interface (The T3 leak resulted in burnout of all probe lead wires).
- The predicted nonsynchronous rotor responses were not observed in the limited steady-state test data obtained prior to the instrumentation failure.
- The second attempt to run an instrumented "all ceramic" gasifier assembly was unsuccessful due to a failure of the ceramic rotor/metal shaft attachment.
- Limited test data verified that mechanical looseness was present in the gasifier rotor prior to the failure.
- The shaft dynamics instrumentation appeared to be intact and can be used in future rig testing pending availability of ceramic gasifier hardware.

### Discussion

Test results from AGT-5 hot rigs utilizing all ceramic gasifiers indicate a potential correlation between gasifier speed and failures associated with bearings, compressor rubs, and rotor tip rubs. To investigate this potential correlation, a finite element rotor dynamics analysis of the gasifier system was initiated. The analysis utilized an axisymmetric model in conjunction with the STRATA/ROTORDYN algorithm. Analyses have been completed for various configurations that include either a 38-bladed metal gasifier rotor or a 20-bladed ceramic gasifier rotor and either of two compressor impeller materials. Initial analyses focused on

critical speed characterization as well as unbalance sensitivity.

Results indicate that all rotor/compressor combinations exhibit similar dynamic characteristics, and these characteristics are relatively insensitive to the particular compressor impeller. Therefore, the discussion herein is focused on a comparison of the metal and ceramic rotors with a baseline compressor impeller. The dynamic analysis (stability and speed sweep) indicates that both systems have the potential for two unstable modes in the operating range. The principal nonsynchronous response occurs near 50,000 rpm and displays a bending mode. A second nonsynchronous response is predicted near 28,000 rpm if the compressor bearing bottoms in the gasifier housing. The mode shape is a turbine whirl. Additional analyses were performed to illustrate that a very small rotor unbalance was more than sufficient to bottom this compressor bearing. Results also indicate that the ceramic rotor system is much more sensitive to unbalance than the metal rotor system. As a consequence, the ceramic rotor system should experience significantly larger deflections for any given amount of rotor unbalance.

In an effort to verify the analytical predictions, two accelerometers (lateral and vertical) were installed on an AGT-5 hot rig case incorporating a ceramic gasifier assembly. The preliminary data indicated that both nonsynchronous modes were indeed present during some phase of the sampled steady-state and transient testing. To characterize the rotor instabilities fully as well as monitor the condition of the rig, additional hot rig shaft dynamics instrumentation was specified. The fully instrumented rig contains lateral and vertical shaft proximity probes, gasifier housing accelerometers, and the case accelerometers. In the event that measured gasifier shaft excursions exceed allowable levels (based on bearing and tip clearance considerations), a preliminary squeeze film damper design has been identified for each bearing location.

Initial hot rig testing of the instrumented gasifier assembly has been completed. At approximately 0.9 hr into the nondurability rig testing, all shaft dynamics instrumentation signals were lost. Subsequent hardware inspection revealed that improper sealing of T3 (burner inlet) air at the gasifier housing/compressor diffuser interface had resulted in complete burnout of the probe lead wires. A replacement set of shaft dynamics instrumentation was procured and installed in an "all ceramic" gasifier assembly. The limited test data (approximately 45 minutes) obtained from the initial running has been reduced and analyzed. A waterfall plot of high speed data for the vertical shaft proximity probe clearly illustrates that predicted nonsynchronous vibrations were not apparent during initial testing; however, a large synchronous vibration was observed.

On further investigation it was discovered that the synchronous vibration resulted from rotor unbalance generated by misalignment between the metal gasifier shaft and ceramic rotor stub shaft. The shaft misalignment issue is currently under investigation and the ceramic rotor assembly has been retired pending final hardware disposition.

The second fully instrumented assembly had completed approximately 18 minutes of low speed steady-state and slow acceleration testing prior to a ceramic failure. Post test inspection of the assembly revealed a failure of the ceramic rotor shaft attachment. Review of the limited dynamics test data confirmed that a mechanical looseness was present in the rotor system during the test. Waterfall plots clearly illustrate mechanical looseness (excitation of multiple engine orders 1EO, 2EO, 3EO, ...).

The shaft dynamics instrumentation appears to be intact and will be preserved for future hot rig testing pending availability of ceramic gasifier hardware.

### 4.1.3.3 Hot Gasifier Rig Development

## Objective/Approach

The objective of the hot gasifier rig development is to bring the rig to the point of being ready for testing of ceramic gasifier components.

## Accomplishments/Results

- A hot gasifier rig exhaust bypass system was used in one hot gasifier rig.
- Design studies of regenerator inlet cavity modifications were conducted with the objective of reducing the rate of insulation degradation in the cavity.
- Regenerator inlet cavity insulation shields were installed and tested in the rig. Testing revealed that the shields reduced the rate of insulation degradation.

## Discussion

A hot gasifier rig exhaust bypass system was designed in 1991 to reduce the back pressure on the gasifier rotor during rig operation to full RPD conditions. One bypass system was obtained and assembled on hot gasifier rig S/N 12 this year. The bypass system was initially checked out with a metal gasifier assembly installed in the rig and then was utilized for all subsequent testing in the rig during the year. The rig ran for 30 hr with the bypass system; no problems were noted. The bypass system allowed more cooling air to be added before the turbine inlet temperature began to increase and result in higher regenerator inlet temperatures. The system was utilized in the all-ceramic gasifier test, which ran the ATTAP durability schedule having three accelerations per 1 hr cycle to 1371°C (2500°F) TIT at 100% speed.

During hot gasifier rig operation testing to full RPD conditions (1371°C [2500°F] at 100%), the insulation material in the regenerator inlet (rotor outlet) cavity suffers significant degradation. Because the hot gasifier rig does not have a power turbine nor an exhaust diffuser, the air velocity and temperature in the cavity are much higher than in an engine. Because the high velocity and temperature are thought to be the cause of the degradation, several rig modifications were designed and analyzed. The modifications attempted to slow down the air exiting the rotor and to inject cooling air further upstream from the insulation to allow for better mixing. Although the modifications would have slowed the air and/or allowed improved cooling air mixing, they were all rejected because of the complexity and cost required to build and assemble the necessary hardware.

To allow continued hot gasifier rig testing without having to repeatedly re-insulate the regenerator inlet cavity, insulation shields were installed into hot gasifier rig S/N 14. The shields were fabricated and installed in a relatively short time period and thus did not significantly affect the ceramic component test schedule. The shields accumulated over 255 hr of operation in the rig with 31.7 hr of the 255 hr total consisting of running the ATTAP durability schedule having three accelerations to 1371°C (2500°F) TIT per 1-hr cycle. Although the insulation in the rotor outlet cavity continued to degrade, the rate of degradation slowed significantly and allowed for increased rig operation between required shutdowns for re-insulation.

### 4.2.3.1 Rotor/Shafting System Rig Test

## Objective/Approach

The objective of this activity is the evaluation of seals, bearings, rotor shaft dynamics, and lubrication systems as necessary to evolve the AGT-5 hot gasifier rig and engine to high temperature test-beds. In addition, room temperature, high speed proof testing of candidate ceramic turbine rotors prior to AGT-5 hot gasifier rig or test-bed engine evaluation is performed.

## Accomplishments/Results

- Proof spin testing of the ceramic power turbine rotors and full RPD capability gearcase was initiated.
- Testing was discontinued because the power turbine was exciting a static structure case mode.

## Discussion

The ceramic power turbine, gearbox, and containment drum were installed on the dynamometer (Figure 4-1) and run to 23% design speed. At this speed, the power turbine could be seen orbiting inside the containment drum. Frequencies, measured by accelerometers on the gearbox, showed the vibration to be driven by

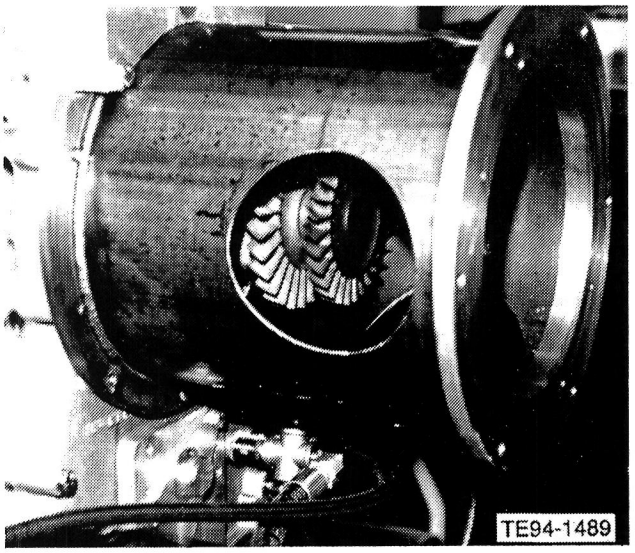


*Figure 4-1. Ceramic power turbine rotors mounted in spin rig using full RPD capability gearbox.*

one excitation per power turbine shaft revolution (1E). The dynamometer was shut down and it was determined that there was a structural bolted from the end of the containment drum to the floor to remove the cantilever bending of the drum. While the dynamometer was off, the structural natural frequencies were again excited and recorded. The dynamometer was then taken up to 25% speed when the response of a higher natural frequency became excessive. Testing was discontinued because this natural frequency, driven by two excitations per shaft revolution (2E), was expected to have even higher response at higher shaft speeds. Further work was required to determine which structural component had this natural frequency and the dynamic behavior of the shaft system.

After reworking the power turbine shafting (Section 1.4.1) the ceramic power turbine is now ready for a second attempt at spin testing.

### 4.2.3.3 Hot Gasifier Rig Test

## Objective/Approach

Hot gasifier rig testing is utilized to screen/proof test and evaluate structural ceramic components (combustors, gasifier turbine components, and regenerators) prior to introduction into the AGT-5 test-bed engine(s). Developmental rig evaluation is continuing while domestic ceramic components are being fabricated for test.

## Accomplishments/Results

- Hot gasifier rig testing accumulated 267.7, 196.5 and 13.5 total test hours respectively, including durability schedule testing with peak conditions of 1371°C (2500°F) at 100%, on three different all-ceramic gasifier assemblies.
- An all-ceramic gasifier assembly ran for 0.4 hours when the assembly suffered a failure.
- An all-ceramic gasifier assembly was tested to 1044°C (1910°F) at 100%.
- Four ceramic gasifier rotors in metal gasifier assemblies were successfully proof tested.
- A SiC ceramic combustor failed during the initial proof test.

## Discussion

Hot gasifier rigs were utilized in 1992 to test over 78 ceramic components, excluding ceramic regenerator cores. Two all-ceramic gasifier assemblies continued testing in 1992 after being proof tested in 1991. Initial proof tests were carried out on three additional all-ceramic gasifier assemblies, four ceramic rotors, and one ceramic burner during the year. Over 450 hours of hot gasifier rig test time were accumulated in 1992, but because of metal component and regenerator core temperature limitations, the ATTAP durability schedule was modified to include only three accelerations to peak conditions during each 1-hr cycle. All durability schedule testing discussed below was run under the modified schedule except as specifically noted. Up to 130.3 hours of ATTAP durability schedule testing were accumulated under the modified schedule with three accelerations per hour to 1371°C (2500°F) TIT at 100% speed. An additional 6.4 hours of running were accumulated under the full ATTAP durability schedule with 15 accelerations per hour to 1371°C (2500°F) TIT at 100% speed.

***Ceramic Component Durability Testing.*** An all-ceramic gasifier assembly consisting of an advanced concept scroll (Kyocera, SN252, P/N

5-81154, S/N KX59815) and a 20-bladed ceramic rotor (Kyocera, SN252, P/N 5-67200, S/N 5K21) was initially proof tested up to 1371°C (2500°F) at 100% speed and then started running on the ATTAP durability schedule. Two turbine tip rubs were apparent during the initial 16 hr of running, but no damage to the ceramic components was noted in two detailed inspections. Because of repeated metal component failures in the rig during the initial 53 hours of durability schedule testing, the schedule was modified after 53 hours to four accelerations per hour cycle up to a peak condition of 1200°C (2190°F) at 100% speed. Subsequent inspections were carried out at 160 and 203 test hours. Turbine rotor tip rubs were apparent during each of the inspections but full FPI inspections revealed no damage to either the rotor or scroll. At 267.7 test hours, the rig automatically shut down and an inspection revealed that all the ceramic components were damaged. Complete failure analysis is discussed in Section 3.1.3.

The all-ceramic gasifier assembly containing the components listed in Table 4-I completed a 100-hr durability test at the end of 1991. A January 1992 complete inspection following the 100-hr test revealed three small cracks in the scroll around the vane pockets, one small surface crack in the scroll shroud area, and two cracked vanes. The two cracked vanes were replaced and the hardware was reassembled. After running up to 1370°C (2500°F) TIT at 100% speed, the assembly ran on the ATTAP durability schedule up to 116 hr when the assembly was removed from the rig for a complete inspection. Although one vane suffered new cracking, no crack growth nor any new cracks were observed in the scroll. The newly cracked vane was not replaced and the assembly continued running on the durability schedule up to 132 total test hours, when it was again removed from the rig for a complete inspection. No new cracks nor crack growth on the scroll were observed, but two vanes had developed new cracks and six new chips were found on the rotor leading edge blade tips. The rotor chips were blended out and the rotor was rebalanced prior to being reassembled, and one of the cracked vanes was replaced. The rig then continued running on the durability schedule up to 196.5 total test hours when the ceramic components were found destroyed following an automatic rig shutdown. Complete failure analysis is discussed in Section 3.1.3.

The all-ceramic gasifier assembly containing the components listed in Table 4-II also completed testing under the ATTAP durability schedule in 1992. This assembly was the first to be built with CBO SiC vanes. The assembly was installed in the hot gasifier rig that had the T6 bypass hardware installed (see Discussion, Section 4.1.3.3). Because the bypass hardware allowed higher peak regenerator inlet temperatures, this assembly ran the full ATTAP durability schedule with 15 accelerations to 1371°C (2500°F) TIT at 100% speed per 1 hr cycle. After running the schedule for 6.4 hours and accumulating 13.5 total test hours, the rig automatically shut down. Inspection revealed that all the ceramic pieces were broken and the metal burner can had severely overheated. Section 3.1.3 provides a complete failure analysis.

***Ceramic Gasifier Assembly Proof Testing.*** Two ceramic gasifier assemblies underwent proof tests in 1992. One continued a proof test that began in 1991 and the other had not been run prior to 1992.

*Table 4-I.*
*Ceramic components in 196.5 hour ceramic gasifier build.*

| Component | Supplier | Material |
|---|---|---|
| Scroll P/N 5-80553, S/N 0001-1 | Kyocera | SN252, $Si_3N_4$ |
| Vane platform P/N 5-80561, S/N 0002-1 | Kyocera | SN252, $Si_3N_4$ |
| Vanes (14) P/N 5-80552 | GTE | PY6, $Si_3N_4$ |
| Vane retaining ring P/N 5-80560, S/N 0001-1 | Kyocera | SN252, $Si_3N_4$ |
| Rotor (15Nb) P/N 5-66946, S/N 5K12 | Kyocera | SN252, $Si_3N_4$ |

*Table 4-II.*
*Ceramic components in 13.5 hour ceramic gasifier build.*

| Component | Supplier | Material |
|---|---|---|
| Scroll P/N 5-80553, S/N 0002-1 | Kyocera | SN252, $Si_3N_4$ |
| Vane platform P/N 5-80561, S/N 0001-1 | Kyocera | SN252, $Si_3N_4$ |
| Vanes (14) P/N 5-80556 | CBO | SiC |
| Vane retaining ring P/N 5-80560, S/N 0001-2 | Kyocera | SN252, $Si_3N_4$ |
| Rotor (15Nb) P/N 5-66946, S/N 5K13 | Kyocera | SN252, $Si_3N_4$ |

The gasifier assembly containing the components listed in Table 4-III ran for 8.5 hours in 1991. Testing was discontinued in order to repair gasifier housing bore problems. After repairing the gasifier housing, the assembly was started and ran for 0.4 hours up to a peak condition of 1305°C (2380°F) TIT at 97.5% speed when the rig automatically shut down. Inspection revealed that all the ceramic components were broken. Section 3.1.3 discusses the complete failure analysis.

A gasifier housing was assembled with additional instrumentation in order to supply data to study gasifier rotor shaft dynamics. Three accelerometers and two proximity probes were installed into the gasifier housing. An all-ceramic gasifier assembly containing the components listed in Table 4-IV was assembled and installed in the rig. Two additional accelerometers were installed on the rig to provide more data for the shaft dynamics study. The rig was taken up to a peak condition of 1045°C (1910°F) TIT at 100% speed when testing was discontinued after 1.2 run hours because of rotor imbalance concerns raised from the shaft dynamics

*Table 4-III.*
*Ceramic components in 8.9 hour ceramic gasifier build.*

| Component | Supplier | Material |
|---|---|---|
| Scroll P/N 5-80567, S/N KX56721 | Norton/ TRW | NT230, SiC |
| Vane platform P/N 5-80561, S/N 0002-2 | Kyocera | SN252, $Si_3N_4$ |
| Vanes (14) P/N 5-80552 | GTE | PY6, $Si_3N_4$ |
| Vane retaining ring P/N 5-80563, S/N KX79532 | Carborundum | α-SiC |
| Rotor (15Nb) (initial build) P/N 5-66946, S/N 5K12 | Kyocera | SN252, $Si_3N_4$ |
| Rotor (20Nb) (subsequent builds) P/N 5-80598, S/N 5S | Norton/ TRW | NT154, $Si_3N_4$ |

data, and a thorough investigation revealed that the ceramic rotor had shifted relative to the metal shaft. A different 20-bladed rotor (Norton/TRW, NT154, P/N 5-80598, S/N 6F) was then installed into the assembly along with new vanes (Kyocera, SN252, P/N 5-81293). This assembly was the first one to contain the Kyocera vanes, which were installed because of better impact resistance characteristics than the GTE vanes previously run in the assembly. The rig was slowly taken up to 92% speed over a 15 minute period, when it automatically shut down. Inspection revealed that the rotor had separated from the shaft and the scroll was damaged in the shroud area. The complete failure analysis is described in Section 3.1.3.

*Table 4-IV*
*Ceramic components in 1.5 hour ceramic gasifier build.*

| Component | Supplier | Material |
|---|---|---|
| Scroll P/N 5-80567, S/N KX59008 | Norton/ TRW | NT230, α-SiC |
| Vane platform P/N 5-80561, S/N 0002-4 | Kyocera | SN252, $Si_3N_4$ |
| Vanes (14) P/N 5-80552 | GTE | PY6, $Si_3N_4$ |
| Vane retaining ring P/N 5-80563, S/N KX79354 P/N 5-80563, S/N KX79350 P/N 5-80563, S/N KX79352 | Carborundum | α-SiC |
| Rotor (20Nb) P/N 5-67200, S/N 5K23 | Kyocera | SN252, $Si_3N_4$ |

***Ceramic Gasifier Rotor and Burner Proof Testing.*** Four ceramic gasifier rotors and one ceramic burner were initially proof tested in hot gasifier rigs in 1992. The rotors and burner initially ran with metal gasifier assemblies prior to any testing with all-ceramic gasifier assemblies. Following successful proof tests, three of the rotors were installed into all-ceramic gasifier builds, two of which were then taken to full RPD conditions (1371°C (2500°F) TIT at 100% speed). One rotor was retired following the proof test. The ceramic burner developed cracks during the proof test.

A 20-bladed $Si_3N_4$ ceramic rotor (Norton/ TRW, NT154, S/N 6F) was initially proof tested for 9.9 hours including 5.1 hours on the ATTAP durability schedule limited to peak TIT at 1150°C (2100°F) due to metal component limitations. During the gasifier testing prior to running the durability cycle, the compressor surged three times. Inspection revealed that a large amount of carbon had formed in the burner, pieces of which had presumably passed through the rotor and caused the compressor surge. No damage to the rotor was noted following the test.

Subsequent to the initial proof test, the rotor was rebalanced, during which material removal from the rotor was required. In order to have as much confidence as possible in the rotor prior to operation in an all-ceramic gasifier build, the rotor was reassembled into a metal gasifier assembly for a second proof test. The rotor was taken up to peak TIT at 1140°C (2085°F) and 99% speed and then ran one cycle of the ATTAP durability schedule up to the same peak condition. The rotor was in good condition following the test and was subsequently used in an all-ceramic gasifier test with the instrumented gasifier housing as discussed above.

Two additional 20-bladed $Si_3N_4$ ceramic gasifier rotors (Kyocera, SN252, S/N 5K21 and S/N 5K23 were successfully proof tested in metal gasifier builds. Both rotors were taken up to 1150°C (2100°F) TIT at 100% speed and were then run on the ATTAP durability schedule. Rotor S/N 5K21 ran the schedule with the same peak condition and accumulated 12.8 total run hours. The rotor was then installed in the all-ceramic gasifier assembly which accumulated 267.7 hours as previously discussed. The rotor accumulated a total of 280.5 total run hours before being destroyed in the all-ceramic gasifier failure. When running rotor S/N 5K23, the schedule was limited to 98% speed and 1140°C (2085°F) TIT because of a noisy speed signal. Running the proof test with a slightly lower peak speed did not lower confidence in using the rotor in an all-ceramic gasifier build. Rotor S/N 5K23 accumulated 11.6 run hours and was then installed into the all-ceramic gasifier assembly with additional instrumentation. As discussed, the rotor shifted relative to the shaft after running for 1.2 hours, and the rotor was then retired with a total of 12.8 run hours.

One 20-bladed $Si_3N_4$ ceramic gasifier rotor (Kyocera, SN252, S/N 5K27) was retired following the initial proof test. After running in a metal gasifier build for 0.5 hours up to a peak condition of 1115°C (2040°F) the rotor was re-

moved from the rig. The engine insulation had deteriorated and carbon had formed in the burner during the test. A detailed inspection revealed that a number of blades had developed cracks during the test, possibly caused by insulation or carbon FOD. Because of the cracks, it was decided not to install the rotor in an all-ceramic gasifier build.

A ceramic combustor with 6 mm thick walls had failed during its initial proof test in 1991. A combustor with 4 mm thick walls (CBO, P/N 5-80583, S/N FX79406) also failed during its initial proof test in 1992. The burner was installed into the hot gasifier rig with a metal gasifier assembly that had been modified to run with the ceramic burner. The rig ran for 1.1 hours up to a peak condition of 1075°C (1965°F) at 93% speed with no abnormal operation noted during the test. Upon disassembly, the burner was observed to be in place but severely cracked. Section 3.1.3 provides detailed failure analysis.

*Component Testing Summary.* Tables 4-V through 4-VII provide a summary of test data accumulated during the reporting period and accumulated to date under the ATTAP program. With the variety of suppliers, materials, and configurations of components placed on test, a substantial data base is being established upon which future efforts can be built.

*Table 4-V.*
*Ceramic rotor data base.*

| Supplier | Rotor S/N | No. of blades | Material | Hours on test: 1992 total | Hours on test: Cumulative total | Peak speed— % | Peak temperature— °C (°F) |
|---|---|---|---|---|---|---|---|
| Norton/TRW | 5S | 20 | NT154 | 0.4 | 224.7 | 100 | 1350 (2460) |
| Norton/TRW | 6F | 20 | NT154 | 12.0 | 12.0 | 100 | 1180 (2155) |
| Kyocera | 5K12 | 15 | SN252 | 96.5 | 229.0 | 101 | 1385 (2525) |
| Kyocera | 5K13 | 15 | SN252 | 13.5 | 22.4 | 100 | 1380 (2515) |
| Kyocera | 5K21 | 20 | SN252 | 279.8 | 279.8 | 100 | 1380 (2515) |
| Kyocera | 5K23 | 20 | SN252 | 12.8 | 12.8 | 100 | 1150 (2100) |
| Kyocera | 5K27 | 20 | SN252 | 0.5 | 0.5 | 100 | 1115 (2040) |

*Table 4-VI.*
*Ceramic scroll data base.*

| Supplier | Scroll type | Scroll S/N | Material | Hours on test: 1992 total | Hours on test: Cumulative total | Peak speed— % | Peak temperature— °C (°F) |
|---|---|---|---|---|---|---|---|
| Norton/TRW | Standard | KX56721 | NT230 | 0.4 | 8.9 | 100 | 1350 (2460) |
| Norton/TRW | Standard | KX59008 | NT230 | 1.5 | 1.5 | 100 | 1050 (1920) |
| Kyocera | Standard | 0001-1 | SN252 | 96.5 | 196.5 | 101 | 1385 (2525) |
| Kyocera | Standard | 0002-1 | SN252 | 13.5 | 13.5 | 100 | 1380 (2515) |
| Kyocera | Advanced Concept | KX59815 | SN252 | 267.7 | 267.7 | 100 | 1380 (2515) |

*Table 4-VII.*
*ATTAP 1987-1992 accumulated hot rotating test times.*

| Period | Engine run hours | Hot rig run hours | Total run hours |
|---|---|---|---|
| October 1987 - 31 December 1989 | 1473 | 142 | 1615 |
| 1 January 1990 - 31 December 1990 | 119 | 710 | 829 |
| October 1987 - 31 December 1990 | 1592 | 852 | 2444 |
| 1 January 1991 - 31 December 1991 | 128 | 719 | 847 |
| October 1987 - 31 December 1991 | 1720 | 1571 | 3291 |
| 1 January 1992 - 31 December 1992 | 147 | 452 | 599 |
| October 1987 - 31 December 1992 | 1867 | 2023 | 3890 |

# V. PERFORMANCE AND DURABILITY TESTING – TEST-BED ENGINES

## 5.2.3.1 Test-Bed Engine Fabrication

### Objective/Approach

Test-bed engine fabrication activities support all engine test activities through instrumentation, build, and repair where necessary (see Section 5.2.3.2). New engine component fabrication activities support the design/development efforts to evolve the AGT-5 to a high temperature durability test-bed engine.

### Accomplishments/Results

- More than 40 gasifier assembly and engine builds were completed.

### Discussion

During 1992, all phases of test-bed engine fabrication were supported for both test stand engine and hot gasifier rig testing. Including teardown for inspection and reassembly, 13 all-ceramic gasifier assembly builds and 8 gasifier builds with ceramic rotors were completed. Five engine builds were also completed during the year. Other fabrication efforts supported everything from high temperature combustion components to instrumentation and simple brackets. Special builds in 1992 included modified burner hardware for insulation injection, instrumenting with accelerometers and proximity probes, and assembling an engine with the new L-seal regenerator seal system. Details of these tests are discussed in Sections 4.2.3.3 and 5.2.3.2.

## 5.2.3.2 Test-Bed Engine Testing

### Objective/Approach

Test-bed engine testing occurs both on the dynamometer stand and in vehicles. Dynamometer stand operation is performed for high temperature durability verification of the test-bed and evaluation of ceramic hot flow-path components and engine insulation. This testing also supports the ceramic redesign process and evaluates new engine hardware as it becomes available. Test-bed engine testing is performed in a vehicle to evaluate ceramic hot flow-path components in a real-world automotive environment, ensuring that ceramic component performance and/or durability design criteria, unique to vehicular gas turbine operation, are not overlooked.

### Accomplishments/Results

- A 100-hour engine durability test with a new regenerator seal system was completed.
- Engine insulation exhaust emissions test work was conducted in the dynamometer cell.
- An engine was run in preparation for a test-bed vehicle installation.
- Exhaust emissions test work in the dynamometer test cell was supported.

### Discussion

In 1992, test-bed engines accumulated 147 hours run time in the dynamometer test cells. Ceramic regenerator cores were installed in engines for 111 hours of the 147 total hours. No other ceramic components were run in complete engines in 1992. Test-bed engine testing supported regenerator seal development, insulation exhaust emissions testing, and pollutant exhaust emissions testing. No engine operation in the test-bed vehicles was conducted, due to the priority placed on ceramic gasifier testing in the hot gasifier rig and due to the unavailability of low emissions burner hardware.

A test-bed engine was assembled with metal turbomachinery and ceramic regenerator cores in preparation for ceramic component (in addition to regenerator cores) testing in an engine. The engine was assembled with the L-seal type regenerator seal system; this engine was the first hot test of the new seal system. The engine ran in the dynamometer test cell in order to establish engine and regenerator seal system reliability. After an initial baseline peak power run up to the metal component speed and temperature limits, the engine accumulated over 100 hours running. The 100 hours consisted of 5.4 hours of steady-state operation and 94.6 hours of durability schedule operation. There were

no shutdowns and restarts while running. Peak gasifier speeds during durability testing were limited to 97% to prevent compressor surge. The initial 21.3 durability hours were run on a schedule consisting of a 64 sec cycle: 48 sec at idle and 16 sec at 97% speed. The remaining 73.3 hours durability testing were on the AT-TAP durability schedule modified to include no shutdowns and with a peak speed of 97%. A comparison of peak power tests run at 1 and at 100 test hours showed no change in engine performance during the test. A complete inspection following the test revealed that the regenerator seals were in excellent condition. Section 1.4.1 provides a more detailed discussion of the L-seal type regenerator seal system.

A test-bed engine ran in the test cell to support the testing of exhaust emissions of insulation material. The engine ran a baseline peak power test and then modified burner hardware was installed to allow injection of insulation material in to the burner cavity. Insulation was injected into a running engine and the amount of insulation that came out of the engine was measured. Section 3.2.2 describes in detail the insulation test. A standard burner was reinstalled in the engine following the test and a repeat of the baseline test showed no change in engine performance.

A third test-bed engine (all metal components) ran in the cell in preparation for installation in the test-bed vehicle. After initial testing revealed high operating temperatures, ceramic regenerators were installed to obtain higher regenerator inlet temperature limits. A subsequent peak power test revealed operating temperatures that were still excessively high for a vehicular installation; however, the engine was made available for an exhaust emissions test. A modified metal burner configuration was installed in the engine and steady-state emissions data were recorded. In order to concentrate build and test work on all-ceramic gasifier assemblies, no further effort was devoted to improving the engine's performance and lowering the operating temperatures.

# APPENDIX A
# ACRONYM LIST

| | |
|---|---|
| AES | General Motors Advanced Engineering Staff |
| AGT | Advanced Gas Turbine |
| AGT-5 | automotive gas turbine test-bed used in Advanced Turbine Technology Applications Project |
| $Al_2O_3$ | aluminum oxide |
| AME | General Motors Advanced Manufacturing Engineering |
| AS | alumino-silicate |
| α-SiC | alpha phase silicon carbide |
| AT | aluminum titanate |
| ATTAP | Advanced Turbine Technology Applications Project |
| ave | average |
| Ba | barium |
| BALCO | The Balancing Company |
| β-$Si_3N_4$ | beta phase silicon nitride |
| BU | build-up |
| BVG | burner variable geometry |
| Ca | calcium |
| CAD | computer aided design |
| CBO | The Carborundum Company |
| CF | centrifugal force |
| CGT | ceramic gasifier turbine |
| CIP | cold isostatic pressing |
| cm | centimeter |
| CMM | coordinate measurement machine |
| cm/sec | centimeters per second |
| CO | carbon monoxide |
| CPS | Ceramic Process Systems, Inc |
| cpsc | cells per square cm |
| cpsi | cells per square inch |
| CTAHE | Ceramics Technology for Advanced Heat Engines |
| CTE | coefficient of thermal expansion |
| D/A | digital to analog |
| DC | direct current |
| deg | degrees |
| DIMOX | directed metal oxidation |
| DOE | Department of Energy |
| DTM | DeskTop Manufacturing |
| EDM-800 | electronic development module (engine controller) |
| EPA | Environmental Protection Agency |
| ERDA | Energy Research and Development Administration |
| FEM | finite element method |
| FOD | foreign object damage |
| FPI | fluorescent penetrant inspection |
| ft lbf | foot-pounds force |
| g/cc | grams per cubic centimeter |
| gm | gram |
| GM | General Motors, Inc |
| GM/AE | General Motors Advanced Engineering |
| gm/mi | grams per mile |
| GMPF | General Motors Parts Fabrication |
| GMR | General Motors Research |
| GTE | GTE Laboratories Inc |
| HC | hydrocarbons |
| HIP | hot isostatic pressing |
| HTML | High Temperature Materials Laboratory (Oak Ridge National Laboratory) |
| I.D. | inside diameter in inches |
| in./in.°F | inches per inch per degree Fahrenheit |
| JP5 | jet petroleum No. 5 (aviation fuel) |
| K | potassium |
| kg | kilogram |
| krpm | kilo-revolutions per minute |
| ksi | kilopounds per square inch |
| ksi-in | kilopounds per square inch inches |
| LAS | lithium alumino-silicate |
| lb | pound |
| lbf | pound force |
| $lb/in^3$ | pounds per cubic inch |
| lbm | pound mass |
| LeRC | NASA Lewis Research Center |
| LoTEC | LoTEC Inc |
| MAS | magnesium alumino-silicate [Cordierite] |
| MAT | mullite aluminum titanate |
| max | maximum |
| MFXR | microfocus X-ray |
| mi | mile |
| MIL-STD | military standard |
| min | minimum |
| mm | millimeter |
| m/m°C | meters per meter per degree centigrade |
| MOR | modulus of rupture |
| MPa | megapascal |
| MPa-m | megapascal meters |
| mpg | miles per gallon |
| mph | miles per hour |
| MR | magnetoresistive |
| MTC | Mountain Technical Center, Schuller International Inc |

| | |
|---|---|
| N | newton |
| 'N' | control number |
| Na | sodium |
| NaCl | sodium chloride |
| NASA | National Aeronautics and Space Administration |
| Nb | number of blades |
| NDE | nondestructive evaluaton |
| no. | number |
| NOx | oxides of nitrogen |
| NTC | Norton/TRW Ceramics |
| N/TRW | Norton/TRW, Inc |
| NZP | (sodium) zirconium phosphate |
| N1 | speed (gasifier shaft speed) |
| °C | degrees Centigrade |
| O.D. | outside diameter |
| ODS | oxide dispersion strengthened |
| ORNL | Oak Ridge National Laboratory |
| °F | degrees Fahrenheit |
| P | phosphorus |
| Pa | pascal |
| PCF | pounds per cubic foot |
| pH | measure of acidity/alkalinity |
| P/N | part number |
| POS | probability of survival |
| ppm | parts per million |
| psi | pounds per square inch |
| Pt/Ps | pressure ratio, total to static |
| P2 | pressure (compressor discharge) |
| P3 | pressure (burner inlet) |
| P5 | pressure (gasifier turbine outlet) |
| RIT | rotor inlet temperature |
| RPD | reference powertrain design |
| rpm | revolutions per minute |
| RT | room temperature |
| sec | second |
| SEM | scanning electron micrograph/microscope |
| SENB | single edged notched beam |
| SiC | silicon carbide |
| Si-SiC | siliconized silicon carbide |
| $Si_3N_4$ | silicon nitride |
| SLS | selective laser sintering |
| S/N | serial number |
| Sr | strontium |
| .STL | computer data file format for rapid prototype fabrication |
| STRATA/ ROTORDYN | mathematical analysis programs using FEM models |
| TIT | turbine inlet temperature |
| T1 | temperature (compressor inlet) |
| T2 | temperature (compressor discharge) |
| T3 | temperature (burner inlet) |
| T4 | temperature (turbine inlet) (TIT) |
| T6 | temperature (regenerator inlet) |
| UHC | unburned hydrocarbon |
| ULEV | ultra-low emissions vehicle |
| VMS-1000 | Vehicular Electronic Controller Instrumentation System |
| WBS | work breakdown structure |
| 2-D | two-dimensional |
| 3-D | three-dimensional |
| 1E | one excitation per power turbine shaft revolution |
| 2E | two excitations per shaft revolution |

# REPORT DOCUMENTATION PAGE

*Form Approved*
*OMB No. 0704-0188*



| 1. AGENCY USE ONLY (*Leave blank*) | 2. REPORT DATE | 3. REPORT TYPE AND DATES COVERED |
|---|---|---|
| | December 1993 | Annual Contractor Report |

**4. TITLE AND SUBTITLE**

Advanced Turbine Technology Applications Project (ATTAP)
1992 Annual Report

**5. FUNDING NUMBERS**

WU–778–32–21
DEN3–336

**6. AUTHOR(S)**

Engineering Department

**7. PERFORMING ORGANIZATION NAME(S) AND ADDRESS(ES)**

Allison Engine Company
P.O. Box 420
Indianapolis, Indiana 46206–0420

**8. PERFORMING ORGANIZATION REPORT NUMBER**

E–9499

**9. SPONSORING/MONITORING AGENCY NAME(S) AND ADDRESS(ES)**

National Aeronautics and Space Administration
Lewis Research Center
Cleveland, Ohio 44135–3191

**10. SPONSORING/MONITORING AGENCY REPORT NUMBER**

NASA CR–195446
DOE/NASA/0336–5

**11. SUPPLEMENTARY NOTES**

Prepared under Interagency Agreement DE–AI01–90CE50300. Project Manager, Paul T. Kerwin, Propulsion Systems Division, NASA Lewis Research Center, organization code 2703, (216) 433–3409.

**12a. DISTRIBUTION/AVAILABILITY STATEMENT**

Unclassified - Unlimited
Subject Categories 07, 27, and 37

This publication is available from the NASA Center for Aerospace Information, (301) 621–0390.

**12b. DISTRIBUTION CODE**

**13. ABSTRACT** (*Maximum 200 words*)

The Advanced Turbine Technologies Application Project (ATTAP) is in the fifth year of a multi-year development program to bring the automotive gas turbine engine to a state at which industry can make commercialization decisions. Activities during the past year included reference powertrain design updates, test-bed engine design and development, ceramic component design, materials and component characterization, ceramic component process development and fabrication, ceramic component rig testing, and test-bed engine fabrication and testing. Engine design and development included mechanical design, combustion system development, alternate aerodynamic flow testing, and controls development. Design activities included development of the ceramic gasifier turbine static structure, the ceramic gasifier rotor, and the ceramic power turbine rotor. Material characterization efforts included the testing and evaluation of five candidate high temperature ceramic materials. Ceramic component process development and fabrication, with the objective of approaching automotive volumes and costs, continued for the gasifier turbine rotor, gasifier turbine scroll, extruded regenerator disks, and thermal insulation. Engine and rig fabrication, testing, and development supported improvements in ceramic component technology. Total test time in 1992 amounted to 599 hours, of which 147 hours were engine testing and 452 were hot rig testing.

**14. SUBJECT TERMS**

Small gas turbine; Ceramic components; Structural ceramics; Automotive; Alternative fuels; Emissions

**15. NUMBER OF PAGES**
102

**16. PRICE CODE**
A06

| 17. SECURITY CLASSIFICATION OF REPORT | 18. SECURITY CLASSIFICATION OF THIS PAGE | 19. SECURITY CLASSIFICATION OF ABSTRACT | 20. LIMITATION OF ABSTRACT |
|---|---|---|---|
| Unclassified | Unclassified | Unclassified | |